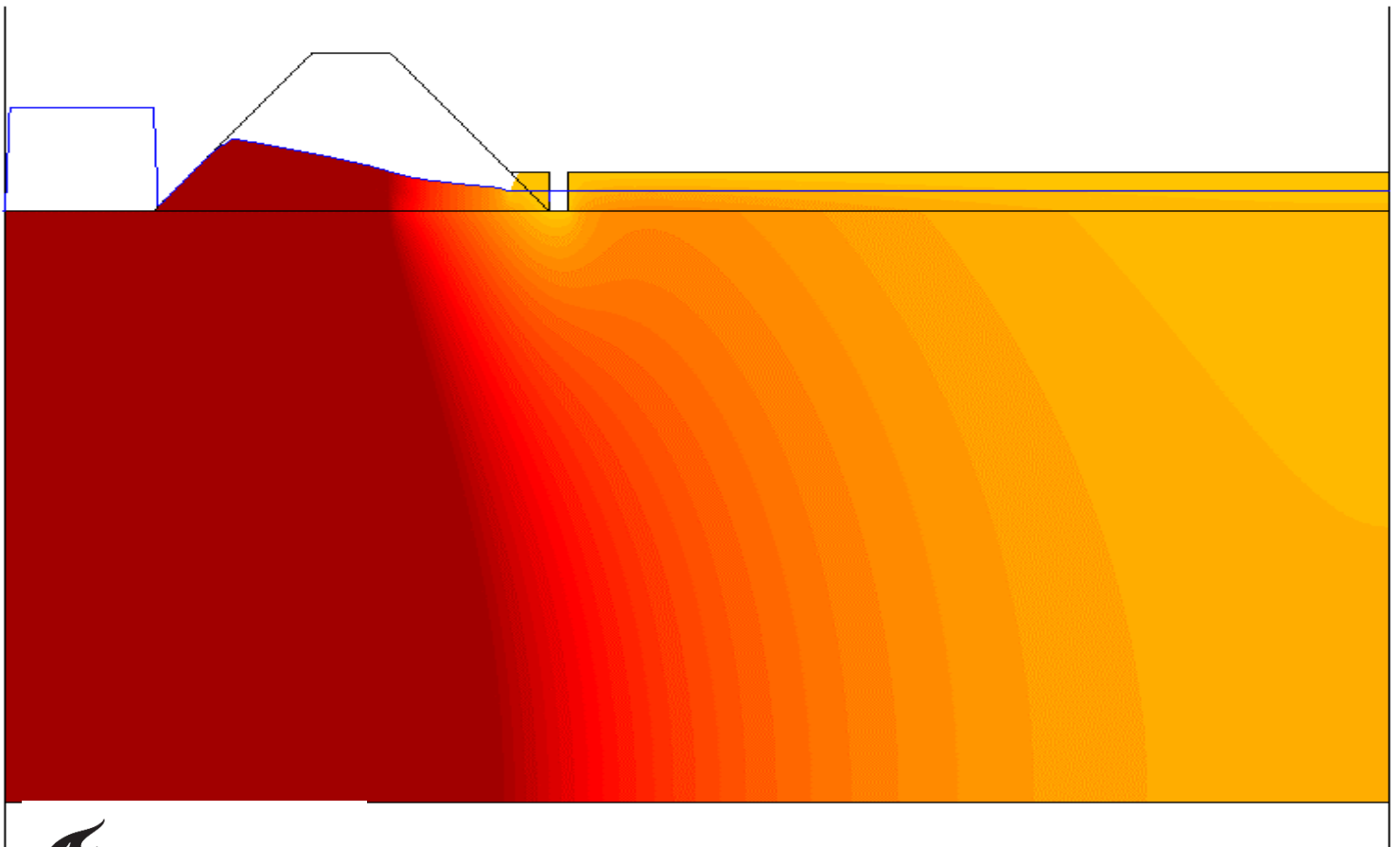


The effect of leakage on backward erosion piping: A modelling study in 2D and 3D

L. Barendsen



The effect of leakage on backward erosion piping: A modelling study in 2D and 3D

by

L. Barendsen

to obtain the degree of Master of Science
at the Delft University of Technology,
to be defended publicly on Friday June 26th, 2020 at 13:00 PM.

Student number: 4152271
Project duration: October 1st, 2019 – June 26th, 2020
Thesis committee: Prof. dr. ir. M. Kok, TU Delft, Chairman
Dr. A. Askarinejad, TU Delft
Ir. J. C. Pol, TU Delft, supervisor
Dr. W. Bartels, Lievense-WSP, supervisor
Drs. B. de Groot, Lievense-WSP, supervisor

An electronic version of this thesis is available at <http://repository.tudelft.nl/>.

Preface

With this thesis I finalise my MSc degree in Hydraulic Engineering with the specialization River Engineering. The process of writing this thesis was a long and bumpy road. One which I could not have taken on my own. Therefore, I would like to thank everyone that helped me in this process. Starting with all of the members in my committee, Prof. Dr. Ir. M. Kok, Dr. A. Askarinejad, Ir. J. Pol, Dr. W.B. Bartels and Drs. B. de Groot who have helped me, whenever I needed their help, and who all showed great interest in everything I did.

First I would like to thank Matthijs Kok for being the chair of my committee. Your guidance and enthusiasm were always greatly appreciated. Next I would like to express my gratitude to Amin Askarinejad, who always had very specific and critical questions. Which always opened my eyes to different perspectives. Furthermore, I would like to thank Joost Pol for all the time he made for me and the critical review, which opened my mind to tracks I would not have thought of on my own. Thank you Bram for your input and willingness to assist either through a discussion or comments on my work. Lastly, I would like to thank Willem-Bart for his enthusiasm and for everything he did for me. You were always able to get me back on the right track and helped me structure my thoughts. Thank you for all the meetings we had and the time you made for me.

Besides my committee, I would like to thank everyone at Lievense-WPS, for giving me a place, where I not only felt welcome from the first day, but where everyone was always very enthusiastic and interested in my thesis topic. Thank you for keeping me in shape and taking me out during the lunch for those nice and really fast walks around Breda.

I want to thank the people around me as well, my friends, my parents and my sister Pien, for reading my thesis and for all the support you have given me in this period. I would especially like to thank Rick, whom has always supported and encourage me, he kept me sane during this time. Lastly, I also want to thank Jens, for all the hard needed brakes and coffees and making my study days more fun.

I hope you enjoy reading my thesis.

Yours sincerely,
L. Barendsen
Delft, June 26th 2020

Abstract

In the Netherlands, dikes are the most commonly used structures to retain water and provide safety against flooding. In order to ensure the safety of these dikes against a number of different failure mechanisms such as backwards erosion piping, wave overtopping and macro stability, a detailed safety assessment has been created. The focus of this thesis is on the failure mechanism known as piping. Which consists of three different sub-mechanisms; uplift, heave and backwards erosion piping.

The safety assessment against piping consists of a multi-step approach. First an elementary assessment is done, followed by a detailed assessment of the different sub-mechanisms and lastly a final analysis is done using more detailed data and software. Currently, Sellmeijer's design rule is used in the detailed safety assessment to design against the sub-mechanism backwards erosion piping. His design rule is the starting point of this thesis.

Before Sellmeijer was able to derive his design rules, he had to make a number of different assumptions and simplifications. The most significant being, simplifying the three-dimensionality of the piping process to a two-dimensional process, by neglecting the meandering nature of the pipe and excluding the effect of the lateral groundwater flow on the pipe progression. By limiting the problem to two-dimensions Sellmeijer derived a mathematical model on which his design rule was based. In his design rule Sellmeijer relates the progression of a pipe to a hydraulic gradient.

Over the years, Sellmeijer's design rule has been adapted three different times. Each adaptation resulted in a more accurate design rule accounting for more and more parameters. However, with each adaptation, Sellmeijer's design rule did not become more transparent. During the derivation of his design rule, Sellmeijer fails to account for the effect of a leaky layer on the critical hydraulic gradient for pipe progression. This limitation in his design rule is the focus of this thesis.

In order to determine if leakage affects the critical hydraulic head for pipe progression, a study is done using a two dimensional groundwater model in which his design rule is implemented. From these simulations it was observed that the presence of a leaky layer results in an increase in the critical hydraulic head. In the simulations studied, a maximum of 12 % increase is observed.

Next an analysis is done on the results of these simulations. On the one hand an attempt is made to determine if and how leakage can be included in Sellmeijer's design rule. The simulations show that the effect of leakage on increasing the critical hydraulic gradient for pipe progression is largely dependent on the hydraulic conductivity of the cover layer. However, in order for a leakage term to be determined, and included in Sellmeijer's design rule, additional simulations should be done.

In MSeep it was also observed that leaky layers significantly impact the groundwater flow under the dike. The effect of this was quantified by looking at the **effective depth**. Which is defined as the portion of the aquifer which is responsible for groundwater flow towards the pipe and uplift channel. In order to further analyse the effect of leakage on groundwater flow, a number of quasi 3D and 3D scenarios were modelled in iMOD. For these simulations the effective depth, the effective width (in 3D) and the discharge in the well is determined. In this way, the effect of leakage can be quantified. In all three of the models similar trends are observed: a increase in the hydraulic conductivity of the cover layer resulted in the decrease of the effective depth. However, in the full 3D model the impact of leakage on the groundwater flow resulted in a larger range in the results.

The results of this thesis, show that derivation of a leakage term would greatly benefit the output of the design rule. As a 'quick fix' it is recommended to derive a leakage term which can be included in Sellmeijer's design rule. However, further developments of a 3D model which correctly implements the effect of a pipe on the groundwater flow is also beneficial.

Contents

1	Introduction	1
1.1	Background information	1
1.1.1	Leaky cover layer	2
1.2	Research objective	3
1.3	Research question	3
1.4	Research methodology	3
2	Background & Literature	5
2.1	Introduction	5
2.2	Piping as a failure mechanism	5
2.3	Piping in the Netherlands	8
2.4	Uplift	9
2.5	Heave	9
2.6	Piping design rules	9
2.7	Factors affecting the critical hydraulic gradient for pipe progression(ΔH_c)	13
I	Sellmeijer's design rule	15
3	Evolution of Sellmeijer's design rule	17
3.1	Mathematical model	17
3.2	Original design rule (1988)	19
3.3	Addition of geometry factor (1989)	20
3.4	Two-force equilibrium (2006)	22
3.5	Recalibration accounting for characteristics of the grains(2011)	23
3.6	Discussion	24
3.7	Conclusions	25
4	Sensitivity Analysis	27
4.1	Aquifer thickness (D)	27
4.2	Seepage length (L)	28
4.3	Characteristic grain size (d_{70})	29
4.4	Hydraulic conductivity (k)	30
4.5	Bedding angle (θ)	31
4.6	Coefficient of White (η)	32
4.7	Conclusions	33
5	Simulations vs. Experimental data	35
5.1	Delta Flume experiments: Silvis (1991)	35
5.2	MSeep	36
5.3	Design rule	37
5.4	Conclusion	39
II	Leakage and Piping	41
6	The effect of leakage on piping	43
6.1	What is leakage?	43
6.1.1	Leakage in The Netherlands	44
6.1.2	Leakage in the Unites States of America	45
6.2	The effect of leakage on piping	45
6.2.1	Lam (2019)	45
6.2.2	MSeep simulations	46

7	Leakage: 2D	49
7.1	General model description	49
7.2	Six scenarios	50
7.3	Engineering approach	52
7.3.1	Discussion	53
7.4	Physics approach	54
7.5	Conclusions	56
8	Leakage: 3D	59
8.1	General model description	59
8.1.1	Effective depth ($D_{effective}$) & Effective width ($W_{effective}$)	61
8.2	Simple groundwater models	62
8.3	Physcis Approach: Effect of leakage	63
8.4	Comparison of MSeep and iMOD modules	65
8.5	Conclusions	66
9	Discussion	67
9.1	Model results	67
9.1.1	MSeep simulations	67
9.1.2	iMOD simulations	68
9.2	Limitations of the research	69
III	Conclusions	71
10	Conclusion	73
10.1	What assumptions were used in the derivation of Sellmeijer's design rule?	73
10.2	How does leakage effect the critical hydraulic head for pipe progression?	74
10.2.1	How does leakage effect the groundwater flow in 3D compared to 2D?.	74
10.3	How can leakage be included in Sellemeijer's design rule?	75
10.4	Concluding remarks	75
11	Recommendations	77
	Bibliography	79
A	MSeep	85
A.1	General model description	85
A.2	Input	86
A.3	Grid	87
A.4	Erosion module	87
A.5	Model sensitivity	89
A.5.1	Mesh size	89
A.5.2	Width ditch	89
B	Delta Flume experiments: Silvis (1991)	91
C	Groundwater and leakage	93
C.1	Confined aquifer with no recharge	95
C.2	Confined aquifer with recharge	96
C.3	Semi-confined aquifer with no recharge	96
C.4	Technical report water pressures in dikes	97
D	Blanket layer theory	99
E	Report: Lam (2019)	105
E.1	KPP Piping - permeability of the cover layer	105

F	MSeep simulations	107
F.1	Case I	107
F.1.1	Geometry	107
F.1.2	Input	107
F.1.3	Boundary conditions	107
F.1.4	Erosion	108
F.1.5	Mesh size	108
F.1.6	Results	108
F.2	Case II	114
F.2.1	Geometry	114
F.2.2	Input	114
F.2.3	Boundary conditions	114
F.2.4	Erosion	115
F.2.5	Mesh size	115
F.2.6	Results	115
G	iMOD	123
G.1	Boundary conditions (BND)	123
G.2	Starting Heads (SHD)	123
G.3	Horizontal permeabilities (K _{HV})	124
G.4	Vertical permeabilities (K _{VV})	124
G.5	Vertical anisotropy(K _{V_A})	124
G.6	Top of aquifers	124
G.7	Bottom of aquifers	124
G.8	Pathline simulation	124
H	iMOD simulations	125
H.1	Geometry	125
H.2	Mesh size	125
H.3	Boundary conditions	126
H.4	Input parameters	126
H.5	Piping	126
H.6	Results	126
H.7	Base case	127
H.7.1	Simple groundwater models	127
H.8	Effect of leakage	128
H.8.1	Comparison of MSeep and iMOD modules	130

1

Introduction

Dikes are the most commonly used structures to retain water and to provide safety against flooding in the Netherlands, because of this an extensive network of both sea dikes and river dikes exist. These dikes have a total length of more than 20,000 km (TAW, 2004). Most of these dikes are river dikes and are constructed using an impermeable material (clay) and are often constructed on top of sandy aquifers. The water level in rivers varies with time, creating a hydraulic gradient over the dike. This hydraulic gradient across the structure results in a groundwater flow through the aquifer (Deltares, 2018), which can result in the movement of sediment. Often the foundations of these dikes and dams are vulnerable to an erosion process known as piping (also known as backward erosion and under-seepage erosion) (van Beek et al., 2013). This process results in the formation of shallow pipes at the interface between a sandy or silty foundation and a cohesive top layer (van Beek et al., 2015). According to van Beek and Hoffmans (2017) backward erosion piping is described by a processes *"whereby particles are transported from granular layers under the action of water flow, leaving a shallow hollow space (a pipe), which progressively develops in the opposite direction of water flow."* (van Beek and Hoffmans, 2017). Once the pipe has fully developed and reached the upstream water level, the increase in flow through the pipe results in the further deepening and widening of the pipe, undermining the structure (van Beek and Hoffmans, 2017). This can cause cracks to form in the dike and cause the dike to eventually fail (van Beek et al., 2011a).

1.1. Background information

Safety assessment in the Netherlands for failure due to piping, consists of a multi-step approach. The first step, is an elementary assessment and consists of a set of simple design rules to determine if backward erosion piping is a possibility. If dikes fail the elementary assessment, a detailed assessment needs to be done, where the failure probability is determined for the different sub-mechanisms; **uplift** of the cover layer, **heave** (transport of particles through a defect) and progression of the pipe (**piping**) (van Beek and Hoffmans, 2017). For the uplift calculation, a comparison of the water pressures in the aquifer and the overlying weight of the **blanket layer** is done. For the vertical transport of sediment through the cracks, a critical vertical gradient of 0.3 across the blanket layer is used. Lastly, the probability of pipe progression is determined using the Sellmeijer rule. Once this detailed assessment has been completed, a final analysis is done using more detailed data and software (van Beek and Hoffmans, 2017).

Up until 2009, the design rule by Bligh (1910) was used in the detailed assessment, to determine the critical hydraulic head for which backward erosion progresses towards the upstream side (van Beek and Hoffmans, 2017). However, after 2009, the design rules by Sellmeijer were adopted. These design rules were adopted, because according to experts, the design rule by Bligh could lead to unsafe results (Vrijling et al., 2010).

Unfortunately, recent analysis of the Dutch dikes using the 2011 version of Sellmeijer design rule has resulted in the conclusion that most of the Dutch dikes would fail with respect to piping, due to the large uncertainties of the input parameters (van Beek and Hoffmans, 2017). For these cases, the calculated critical hydraulic head difference is too large for the limited **seepage length** (L_s) under the dike.

Where the seepage length is defined as the distance that the pipe must cover between the upstream level and downstream level (Figure 1.1) (van Beek and Hoffmans, 2017). Fortunately, according to experts, the predictions made using Sellmeijer's (2011) design rules are for some cases conservative; resulting in a need for impossibly long seepage lengths.

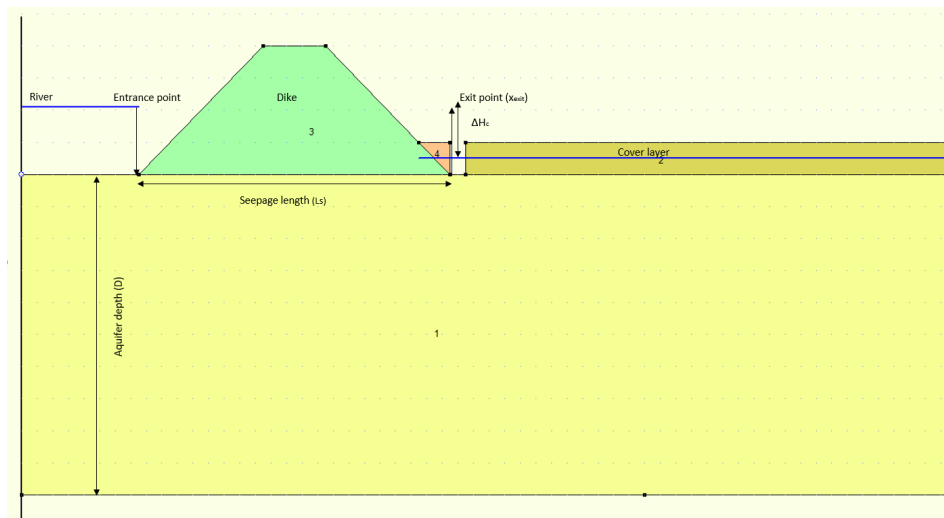


Figure 1.1: Cross sectional view of a dike with an exit point.

1.1.1. Leaky cover layer

Often the cover layer consists of semi-permeable/leaky clay. Resulting in leakage though these layers as a result of a difference in potential in the clay and sand. The magnitude of leakage depends on the hydraulic conductivity of the cover layer, the confined layer and the thickness of both of these layers and is expressed using the **leakage factor** (λ).

The presence of a leaky cover layer significantly effects the streamlines in the aquifer under a dike. Figure 1.2 shows the streamlines under a dike for a situation where there cover layer is impermeable. In Figure 1.2 it can be seen that all the streamlines converge towards the ditch and that all of the water flows out via the ditch. Figure 1.3 shows the streamlines under a dike for a very leaky (larger hydraulic conductivity) cover layer. It can be seen that a portion of the streamlines flow towards the ditch, while a significant portion also flows towards the hinterland and eventually towards the surface. Through the cover layer.

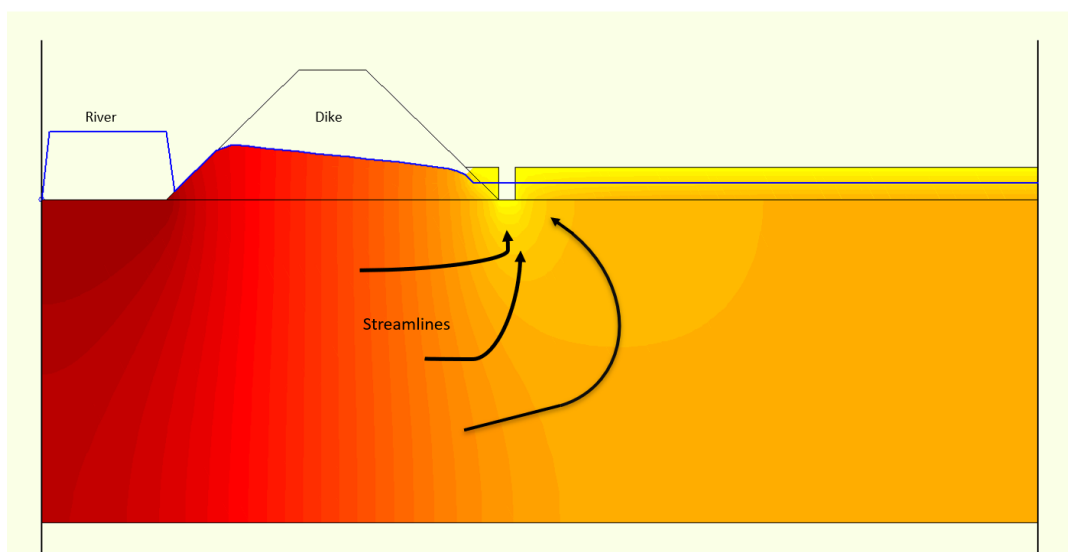


Figure 1.2: Potentials and streamlines in the aquifer for an impermeable cover layer.

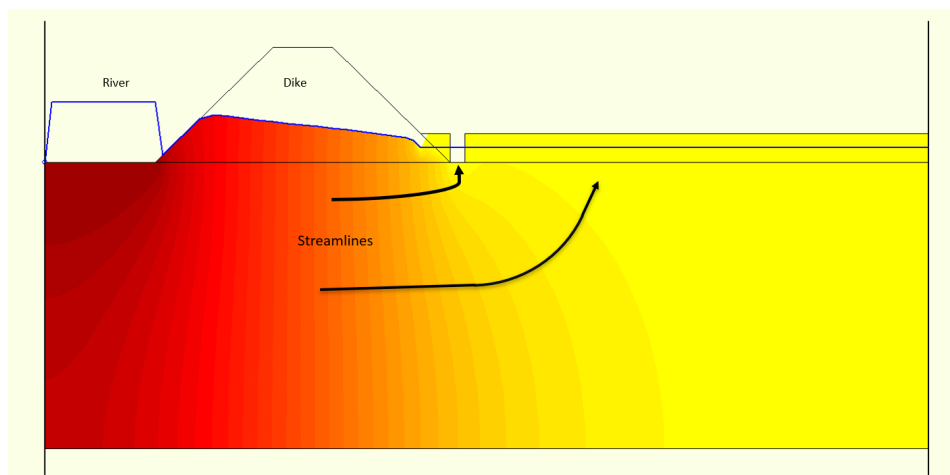


Figure 1.3: Potentials and streamlines in the aquifer for a leaky cover layer

1.2. Research objective

Currently, the Dutch guidelines for piping use the 2011 version of Sellmeijers' design rule. The rule is based on a basic dike configuration (Figure 1.1) and accounts for groundwater flow in two-dimensions; horizontally (under the dike towards the hinterland) and vertically. Over the years, the design rule by Sellmeijer has been adapted a number of times, one of these adaptations resulted in the inclusion of the geometry factor. This factor accounts for a more realistic approach of the geometry, by accounting for a finite thickness of the sub-soil as well as the presence of a cover layer (Weijers and Sellmeijer, 1993). In his mathematical model, Sellmeijer assumes that the cover layer is impermeable and that the vertical discharge is equal to zero. Based on this assumption, it can be concluded that the effect of leakage towards the hinterland (since along this boundary the vertical discharge vanishes) is unaccounted for. However in actuality, leakage towards the hinterland does occur (Hoffmans and Van Rijn, 2018). Therefore, the goal of this thesis is *to asses the effects of leakage on groundwater flow, and how this affects the critical hydraulic gradient for which a pipe progresses.*

1.3. Research question

In order to achieve the above mentioned objective, the following research questions have been determined:

1. What assumptions were used in the derivation of Sellmeijer's design rule?
2. How does leakage towards the hinterland effect the critical hydraulic head for pipe progression?
 - 2.1 How does leakage effect the groundwater flow in 3D compared to 2D?
3. How can leakage be included in Sellmeijer's design rule?

1.4. Research methodology

In this thesis, the focus will be on the effects of leakage on the critical hydraulic gradient for which a pipe progresses. First a general introduction will be given to the failure mechanism known as piping. After this, the thesis will be split up into three different sections (Figure 1.4). The first section, will focus on answering the first research question. The second will focus on the effects of leakage and piping and is used to answer the second and third research question. The third, and final section will focus on the conclusions of this research and recommendations for further research.

As was previously mentioned, the first section will focus on the design rules by Sellmeijer. Specifically how these design rules have evolved since their first appearance. Secondly, a sensitivity analysis will be done of the four different versions of Sellmeijer's design rule, for each version a number of different input parameters will be varied. Next, the focus will be on three large scale piping experiments done by Silvis et al. (1991) in the Delta Flume. Before these experiments were performed, MSeep (Finite Element groundwater model) calculations were done, in order to predict the expected outcome of the

pipng results. Since the goal of this thesis is to determine leakage towards the hinterland, a MSeep model needs to be constructed. By first replicating the results of the simulations done by Silvis, the implemented boundary conditions are studied. As well as the difference in results of the experiment, models and design rule.

The second section focuses on leakage and the effect of leakage on piping. Here leakage is defined and how it affects the critical hydraulic gradient for pipe progression is studied. Next, an analysis using a two-dimensional model (MSeep, with an erosion module) is done to determine the effect of leakage on the critical hydraulic gradient as well as on the groundwater flow. Followed by an discussion in which the possibilities of including leakage in Sellmeijer's design rule are presented.

Next, an analysis is done using iMOD in which both quasi 3D and full 3D simulations are done. An erosion tool has not been included in iMOD, so in order to study the effect of a pipe on groundwater flow, a very permeable strip is included directly under the dike. Lastly, a comparison is made between the results of MSeep and iMOD.

After the results of the model have been presented, the results will be evaluated in the discussion. Here the limitations of the research will also be discussed.

In the final section, the conclusions of the thesis are given. Followed by recommendations for further research.

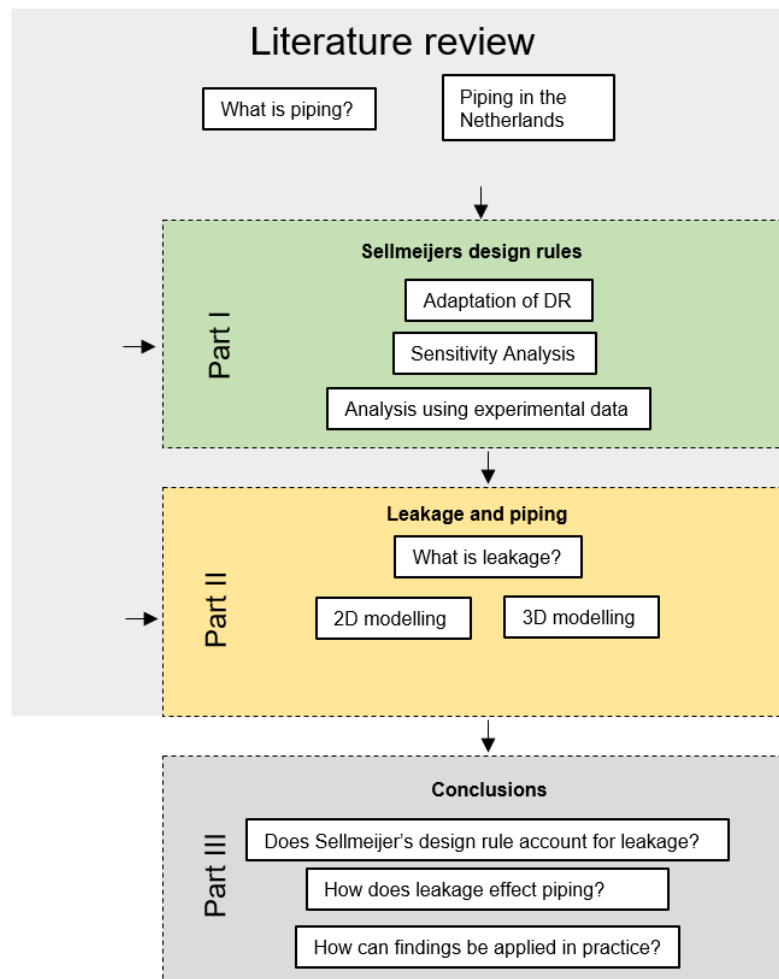


Figure 1.4: Research approach

2

Background & Literature

2.1. Introduction

In this chapter, the relevant literature will be discussed. The chapter will start with a step by step explanation of the piping process followed by a brief overview of the historical failures of dikes due to piping in the Netherlands. Next, an overview of the different sub-mechanisms will be given followed by an overview of the historical methods used to determine the critical hydraulic gradient for which failure due to piping would occur. Lastly, factors which affect the critical hydraulic gradient will be discussed.

2.2. Piping as a failure mechanism

According to van Beek et al. (2011b) four distinct phases of the failure mechanism known as piping can be seen; **seepage**, **backward erosion**, **widening of the channel** and **failure of the dike**. In the next few sections each of these four phases will be explained in detail.

Seepage

For failure to occur through backwater erosion piping, first seepage needs to occur. Seepage is induced by a water level difference across the water retaining structure, in this case a dike. The groundwater flow through the sandy aquifer can be described by Darcy's Law (which assumes laminar groundwater flow). In order for seepage to lead to backward erosion, an exit point needs to be located somewhere on/ along the inner side of the dike. An **exit point** can form due to a process known as **uplift**. Uplift can occur when there is an increase in water pressure in the aquifer (due to the increase in hydraulic gradient over the dike), and as a result, the upward force is larger than the overlying weight of the blanket layer (Figure 2.1).

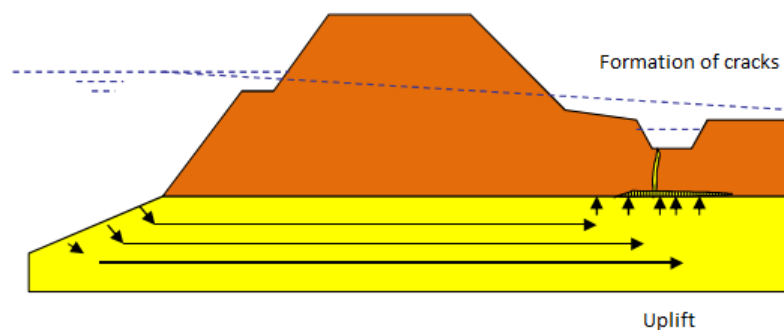


Figure 2.1: Formation of cracks due to Uplift (de Bruijn, 2013).

This can result in the formation of cracks in the blanket layer (Figure 2.2 & Figure 2.3a)(van Beek et al., 2011b)(van Beek et al., 2013). In some cases uplift and seepage can occur for lower critical hydraulic gradients, as a result of existing weaker spots in the cover layer. These weaker spots can be a consequence of tree roots, or burrow holes of animals (van Beek et al., 2013).

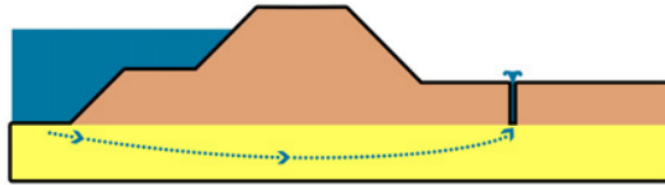


Figure 2.2: Phase 1: Seepage (Vandenboer et al., 2018).

Backward erosion

Once uplift has occurred, the next two steps are **heave** and **backward erosion**. According to van Beek et al. (2013), backward erosion piping can be split-up into four different phases:

1. The **single grain transport** phase:

In this phase, the first signs of erosion can be observed. Single grains are pushed out through the crack in the cover layer. The smaller-sized grains are removed first since these are more mobile, under the considered conditions. The erosion of these particles can result in the formation of micro-scale holes(de Wit et al., 1981), creating pore-scale pipes. For all of the studied experiments, this micro-scale erosion stops and stabilizes until the head is increased (van Beek et al., 2011b). This results in the formation of preferential flow paths (van Beek et al., 2013).

2. The **boiling** phase (Figure 2.3a, Figure 2.3b):

The bed expands as a result of an increase in pore pressures near the exit hole resulting in local fluidization of sand particles. This fluidized sand is pushed up due to the flow of the water (**heave**). However, sand wells, resulting in the formation of the pipe do not form yet. This is because the water flow is insufficiently strong to push the sand boils up and out, the sand is instead dropped back into the center of the boil (van Beek et al., 2013).



(a) Formation of a well which only excretes water (de Bruijn, 2013).



(b) Due to a further increase in hydraulic head, the sand fluidizes and becomes mobile, sand is deposited and forms shape similar to a well (de Bruijn, 2013).

Figure 2.3: Development of wells

3. The **regressive backward erosion** phase:

If the hydraulic gradient increases further, the sand boiling will intensify and sand will be deposited near the exit point. Hollow spaces will form in the sand body. Often at this point the critical head, has not yet been exceeded. After some time, the pipe progression will cease. An equilibrium in pipe formation can be observed and is therefore known as the regressive or equilibrium phase (van Beek et al., 2013). Several causes have been discussed for this equilibrium phase. In the experiment by de Wit et al. (1981), the circular vertical hole was slowly filled with

sand, but the level of fluidization remained constant until there was a further increase in hydraulic gradient. Eventually, the water pressure increased, and caused the sand to be ejected out of the tube and onto the cover layer, forming a well.

For larger hole diameters (0.04 m in the de Wit et al. (1981) experiments and 0.013 m in Miesel (1978) experiments) equilibrium was no longer observed at this stage. The pipe continues to develop until the upstream side without a need for a further increase in head. For smaller diameter exit holes (< 0.013 m) equilibrium can still occur after sand ejection. This equilibrium can be due the decrease in hydraulic gradient, in the sand further away from the exit point. This limits the inflow to the pipe and the gradient at the head of the pipe with increasing length (van Beek et al., 2013). Finally, equilibrium can occur, if a cut-off wall or structure is present. Once the pipe reaches the structure, the pipe will propagate parallel to the structure until the head difference in larger enough to bring the pipes underneath the cut-off (de Wit et al., 1981),(van Beek et al., 2011b).

In some experiments, equilibrium in pipe formation is not observed. These experiments are mainly plane and slope exit type experiments. In these experiments the critical head for progression is already exceeded once the pipe formation has started. Since the required head for fluidization is larger than the head required for progression.

According to Hanses (1985) there are two different types of erosion for the progression of a pipe. The first is known as **primary erosion**, and is defined as the erosion at the pipe tip causing the pipe to lengthen (Figure 2.5a & Figure 2.5b). This type of erosion occurs when the critical hydraulic gradient at the tip of the pipe is reached, resulting in the fluidization of sand, so that transport can occur (van Beek et al., 2013). The second is known as **secondary erosion** and is defined as erosion of the pipe walls and bottom causing the pipe to deepen and widen in the downstream direction (Figure 2.4).

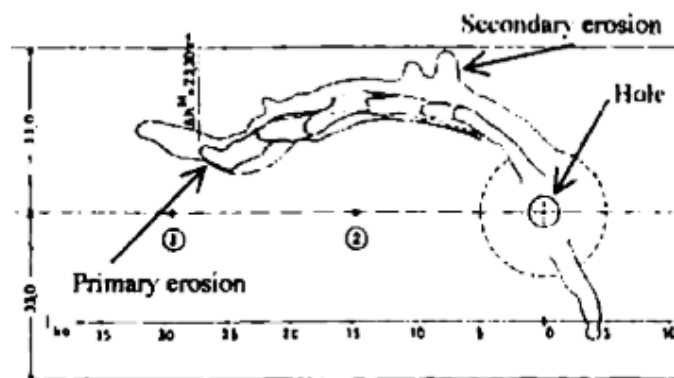


Figure 2.4: Drawing of the pipe development showing both primary and secondary erosion (Hanses, 1985).

4. The **progressive backward erosion** phase (Figure 2.5a, Figure 2.5b):

The pipe continues to develop towards the upstream side. According to Müller-Kirchenbauer et al. (1993), this phase is often reached once the pipe had developed to 1/3 or 1/2 of the seepage length. From this moment onward, the gradient and flow towards the pipe increase and equilibrium is no longer possible. For situations in which a cut-off structure is present, the progressive phase has been reached once the pipe has passed this cut-off structure (van Beek et al., 2013).

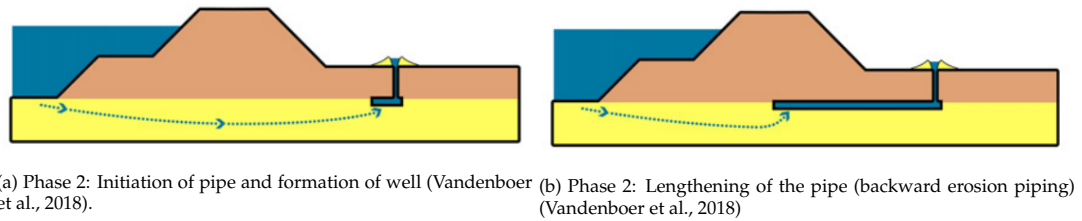


Figure 2.5: Backward erosion piping

Widening of the channel

Once the pipe has reached the full length of the base of the dike, and the upstream and downstream sides are connected, initially the flow through the pipe will increase drastically. This increase in flow velocity through the pipe will result in a further increase of the erosion rate of the pipe starting upstream (van Beek et al., 2013). This large increase in sediment volume which needs to be transported through the pipe can result in the blockage of the pipe. A new process of backwards erosion will need to start in order to unblock/ re-connect the widened pipe with the downstream pipe (van Beek et al., 2013). Eventually, the widened pipe has reached the whole width.

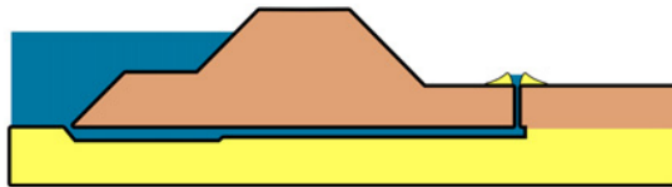


Figure 2.6: Phase 3: Widening of the pipe (Vandenboer et al., 2018).

Failure of the dike

Once the widening of the channel has reached the full length of the dike. The increased flow through the dike results in further erosion and scouring of both the dike and the sandy aquifer in such a way that the dike deforms and cracks resulting in the failure of the dike (van Beek et al., 2013).



(a) Phase 4: Cracking and deformation of dike (Vandenboer et al., 2018). (b) Phase 4: Dike breach (dike failure) (Vandenboer et al., 2018).

Figure 2.7: Complete failure of the dike

2.3. Piping in the Netherlands

Throughout history, the failure of dikes in the Netherlands has only occurred at three different times (Förster et al., 2012). During this time, the failure mechanisms known as piping was still undiscovered. These accounts are based on historical reports describing the failure of the dike. These three instances are:

1. Dike breach in the polder at Nieuw-Strijen in Tholen (1894)
2. Dike breach at Heidijk in Nieuwkuijk (1880)
3. Dike breach in Zalk (1926)

Besides these three instances when failure of the dike occurred, there have been a few more instances when failure of the dike due to piping was imminent. However due to mitigation measures, the

pipe was unable to grow and cause failure of the following dike reaches; Landsdijken Gelderland, Galgendaalsedijk, Hondbroeksche Pleij and Vianen (Förster et al., 2012).

2.4. Uplift

As was mentioned earlier, before a dike fails because of piping. First three sub-mechanisms need to occur; **uplift**, **heave** and finally **piping**. The first sub-mechanism will be discussed here. In order for uplift to occur a criterion for uplift needed to be determined. The following equation is used to determine if uplift can occur at a specific location with a specific piezometric head (Equation 2.1). A safety factor is included so that uncertainty due to variation of the subsoil can be taken into account.

$$(\phi_z - h_p) \leq \frac{1}{\gamma} (\phi_{z,g} - h_p) \quad (2.1)$$

With:

$$\phi_{z,g} = h_p + d \frac{\gamma_{wet} - \gamma_w}{\gamma_w} \quad (2.2)$$

Where:

- γ is the safety factor [-]
- γ_{wet} is the volumetric weight of the wetted sand grains [kN/m³]
- γ_w is the volumetric weight of water [kN/m³]
- ϕ_z is the piezometric head directly under the cover layer [m]
- $\phi_{z,g}$ is the critical potential for which uplift can occur [m]
- d_{cover} is the thickness of the cover layer [m]
- h_p is the head in the polder [m]

2.5. Heave

Next, the sub-mechanism heave needs to occur. In 1922, a concept based on the vertical critical gradient was presented by Terzaghi. This gradient occurs when the vertical seepage forces acting on a sand grain exceeds the downward force acting on these grains (weight) (Terzaghi, 1922). This equilibrium as described by Terzaghi (Equation 2.3) can be used as means for determining if particle movement will occur and initiation the downstream seepage exit (Robbins and van Beek, 2015).

$$i_c = \frac{\gamma_{sat} - \gamma_w}{\gamma_w} = \frac{\gamma'}{\gamma_w} \quad (2.3)$$

This process, is currently known as heave and Equation 2.4 can be used to calculate the critical gradient for heave. If the the water pressure in the soil is less than the critical gradient, safety against heave can be guaranteed.

$$i_c = \frac{\gamma'}{\gamma_w} = \frac{(1 - n)(\gamma_p - \gamma_w)}{\gamma_w} \geq \frac{\phi_o - h_p}{x} \quad (2.4)$$

Where:

- ϕ_o is the piezometric head at the bottom of the seepage screen where the exit gradient is largest [m]
- n is the porosity in the sand layer [-]
- x is the location where the hydraulic gradient of the exit point is largest [m]

2.6. Piping design rules

In this section, the following piping design rules will be discussed; Bligh (1910), Lane (1935), Sellmeijer(2011) together with the adapted Sellmeijer rule (0.3d) and finally the Shields-Darcy (Hoffmans, 2014) design rules.

Bligh (1910)

Bligh's design rule was based on failure of several brick dams constructed on steel foundations, for various earth foundations located in India (Bligh, 1910). These dams were analysed and Bligh came up with the following empirical relation:

$$\Delta H \leq \Delta H_c = \frac{L}{C_{creep}} \quad (2.5)$$

Where:

- H is the hydraulic head [m]
- ΔH_c is the critical hydraulic head difference [m]
- L is the minimum seepage length [m]
- C_{creep} is the creep factor [-]

Bligh's design rule calculates the maximum allowable difference in head over the flood defence structure so that failure due to piping does not occur. Bligh (1910) takes into account both the horizontal and vertical line of creep (seepage length) under a water retaining structure for specific soil types (Bligh, 1910).

Adaptation of Bligh's design rules for Dutch dike design

Once, Bligh's design rule was implemented in the Netherlands, it needed to include a correction for the presence of a blanket layer (Equation 2.6) (Lonsdale, 2001).

$$\Delta H_c \geq \Delta H_e = \Delta H - 0.3 \cdot d \quad (2.6)$$

Where:

- d is the thickness of the blanket later [m]

Lane (1935)

In 1935, Lane investigated 278 brick dams, constructed on different foundations. The goal of the research was to determine the required seepage length in order for piping to not occur. According to Lane, the vertical resistance to seepage was significantly larger than the horizontal resistance to seepage. This was the basis of Lanes' relation, as a result, the horizontal seepage length is reduced by a factor 3 (Equation 2.7) (Lane, 1935). The creep factor used by Lane is also more conservative than the creep factor according to Bligh (Table 2.1). Where the creep factor is defined as the extent to which the subsoil is resistant against washing out (Deltares, 2017a).

$$\Delta H \leq \Delta H_c = \frac{\frac{1}{3}L_h + L_v}{C_{w,creep}} \quad (2.7)$$

Where:

- L_h is the horizontal seepage length [m]
- L_v is the vertical seepage length [m]
- $C_{w,creep}$ is the weighted creep factor [-]

Table 2.1: Overview of the different creep factors for both Bligh and Lane (Förster et al., 2012).

Soil type	Median grain size [mm]	C_{creep} (Bligh)	$C_{w,creep}$ (Lane)
Very fine sand, silt	< 0.105		8.5
Fine sand	0.105 - 0.150	18	
Fine sand (mica)		18	7
Moderately fine sand (quarts)	0.150 - 0.210	15	7
Moderately coarse sand	0.210 - 0.300		6
Very coarse sand	0.300 - 2.00	12	5
Fine gravel	2.0-5.6	9	4
Moderately coarse gravel	5.6 - 16		3.5
Very coarse gravel	> 16	4	3

Sellmeijer (2011)

Currently, the 2011 version of the design rule by Sellmeijer is used in the Netherlands. This rule was based on a mathematical model by Sellmeijer (1988). Over the years, the design rule by Sellmeijer has under gone three main adaptations. A detailed analysis and discussion of these adaptation can be found in chapter 3.

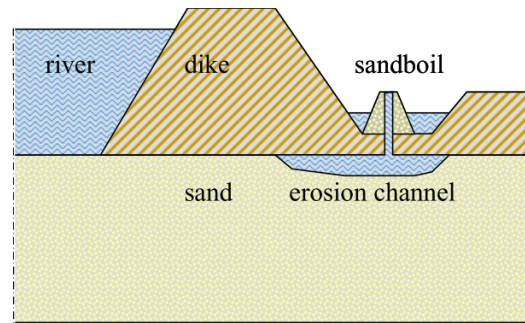


Figure 2.8: A simplified cross section of a dike used by Sellmeijer (Sellmeijer, 2006)

The design rule is used to determine a critical hydraulic gradient for which the progression of a pipe to the upstream side can occur. In the design rule, the soil properties are related to the hydraulic head and a seepage length (Sellmeijer, 1988). The design rule was based on an idealized situation in which the aquifer was assumed to be homogeneous and have a constant thickness (Figure 2.8). At the interface, between the sand and clay layer a completely horizontal boundary was assumed. Later on, variations were accounted for by including a geometry factor in the design rule. The main driving force for piping is groundwater flow as a result of a difference in potential over the dike. The main resistance force is the stability of the sand grains in the piping channel (the weight of the sand grains and the drag force on the grains due to the flow of groundwater) (Sellmeijer and Koenders, 1991). These processes resulted in the resistance factor in the design rule Equation 3.19.

$$\frac{H_c}{L} = F_R F_S F_G \quad (2.8)$$

$$F_R = \eta \frac{\gamma_{p'}}{\gamma_w} \tan \theta \left(\frac{RD}{RD_m} \right)^{0.35} \left(\frac{U}{U_m} \right)^{0.13} \left(\frac{KAS}{KAS_m} \right)^{-0.02} \quad (2.9)$$

$$F_S = \frac{d_{70}}{\sqrt[3]{\kappa L}} \left(\frac{d_{70,m}}{d_{70}} \right)^{0.6} \quad (2.10)$$

$$F_G = 0.91 \left(\frac{D}{L} \right)^{\frac{0.28}{\left(\frac{D}{L} \right)^{2.8} - 1} + 0.04} \quad (2.11)$$

Where:

- γ_p is the volumetric weight of the sand [kN/m³]
- γ_w is the volumetric weight of water [kN/m³]
- θ is the bedding angle [°]
- η is the coefficient of White [-]
- κ is the intrinsic permeability of the piping sensitive sand layer [m²]
- d_{70} is the particle diameter for which 70% passes through a sieve [m]
- d_{70m} mean d_{70} in the small scale tests [m]
- D is the aquifer thickness [m]
- H_c is the critical hydraulic head [m]
- L is the seepage length [m]
- RD is the relative density [-]
- RD_m is the average relative density in small scale tests (0.725) [-]

As can be seen in the above mentioned equations (Equation 2.8, Equation 2.9, Equation 2.10 and Equation 2.11) the design rule by Sellmeijer requires quite a number of different input parameters. These input parameters require a better understanding of the surrounding sub-soil conditions. Once these parameters have been determined (often due to local measurements) the question arises whether or not it is useful and acceptable to apply these conditions for the whole section under a dike, due to the large variation of sub-soil features.

According to the design rules, if the hydraulic gradient present is smaller than the critical hydraulic gradient, a small pipe will form and slowly start to progress to the upstream side (Förster et al., 2012). This pipe will continue to grow until the length of pipe which corresponds to this gradient has formed. Once the pipe has formed, the decrease in concentration of flow lines results in a decrease in flow velocity, as a result, the pipe will stop growing. If the hydraulic head gets increased even further, the pipe will start to grow again. This process will continue if the hydraulic gradient remains below the critical hydraulic gradient. Once the critical hydraulic gradient has been exceeded, the pipe will no longer stop growing and a small canal under the dike will form (Förster et al., 2012). The hydraulic gradient is largely affected by; the length of the flood defence structure compared to the length of the pipe, the permeability of the aquifer, the drag coefficient (Coefficient of White), the diameter of the sand grain and its resistance to rolling. The resulting gradient for which sand grains are still in equilibrium is known as the critical hydraulic head (H_c).

This version of the Sellmeijer design rules accounts for the influence of the relative density on the piping mechanism. According to Knoeff et al. (2009), in laboratory experiments, the occurrence of piping is strongly dependent on the relative density of the sandy aquifer. In the adapted model of Sellmeijer, the influence of the relative density is accounted for by taking the ratio of the relative density in the sandy layer over the average relative density in small scale tests (0.725). The assumption for the method in which the sand grains are transported in the pipe are also slightly adjusted. Previously, it was assumed that the sand grains were only transported through rolling in the pipe. Now, it has been assumed that the grains are not only transported through rolling but also through shearing/translation (van Esch et al., 2012).

Sellmeijer's design rule differs to both that of Bligh (1910) and Lane (1935). Since, the design rule by Sellmeijer is based on theoretical assumptions instead of solely on empiricism (Sellmeijer, 1988). Numerically, the design rule by Sellmeijer is of a similar nature to that of Bligh and Lane. However, the difference between Bligh and Lane compared to Sellmeijer, is the fact that the factors (c , C_{creep} , etc.) which are used to calculate the critical hydraulic gradient are "specified in terms of soil parameters rather than empirical soil classification" (Sellmeijer, 1988). Furthermore, the design formula by Sellmeijer, predicts values for which the structure will fail, meaning that no safety margins are accounted for. In the design rules by Bligh (1910) and Lane (1935), this is not clear, however, according to Sellmeijer (1988), there are indications that the authors meant it to also be that way. However, the design rules by Bligh (1910) and Lane (1935) have been applied successfully in Dutch polders, without considering additional safety coefficients. So according to this, the design rules by Bligh (1910) and Lane (1935) can also be used to predict safe circumstances (instead of failure).

Sellmeijer model (2011): 0.3 rule

The adapted method of Sellmeijer takes into account the reduction in hydraulic head by 0.3 times the thickness of the cover layer. In this way, the resistance created by the fluidized sand grain in the uplift channel can be taken into account (Förster et al., 2012).

$$(\Delta H - 0,3d) \leq \frac{\Delta H_c}{\gamma} \quad (2.12)$$

Where:

d is the thickness of the cover layer [m]

γ is the safety factor 1.2 [-]

Shields-Darcy (2014)

The Shields-Darcy model made by Hoffmans and Van Rijn (2018), is used to approximate the two-dimensional groundwater flow towards a pipe for homogeneous and isotropic sand aquifer (van Beek and Hoffmans, 2017). In this model, the groundwater flow in the sandy layer is schematized by two different zones. **Zone A** which has a thickness D_{ref} close to the pipe is also known as the influence zone (in the area close to the pipe, where there is a dip in the hydraulic gradient). **Zone B** is located at a greater depth, where the hydraulic head is assumed to be unaffected by the flow towards the pipe (van Beek and Hoffmans, 2017). Lastly, Hoffmans (2014) assumes that the flow upstream of the pipe is horizontal, and therefore the gradient upstream of the pipe is constant.

$$\frac{H_c}{L} = S_{pipe,c} + \left(1 - \frac{\ell_c}{L}\right) (S_{sand,c} - S_{pipe,c}) \quad (2.13)$$

Where:

- $S_{pipe,c}$ is the hydraulic pipe gradient [-]
- $S_{sand,c}$ is the hydraulic sand gradient [-]
- ℓ_c is the critical length of the pipe [m]

Both the Sellmeijer and Shields-Darcy model depend only on secondary erosion, and therefore base the progression of the pipe on the critical conditions in the pipe (van Beek and Hoffmans, 2017). However, the Shields-Darcy model, the pipe widens, lengthens and deepens when the average gradient in the pipe increases (exceeds a critical value $S_{pipe,c}$). The progression of the pipe is therefore determined by the equilibrium of particles in the pipe, instead of the erosion of the particles upfront of the pipe (primary erosion) (van Beek and Hoffmans, 2017).

2.7. Factors affecting the critical hydraulic gradient for pipe progression(ΔH_c)

The critical hydraulic gradient for pipe progression is affected by many different factors, the most significant factors will be discussed here.

Exit point location x_{exit}

Often, for situations with a horizontal ground level behind the dike, the location of the exit point is assumed to be located at the inner toe of the dike. If a ditch is present in the hinterland, and this ditch has either a thin clay cover or no cover, piping calculations are done with the exit point located in the ditch. However, for situations where the hinterland consists of uneven ground, the location of the exit point is guessed. For these situations often more, than one piping calculations needs to be done for different locations of the exit point (Förster et al., 2012). If the exit point is located close to the dike, the hydraulic gradient over the dike is larger, than for a situations where the exit point is located further inland.

Entrance point

The entrance point is the location closest to the dike, where the water retaining sandy layer is in direct contact with the water outside in the river, or where the water potential in the sandy layer is equal to the hydraulic head in the river. In order to determine the location of the entrance point, the presence of a clay cover layer needs to be determined. Often the location of the entrance point is assumed to be located at the toe of the outer-side of the dike. If according to this location, uplift occurs of the cover layer on the inside of the dike, a more detailed analysis of the subsoil outside of the dike needs to be done to accurately determine the location of the entrance point. The location of the entrance point in the foreland can result in a significant reduction of the of the potential in the sand layer, reducing the chance of uplift. During this analysis, the permeability of the dike needs to be determined, as well as the use and state of the clay layer needs to be determined (Förster et al., 2012).

Aquifer depth D

According to Robbins and van Beek (2015), the process of backwards erosion is largely influenced by the scale, because of this, laboratory experiments are not directly applicable to practice. With respect to the aquifer depth, if the depth is larger, the area from which the flow originates is also larger and as a result more water will be conveyed towards the pipe head or exit. As a result the flow velocity and gradients near the pipe head will increase with scale, and the critical gradient will decrease with scale.

Inclination of the pipe path

In laboratory experiments, the path which the pipe follows is often schematized as perfectly horizontal and smooth. However, in reality the interface between the cohesive clay layer and the sand layer in neither smooth nor perfectly horizontal. According to van Essen et al. (2014), the critical gradient for pipe progression was found to increase by a factor of 3 for beds with an inclination of 20 degrees.

Permeability of clay layer k

The permeability of the clay layer largely effects the water potential in the sand layer. If the clay has a very high hydraulic conductivity, the entrance point should be located closer to the dike. Downstream of the dike, the permeability of the clay layer also effects the hydraulic gradient in the sand. This effect is translated into a leakage factor. Where the leakage factor describes the distribution of leakage through a aquitard into a leaky layer (clay). The higher the hydraulic conductivity, the steeper the hydraulic gradient in the sand layer.

Relative density RD

The relative density of the aquifer describes the state of the granular structure (Robbins and van Beek, 2015). Dense sand layers can result in an additional strength due to the interlocking of grains and dilatancy. Fluidization of grains is easier in loosely packed soils. Loosely packed beds are also more permeable and as a result, more flow enters the pipe. The increase flow, results in an increase in the drag force of the particles in the pipe resulting in higher erosion rates.

Grain size d

The characteristic grain size of the sand in the aquifer in turn affects the permeability of the sandy layer and in turn also the hydraulic conductivity of the aquifer. Aquifers consisting mainly of finer grains often have a lower hydraulic conductivity, resulting in higher hydraulic gradients. The influence of grain size remains difficult to asses, because a change in grain size is often accompanied by changes in other soil characteristics. However, according to van Beek et al. (2013), the grain size has a significant impact on the critical shear stress required for the onset of grain movement, and is therefore also likely to affect the progression gradient

I

Sellmeijer's design rule

3

Evolution of Sellmeijer's design rule

In the next few sections, the original mathematical model on which the design rules by Sellmeijer are based on will be discussed. Followed by the evolution of his design rules over the years (Figure 3.1). The design rule has been adapted three times. The first adaptation, accounted for the inclusion of the effect of the geometry of the dike profile on the critical hydraulic gradient. Followed by the change from a four-force equilibrium acting on the sand grains in the piping channel to a two-force equilibrium. Finally, the third and last adaptation accounts for the effect of the characteristics of the grains on the critical hydraulic head for pipe progression.

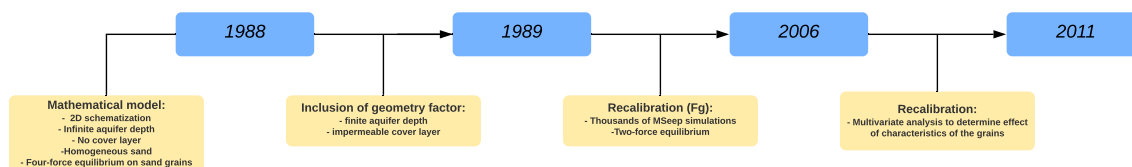


Figure 3.1: Evolution of Sellmeijer's design rule.

3.1. Mathematical model

Over the years, many different experiments have been done to study backwards erosion piping. In these experiments small piping channels or slits have been observed, extending from the downstream corner of the structure slowly extending upstream (Sellmeijer and Koenders, 1991). These channels are formed due to an erosion process initiated by a hydraulic gradient over the sand layer. Once this channel has formed (pipe), the permeability in the channel is much larger than in the surrounding soil, and as a result, the hydraulic gradients which resulted in the initiation of erosion are damped down and an equilibrium situation can be reached. According to Sellmeijer and Koenders (1991) in order to accurately model this effect, the channel must be taken into account in the model.

In 1988, Sellmeijer came up with a mathematical model which can be used to describe the backward erosion piping process under a dike. A two-dimensional approach was taken (Figure 3.2). The structure was assumed to have a horizontal bottom with length L , because of this, the upper boundary of the flow domain is also flat. The length of the sand boil is annotated using the letter b , and the boil together with the piping channel will have a total length l . The piping channel also consists of a vertical slit, this will be known as a . The difference in water level over the structure is annotated with the letter H . Lastly, the subsoil is taken to be homogeneous and have a specific hydraulic conductivity k (Sellmeijer and Koenders, 1991).

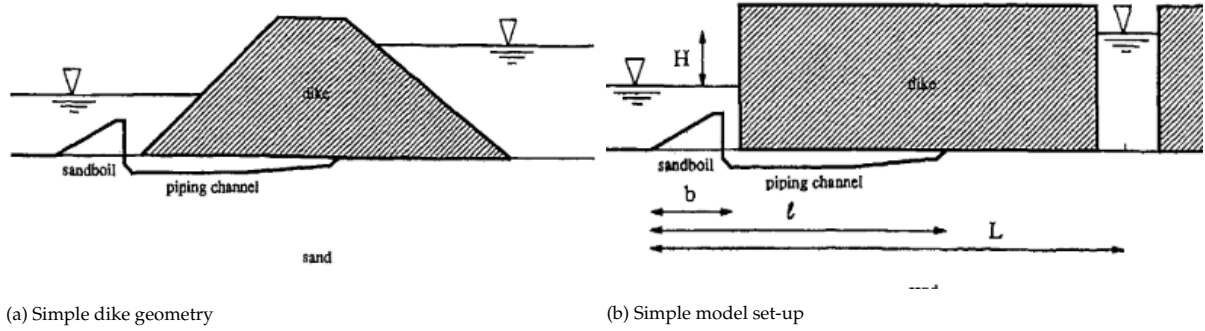


Figure 3.2: A simplified cross section of a dike geometry (Figure 3.2a) on which Sellmeijer based his model schematization (Figure 3.2b).

Figure 3.2a shows the two-dimensional schematization of Sellmeijer's model. The goal of his model was to determine the possible equilibrium situations which could occur without further washing away of dike material. In order to achieve this, an analysis of the forces acting on the grains in the lower edge of the piping channel was done. In his model, Sellmeijer accounts for the groundwater flow problem, for a situation where there is a narrow slit present under a dike. The eroded material, from the slit is deposited downstream of the dike in a sand boil. In order to describe this erosion process at limit equilibrium, a critical shear stress as according to White (1940) was used. White related the equilibrium of forces acting on the grains to the distribution of the load over a group of particles (White, 1940).

$$\frac{\pi a}{3\eta d} \frac{\partial \phi}{\partial x} = \frac{\gamma'_p}{\gamma_w} \frac{\sin(\vartheta + \alpha)}{\cos \vartheta} \quad (3.1)$$

According to Sellmeijer and Koenders (1991), the main problem of the mathematical model was the ability to accurately model the physical behaviour of the eroded material near the downstream corner of the structure. In Sellmeijer's model, the upstream boundary conditions were not assumed to be critical and were adapted for mathematical convenience. The main variable, was the piezometric head (ϕ), which was expressed in equivalent water height. In the subsoil, the piezometric head follows Darcy's Law and the equation of continuity holds resulting in the Laplace equation for two-dimensional groundwater flow (Equation 3.2).

$$\left(\frac{\partial^2}{\partial x^2} + \frac{\partial^2}{\partial y^2} \right) \phi = 0 \quad (3.2)$$

In the piping channel Sellmeijer (1988) assumes a four-force equilibrium acting on the sand grains. Sellmeijer accounted for a drag force, a horizontal and vertical force due to (horizontal and vertical) seepage gradients and lastly the weight of the particle. In his mathematical model, at the upstream boundary the potential in the sand layer is equal to the potential in the water. This implies that the sand layer is in direct contact with the water. Downstream, at the location of the exit point, the potential in the sand is equal to, either the water level downstream or for the case of a dike often equal to the polder level (or the water level in the ditch). These boundary conditions, which are based on the theory by Verruijt (1970) (Figure 3.3b) are further explained below (Figure 3.3a):

- $0 \leq x < l, y = 0$ The piezometric head satisfies a function $F(\partial\phi/\partial x, \partial\phi/\partial y, \phi) = 0$
- $x = 0$ the pressure has a fixed value $\phi = \phi_0$ (often equal to 0 m N.A.P)
- $x = l, y = 0$ The impermeability condition is imposed and the vertical discharge vanishes ($\partial\phi/\partial y = 0$)
- $x = L$ The piezometric head is fixed and equal to H

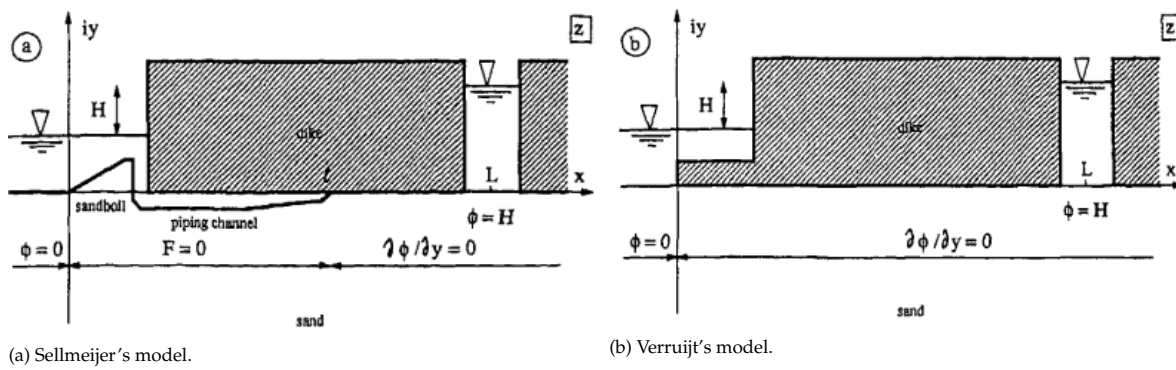


Figure 3.3: Boundary conditions imposed a) Sellmeijers mathematical model Sellmeijer and Koenders (1991) b) according to Verruijt (1970).

In Sellmeijer's mathematical model, he accounts for a limit equilibrium in both the sand boil and the piping channel (Sellmeijer and Koenders, 1991). He also assumes steady laminar flow through the slit and assumes that the erosion is concentrated in the piping channel under the structure (confining layer) (Sellmeijer et al., 1989). Lastly, Sellmeijer also accounts for the resistance created by the geometry of the sand boil and slit at the downstream side of the structure. As a result, the model was based on mathematical descriptions of three processes (Sellmeijer and Koenders, 1991):

1. An analytical solution for the groundwater flow towards the lee side of the dike and to the slit.
2. An analytical description of the flow through that slit.
3. An analytical description of the stability of the grains at the bottom of the slit.

In the next section, Sellmeijers' original design rule will be discussed. His rule is a simplification of his described mathematical model and accounts for the same three processes as mentioned above.

3.2. Original design rule (1988)

In 1988, Sellmeijer used the technique of curve fitting and came up with a design rule (Equation 3.4) (Sellmeijer, 1988), in which the difference in water head over the structure and the length of the slit were coupled. In this version of his design rule, he assumes that the sand layer has an infinite thickness and that no cover layer is present (Weijers and Sellmeijer, 1993). In his analysis, Sellmeijer found that all variables can be grouped into meaningful clusters:

$$\frac{H_c}{L} = \frac{H}{L} \left(\frac{l}{L}; \frac{\kappa}{d^2}; \frac{d}{L}; \Phi, \theta, C, \eta, \frac{\gamma'_p}{\gamma'_w}, \frac{\gamma'_s}{\gamma'_w} \right) \quad (3.3)$$

Where:

- C is the surface factor [-]
- d is the particle diameter [m]
- H is the hydraulic head across the structure [m]
- H_c is the critical hydraulic head across the structure [m]
- l is the erosion length [m]
- L is the structure length [m]
- γ'_p is the submerged unit weight of particles [kN/m^3]
- γ'_s is the (apparent) volumetric weight of sand grains under water [kN/m^3]
- γ'_w is the volumetric weight of water [kN/m^3]
- η is the coefficient of White ($\eta = 0.25$) [-]
- θ is the bedding angle ($\theta = 41^\circ$ according to TAW 1999, Sellmeijer argues $\theta = 39^\circ$) [$^\circ$]
- κ is the intrinsic permeability [m^2]
- Φ is the piezometric head in the slit [m]

H/L is a design quantity of the structure, and it is a function of a number of different variables. All the remaining variables, except for l/L are characteristics of either the soil or the groundwater. Figure 3.4 shows the value of H/L as a function of l/L (ratio between the length of the piping channel

and the length of the structure). According to observations done by Sellmeijer and Koenders (1991) of the piping experiments, H/L is often at a maximum when l/L roughly equals $\frac{1}{2}$. For situations when the piping channel is shorter than half the structure length (L), small variations in water level will lead to small variations in slit length. This is because for $l/L < 0.5$, equilibrium in the slit is assumed to be present. However, if $l/L > 0.5$ an increase in water level would require a shortening of the slit length. Yet, this is impossible, since slit formation is irreversible. Therefore, the maximum values of the curves in Figure 3.4 represent the critical design values. These maxima are expressed in the following design formulas (Equation 3.4, Equation 3.5). These formulas were obtained by curve fitting, and summarizing many calculations for a large variation of soil parameters (Sellmeijer and Koenders, 1991). According to Sellmeijer and Koenders (1991), the parameters of the sand boil do not significantly affect the maximum H/L ratio.

$$\frac{H_c}{L} = c \frac{\gamma'_p}{\gamma_w} \tan \theta (1 - 0.65c^{0.42}) \quad (3.4)$$

With:

$$c = \frac{1}{4} \pi \eta^3 \sqrt{\frac{d^2}{\kappa} \frac{d}{\frac{1}{2}L}} \quad (3.5)$$

Where:

c is the cluster of soil parameters [-]

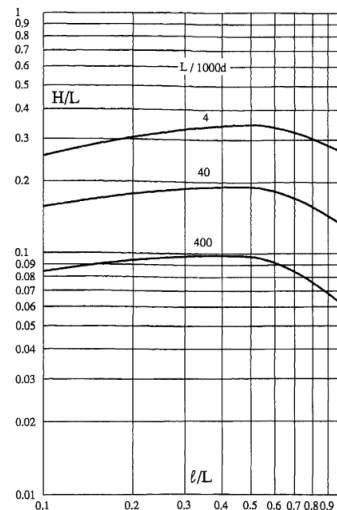


Figure 3.4: Hydraulic head versus erosion length of the pipe (Sellmeijer and Koenders, 1991).

In Sellmeijer's design rule, he uses a representative particle diameter between d_{65} and d_{75} , because, finer particles are more mobile and can be easily transported compared to larger particles (Sellmeijer, 1988). As a result, the larger grains in the pipe determine the resistance in the pipe and are therefore the limiting factor of the erosion process.

In order for the design rule to be applied, first uplift and heave have to occur. In this model, an equilibrium of four forces is assumed, since the sand grain is strongly embedded in the bed. The four forces which are acting on the sand grain are; the weight of the sand grain, the drag force, the horizontal seepage force and the vertical seepage force (Sellmeijer, 1988).

3.3. Addition of geometry factor (1989)

The original design rule had two major shortcomings (Sellmeijer et al., 1989). The first shortcoming was that in Sellmeijer's mathematical model, the presence of an impervious cover layer was unac-

counted for and as a result a simple but conservative upstream boundary condition was applied. The second short coming was that in the model, the aquifer was assumed to have an infinite depth. These restrictions were assumed to significantly affect the flow pattern in the aquifer and in turn affect the development of the pipe.

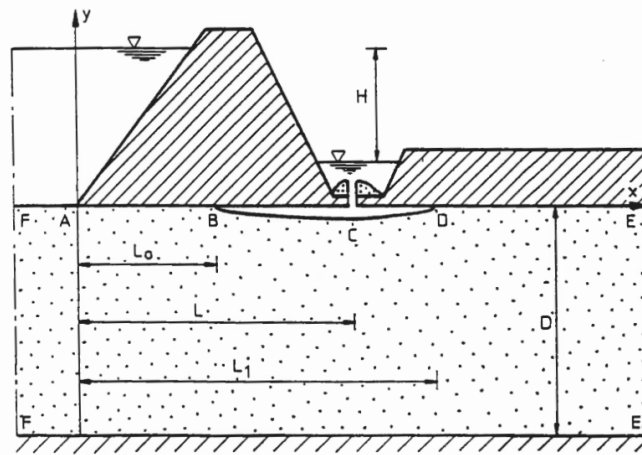


Figure 3.5: Modified geometry of a dike used by Sellmeijer et al. (1989).

In 1989, Sellmeijer's mathematical model was enhanced by introducing a more realistic approach of the geometry (Figure 3.5). Now a finite thickness of the subsoil was included as well as a cover layer on the lee side of the dike (Weijers and Sellmeijer, 1993). The following boundary conditions were now applied (Figure 3.5) to the mathematical model (Sellmeijer et al., 1989):

- F-A The head is constant ($\partial\phi/\partial x = 0$).
- A-B A impermeability condition is imposed and the vertical discharge vanishes ($\partial\phi/\partial y = 0$).
- D-E-E-F A impermeability condition is imposed and the vertical discharge vanishes ($\partial\phi/\partial y = 0$).
- B-C-D The sand is in a state of limit equilibrium.

Next a large number of simulations were done with the above mentioned boundary conditions, for certain soil characteristics and geometries. Quantitative results of the computer model could have been used as an input for the design rule, however this was very time consuming. The choice was made to derive an approximate solution. Observations of the model output (showing H vs L, accounting for different D/L ratios) shows that the positions of a group of curves (H vs. L) with the same soil properties depends on the aquifer thickness alone (Figure 3.6) (Sellmeijer et al., 1989).

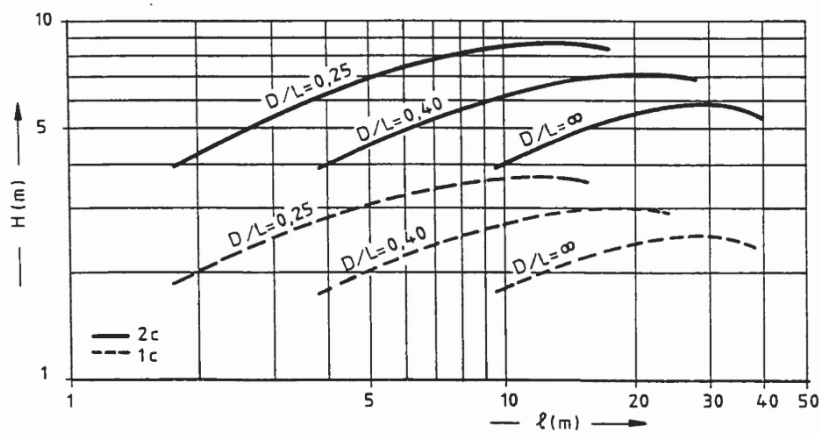


Figure 3.6: Relation between the hydraulic head and slit length (Sellmeijer et al., 1989).

Curve fitting has been applied once again resulting in the following factor:

$$\alpha = \left(\frac{D}{L}\right) \frac{0.28}{\left(\frac{D}{L}\right)^{2.8} - 1} \quad (3.6)$$

This adaptation in the boundary conditions also resulted in a slight change in the cluster of soil parameters c (Sellmeijer et al., 1989):

$$c = \eta \sqrt[3]{\frac{d^3}{\kappa L}} \quad (3.7)$$

According to Sellmeijer et al. (1989), by accounting for a cover layer and a limited but constant aquifer depth, there was an improvement in describing more realistic situations. This addition significantly reduced the risk of piping and resulted in the following design formula:

$$\frac{H_c}{L} = \alpha c \frac{\gamma_{p'}}{\gamma_w} \tan \theta (0.68 - 0.1 \ln c) \quad (3.8)$$

$$c = \eta \sqrt[3]{\frac{d^3}{\kappa L}} \quad (3.9)$$

$$\alpha = \left(\frac{D}{L}\right) \frac{0.28}{\left(\frac{D}{L}\right)^{2.8} - 1} \quad (3.10)$$

Where:

α is the geometry factor [m]

3.4. Two-force equilibrium (2006)

Since the goal of the design rule was to determine sand transport at limit equilibrium a two-force equilibrium should be used instead of the four-force equilibrium (van Esch, 2015). According to Sellmeijer (2006), for heterogeneous mixtures in steady state, a distribution of the grains was seen where the large grains stick out and the small grains are well buried. Between these larger grains, large open spaces exist. As a result, the forces due to a seepage gradient do not effect these grains at the top of the interface (Sellmeijer et al., 2011). Therefore, the four-force equilibrium became a two-force equilibrium and the two forces which are taken into account are the gravitational force and the drag force, neglecting the forces due to the vertical and horizontal hydraulic gradients (Figure 3.7)(van Esch, 2015). The model follows the assumption that the grains are at rest (immobile) if the drag force is less than the counteracting gravitational force. This is indeed the case when the shear stress exerted by the water is less than the critical shear stress (τ_c)(van Esch et al., 2012).

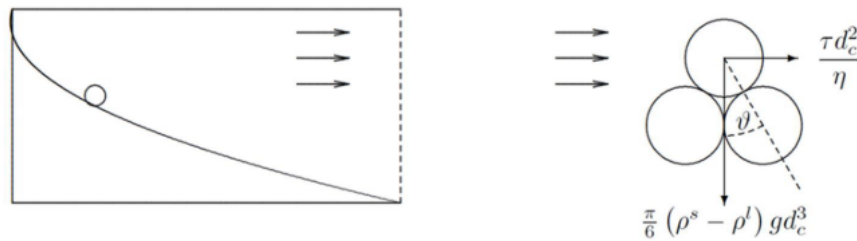


Figure 3.7: Grain equilibrium according to Sellmeijer, where the sand grains area already sticking out of the bed (van Esch, 2015),(Sellmeijer, 1988).

This transition from a four-force to a two-force equilibrium, together with the recalibration of Sellmeijer's design rule with the use of thousands of MSeep calculations, has been accounted for in the

geometry factor of the design rule (Sellmeijer et al., 2011)(van Beek and Hoffmans, 2017). Transitioning from:

$$F_G = \{0.68 - 0.1 \ln(\eta F_S)\} \left(\frac{D}{L}\right)^{\frac{0.28}{\left(\frac{D}{L}\right)^{2.8} - 1}} \quad (3.11)$$

to

$$F_G = 0.91 \left(\frac{D}{L}\right)^{\frac{0.28}{\left(\frac{D}{L}\right)^{2.8} - 1} + 0.04} \quad (3.12)$$

Where according to (Sellmeijer et al., 2011):

θ is the bedding angle ($\theta = 37^\circ$) [$^\circ$]

The Sellmeijer design rule now also has a different form and consist of three different factors: the resistance term (F_R , Equation 3.14), the scale term (F_S , Equation 3.15) and the geometry term (F_G , Equation 3.16).

$$\frac{H_c}{L} = F_R F_S F_G \quad (3.13)$$

$$F_R = \eta \frac{\gamma'_p}{\gamma_w} \tan \theta \quad (3.14)$$

$$F_S = \frac{d_{70}}{\sqrt[3]{\kappa L}} \quad (3.15)$$

$$F_G = 0.91 \left(\frac{D}{L}\right)^{\frac{0.28}{\left(\frac{D}{L}\right)^{2.8} - 1} + 0.04} \quad (3.16)$$

In the 2006 version of Sellmeijer's design rule, the grain size (d) has transitions to the (d_{70}) (TAW, 2004).

3.5. Recalibration accounting for characteristics of the grains(2011)

In 2011, a multivariate analysis was done on small-scale tests, where different material properties were varied. The following variables were used in the analysis; the relative density (RD), uniformity (U), the angularity (KAS), permeability (k) and the grain size (d_{70}) (Sellmeijer et al., 2011). The multivariate analysis linearises the influence of the involved variables. In order for the results to become independent of the variable dimensions, the data is transformed into a logarithmic domain, producing weights rather than coefficients. The multivariate approach on the small-scale tests can be formulated as:

$$\frac{H_c}{L} = \left(\frac{H}{L}\right)_m \exp(\beta_0) \left(\frac{RD}{RD_m}\right)^{\beta_{RD}} \left(\frac{U}{U_m}\right)^{\beta_U} \left(\frac{KAS}{KAS_m}\right)^{\beta_{KAS}} \left(\frac{\kappa}{\kappa_m}\right)^{\beta_\kappa} \left(\frac{d_{70}}{d_{70m}}\right)^{\beta_{d/2}} \quad (3.17)$$

The results of this analysis can be seen in Table 3.1. The influence of each factor on the critical head can be seen. Negative factors indicate that the variable is inversely proportional.

Table 3.1: Multivariate regression factors (Sellmeijer et al., 2011).

	RD	κ	d_{70}	U	KAS	fitting
β	0.35	-0.35	0.40	0.13	-0.02	-0.079

By combining the piping rule with the results of the multivariate analysis, the design rule for piping can be written as:

$$\frac{H}{L} = F_R F_S F_G \quad (3.18)$$

$$F_R = \eta \frac{\gamma_{p'}}{\gamma_w} \tan \theta \left(\frac{RD}{RD_m}\right)^{0.35} \left(\frac{U}{U_m}\right)^{0.13} \left(\frac{KAS}{KAS_m}\right)^{-0.02} \quad (3.19)$$

$$F_S = \frac{d_{70}}{\sqrt[3]{\kappa L}} \left(\frac{d_{70,m}}{d_{70}} \right)^{0.6} \quad (3.20)$$

$$F_G = 0.91 \left(\frac{D}{L} \right) \left(\frac{D}{L} \right)^{\frac{0.28}{2.8-1} + 0.04} \quad (3.21)$$

The test results refer to the small-scale tests. It is not yet clear if for large structures less prominent effects may occur (Sellmeijer et al., 2011). The newly adapted piping rule may only be applied within the limits of the involved parameters during testing. The limits of the design rule are found in Table 3.2

Table 3.2: Parameter limits (Sellmeijer et al., 2011).

Parameter	Minimum	Maximum	Mean
<i>RD</i>	50 %	100 %	72.5 %
<i>U</i>	1.3	2.6	1.81
<i>KAS</i>	35 %	70 %	29.9 %
<i>d</i> ₇₀	150 μm	420 μm	208 μm

The new rule was used to predict the large scale IJkdijk tests. For fine sand, the rule was able to predict the outcome of that large scale tests well (Sellmeijer et al., 2011). Unfortunately, for coarse sand, only one test was carried out and for this test a difference of 25 % was observed between the prediction and observations.

3.6. Discussion

In this section, the different advantages and disadvantages of Sellmeijer's design rule are discussed. First the advantages of Sellmeijer's model will be discussed. One of the advantages of Sellmeijer's design rule compared to other methods which have been used to determine the critical hydraulic head for which progression of a pipe occurs is that Sellmeijer's model was based on theory. While the models by both Bligh and Lane were only based on empiricism (Sellmeijer, 1988). Sellmeijer's design rule is based on a theoretical model in which he attempts to describe three different processes (Sellmeijer and Koenders, 1991):

1. An analytical solution for the groundwater flow towards the lee side of dike and to the slit.
2. An analytical description of the groundwater flow through the slit
3. An analytical description of the stability of the grains at the bottom of the slit.

The inclusion of the geometry factor has significantly impacted and improved the results of the design rule as it has increased the range of applicability significantly for dikes in the Netherlands. By limiting the depth of the aquifer, a more realistic flow pattern of the groundwater in the aquifer can be modelled as well as a more realistic assumption from where the water flowing towards the pipe originates from.

Sellmeijer's design rule accounts for site specific conditions when calculating the seepage length. This makes the model adjustable to specific locations as well as flexible (within the range for which it has been derived) (Calle et al., 1989).

The transition from a four-force equilibrium to a two-force equilibrium attempts to account for the effect of a heterogeneous sand mixture. By limiting the forces acting on the sand grains in the channel to the gravity force and the drag force (Sellmeijer et al., 2011). Thus improving the applicability, since in reality, no sand is homogeneous.

Unfortunately, the theoretical model also has quite some limitations, one of the main limitations is that it can only be applied to scenarios which match the two-dimensional seepage conditions considered, when deriving the model (Robbins and van Beek, 2015). The aquifer is assumed to have a constant thickness and hydraulic conductivity, and the boundary between the aquifer and the confining layer is completely horizontal. While in reality the thickness of the aquifer and the hydraulic conductivity can vary significantly. However, more difficult scenarios can be modelled with the use of finite element models such as MSeep or D-GeoFlow. Both of these models contain a piping module.

As was discussed earlier, the design rule has been adapted three times, each adaptation has resulted in a design rule which better describes the piping process in two-dimensions. Unfortunately, each adaptation fails to account for the three-dimensional nature of the piping process. In three dimensional experiments, the meandering nature of the pipe has been observed as well as critical hydraulic gradients significantly lower (factor two lower) than the predicted critical hydraulic gradients (van Beek and Hoffmans, 2017). This difference in hydraulic gradient can be due to the fact that groundwater flow in the third dimension has been unaccounted for (Figure 3.8).

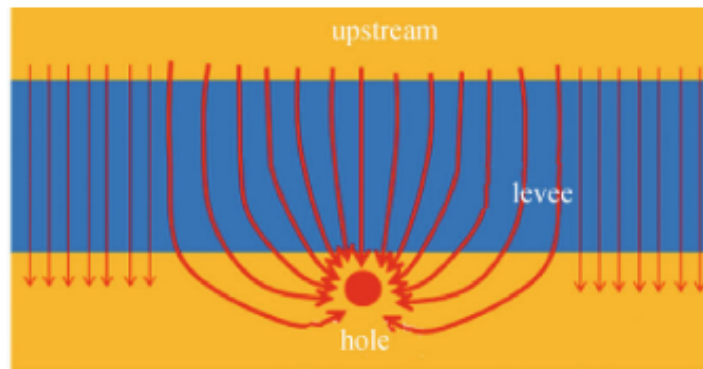


Figure 3.8: Schematic drawing showing lateral groundwater flow towards x_{exit} (Vandenboer et al., 2014)

The meandering nature of the pipe is significantly influenced by the local characteristics of the sand and the spatial variability of the different sand types (heterogeneity). How the heterogeneity effects the meandering nature of the pipe is unaccounted for. Since, Sellmeijer assumes that the sand mixture in the aquifer is homogeneous. However, in later versions of his design rule, Sellmeijer has made a transition from a four-force equilibrium acting on the sand grains to a two-force equilibrium acting on the sand grains. According to (Sellmeijer, 2006), this transitions accounts for the influence of heterogeneity on the initiation of motion of the sand grains in the piping channel and that for heterogeneous mixtures, there are no seepage forces acting on the sand grains.

While deriving the geometry factor in 1989, Sellmeijer assumed that an impermeable cover layer was present in the hinterland. He accounted for this in his mathematical model by assuming that there is no vertical discharge through the cover layer. Often, this is not the case, and the cover layer consists of a semi-permeable (leaky) layer which allows vertical discharge. This leakage is often accounted for with the use of the leakage factor and accounts for the difference in hydraulic conductivity between the aquifer and the cover layer and the thickness of these layers.

As a result of the models adjust-ability and flexibility, a larger number of soil parameters need to be known. These soil parameters are often difficult to estimate, and as a result, substantial uncertainty can be involved. This uncertainty will also be present in the results of the calculation (Calle et al., 1989), since the results are very sensitive to these input parameters: grain size (d_{70}) and hydraulic conductivity (k) (Robbins and van Beek, 2015).

Lastly, in Sellmeijer's theoretical model, he assumes laminar flow in the pipe, which is the case for fine sand. However, for coarse sand the assumption of laminar flow no longer holds, the flow in the slit is instead turbulent (Weijers and Sellmeijer, 1993). Limiting the range of applicability of Sellmeijer's design rule.

3.7. Conclusions

Currently, the 2011 version of Sellmeijer's design rule is the most advanced and widely used tool in the Netherlands to design against backwards erosion piping. Even though his design rule has a number of different shortcomings. The most significant shortcoming is that a two-dimensional model has been used to describe a three-dimensional problem. However, since the three-dimensionality of the piping process is very location specific, due to the heterogeneity of the subsoil. Accounting for this will remain very difficult. A second limitation of Sellmeijer's design rule is that Sellmeijer does not

accounting for the effect of leakage on the piping process. In his model he assumes that the cover layer is impermeable. However, this is often not the case, since the cover layer is made of clay therefore is often semi-permeable. The effect of leakage on the piping process will be determined in Part II of this report.

4

Sensitivity Analysis

In this chapter, a sensitivity analysis is done for the four different versions of Sellmeijer's design rule (1999, 1989, 2006 and 2011). The goal of the sensitivity analysis is to see which parameters significantly effect the critical hydraulic head for pipe progression and how this varies for the different versions of the design rules. For each of the four versions, the following six parameters are varied:

1. The thickness of the aquifer (D)
2. The seepage length (L)
3. The characteristic grain size (d_{70})
4. The hydraulic conductivity (k)
5. The bedding angle (θ)
6. Coefficient of White (η)

For every parameter, the influence on the critical hydraulic head is compared to a base case, so that a relative change can be quantified. The base case has the following input values; the seepage length is 18 m, the thickness of the aquifer is 15 m, the hydraulic conductivity of the sandy layer is 1.5 E-4 m/s, the characteristic grain size (d_{70}) is equal to 200 μm , the bedding angle is equal to 37° and the Coefficient of White which is used is equal to 0.25. The calculations results of the base case using the different versions of the design rule can be found in Table 4.1.

Table 4.1: Results of the different design rules for the base case.

Design rule	Sellmeijer 1988	Sellmeijer 1989	Sellmeijer 2006	Sellmeijer 2011
H_c	1.37 m	1.90 m	1.85 m	2.16 m

As can be seen, in Table 4.1, the different versions of the design rule results in significantly different results. The difference between the 1989 and 2006 version is the smallest. The difference between these two formulas was also the least significant, namely from a four-force equilibrium to a two-force equilibrium acting on the sand grains. These results will be used as a base case to which all of the other calculations will be compared.

In the next few sections the influence of the different parameters will be discussed. In each section, only one parameter will be varied. This is done so that the effect of changing a specific parameter can be determined for the various versions of the design rule. In order to do this, both the relative change in the critical hydraulic head, as well as the relative change in the parameter is compared to the base case.

4.1. Aquifer thickness (D)

The first parameter which will be varied is the thickness of the aquifer. Calculations are done using the four different versions of the design rule, for a larger variation in aquifer thickness's. Each calculation is compared to the base case with an aquifer depth of 15 metres. In Figure 4.1, the relative change in the

critical hydraulic head is plotted on the vertical axis and the relative change in thickness of the aquifer is plotted on the horizontal axis. Figure 4.1, shows that for the 1988 version of Sellmeijer's design rule, the critical hydraulic gradient is not effected by the aquifer depth. This is because, for this version of the design rule, the geometry of the dike and aquifer were not taken into account. In the 1988 version of the design rule, Sellmeijer assumes that the aquifer has an infinite depth and therefore a change in aquifer depth should not affect the calculation, which is indeed the case.

In the later three versions of his design rule, Sellmeijer does account for the effect of the geometry of the aquifer. For these three versions, it can be observed that an increase in aquifer thickness will result in a decrease in the critical hydraulic gradient (ΔH_c). These results are in accordance with the conclusions drawn by Robbins and van Beek (2015), whom agrues that for a larger aquifer depth, the area from which the flow originates is also larger, and as a result, more water will be conveyed towards the pipe or exit. This in turn results in higher flow velocities and larger gradients near the pipe head (Robbins and van Beek, 2015).

In Figure 4.1, an outlier can be observed, this value is for calculations where the thickness of the aquifer is equal to the seepage length. This is because in python, the design rule is still solved, while in actuality this should not be the case. For simulations where this ratio is larger than 1, the critical hydraulic head continues to decrease tending towards a minimum value.

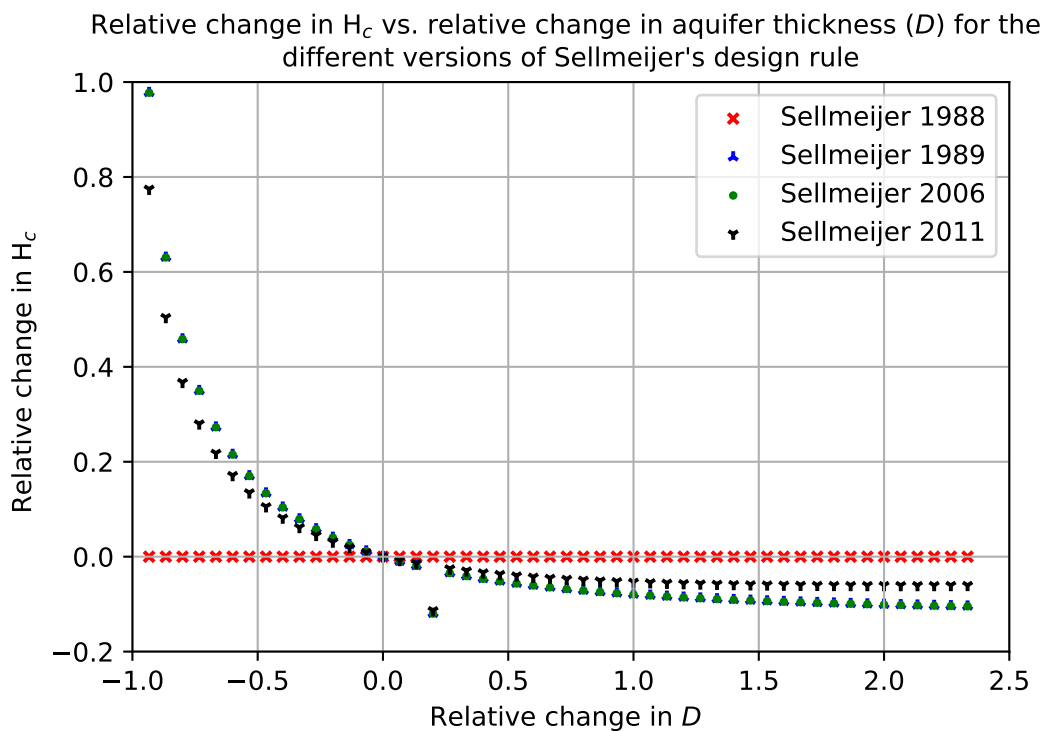


Figure 4.1: Relative change in the critical hydraulic head calculation for varying aquifer thickness.

4.2. Seepage length (L)

The second parameter which is varied is the seepage length (L). A large number of calculations are done for various seepage lengths, each calculation is compared to the base seepage length of 18 metres. As can be seen in Figure 4.2, all version of the design rule are effected by the seepage length. In the original version of the design rule (Sellmeijr 1988), the seepage length is accounted for in both the scale term as well as in the general form of the equation to determine the the maximum allowable hydraulic head. The original version of the design rule shows that there was a limited effect on the critical hydraulic head for a larger seepage length. Where as for the other three versions of the design rule, a nearly linear increase can be seen.

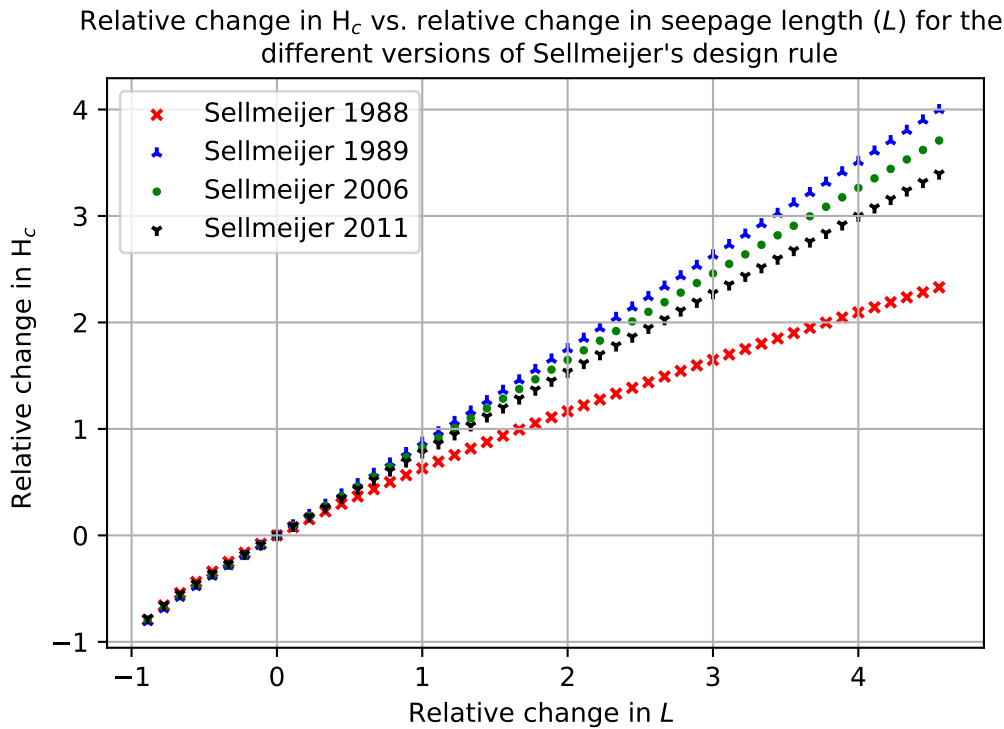


Figure 4.2: Relative change in the critical hydraulic head calculations for varying seepage lengths

The last three versions of the design rule (accounting for the geometry of the structure), show that the seepage length significantly effects the critical hydraulic gradient for pipe progression. The longer the seepage length the higher the gradient can be over the structure. This is because for longer structure lengths, the difference in head needs to be larger to achieve the same gradient in potential in the sand layer. This gradient affects the flow velocities in the sandy layer and therefore also the piping process.

4.3. Characteristic grain size (d_{70})

In this section, the characteristic grain size is varied between 10 to 400 μm . For smaller grain sizes, it can be seen than failure due to piping will occur for a much lower critical hydraulic gradient, than compared to larger grain sizes (Figure 4.3). Difference in grain size, has a significant impact on the critical shear stress required for the onset of grain movement, and is therefore also likely to affect the gradient for which the pipe progresses (van Beek et al., 2013).

The first two versions of the design rule (1988 and 1989) are based on the four-force equilibrium assumption acting on the sand grains and assumes that the sand mixture is homogeneous (Sellmeijer, 1988). The last two version of the design rule (2006 and 2011) are based on the assumption that the sand mixture is heterogeneous, and therefore follow the two-force equilibrium assumption. The earlier three versions of Sellmeijer's design rule behave nearly linear. Yet for the 2006 version of Sellmeijer's design rule a slightly steeper gradient can be observed. An increase in the critical hydraulic head is most likely a result of the transition from a four force equilibrium to a two-force equilibrium acting on the sand grains. Lastly, it can be seen that the 2011 version of Sellmeijer's design rule follows a different trend, and appears to tend towards a maximum. In this version of the design rule, the characteristics of the grains were included.

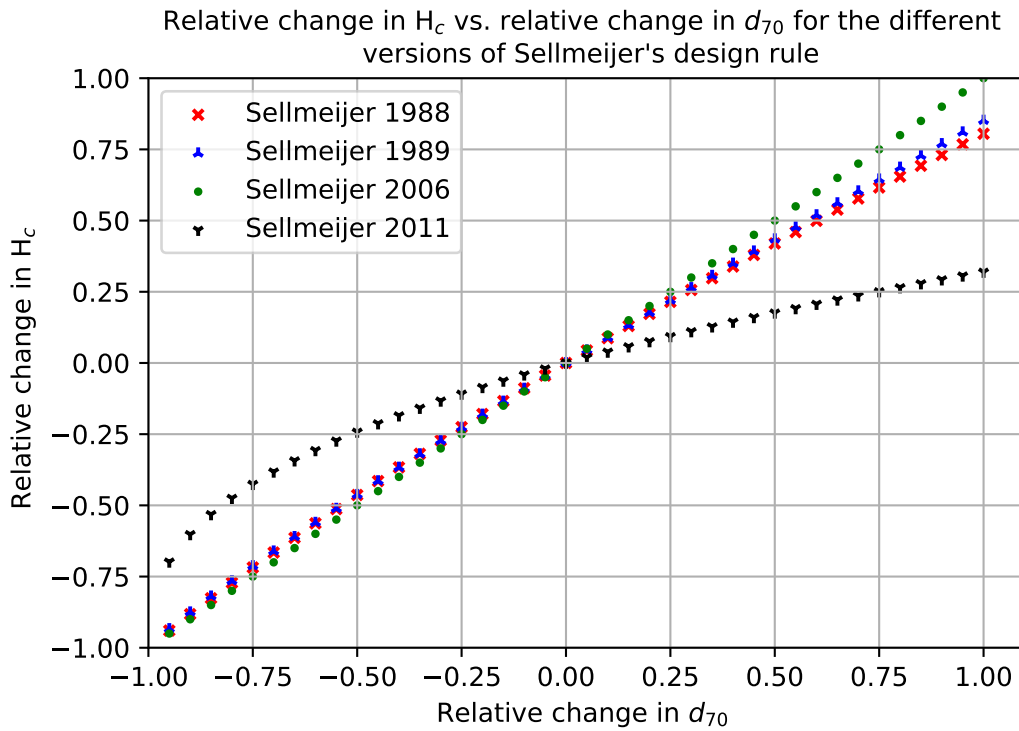


Figure 4.3: Relative change in the critical hydraulic head calculation for varying characteristic grain sizes

According to Weijers and Sellmeijer (1993), Sellmeijer's design rules are unable to accurately predict the critical hydraulic head for coarse sand. Since the design rules are based on a mathematical model which assumes that the flow in the slit is laminar. However, for coarse grains this assumption no longer holds and the flow in the slit is turbulent. This increase in variation between the four versions of the design rule for larger grain sizes (≥ 0.5) is also seen.

4.4. Hydraulic conductivity (k)

Calculations were done for values of the hydraulic conductivity ranging between 0.5 E-4 to 2.5 E-4 m/s. Figure 4.4 shows that an increase in the hydraulic conductivity results in a decrease in the critical hydraulic head for pipe progression. However, in reality, an increase in the hydraulic conductivity is often paired with an increase in grain size. Therefore, in order to have an accurate representation of the effect of a changing hydraulic conductivity on the critical hydraulic gradient, combinations should be modelled for sand mixtures with specific grain sizes and their corresponding hydraulic conductivity.

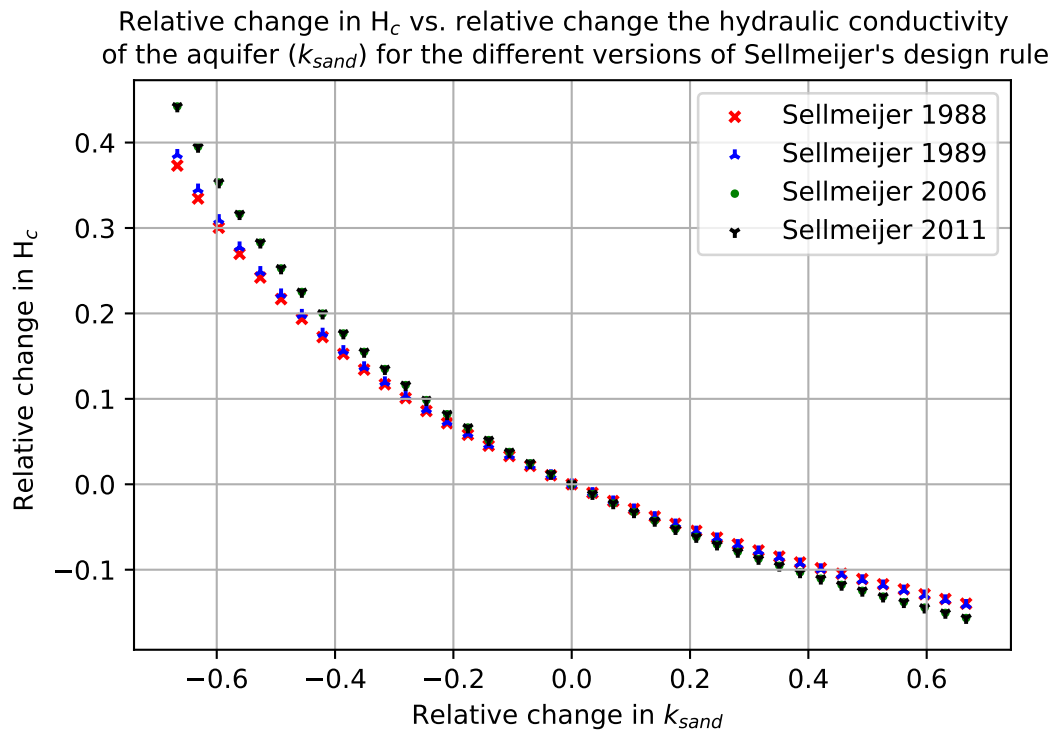


Figure 4.4: Relative change in the critical hydraulic head calculations for varying hydraulic conductivities of the sand layer

4.5. Bedding angle (θ)

Over the years, a number of different values have been suggested by both Sellmeijer and the TAW 1999 for the bedding angle. The most recent version of the Sellmeijer design rule uses a bedding angle of 37 degrees, while the older versions use 39 or 41 degrees. Therefore, the choice is made to model the effect of a bedding angle ranging between 30 and 51 degrees on the critical hydraulic gradient.

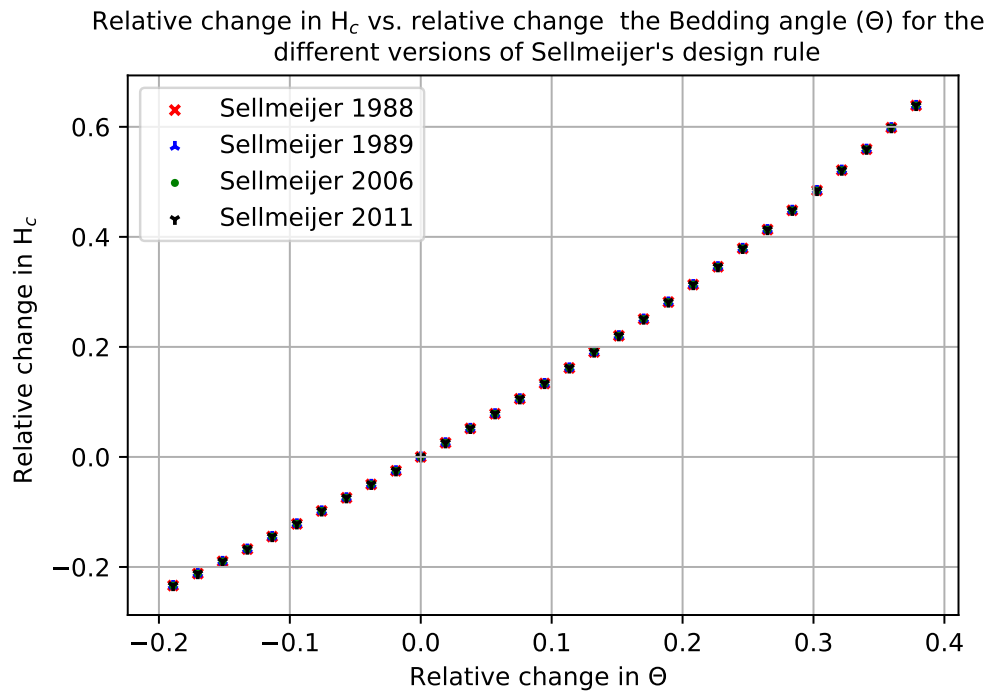


Figure 4.5: Relative change in the critical hydraulic head calculations for varying values for the Bedding angle

For all of the different versions of the design rule, it can be observed (Figure 4.5) that an increase in the bedding angle results in an increase in the critical hydraulic gradient. Very small differences between the four versions of the design rule are observed.

4.6. Coefficient of White (η)

The effect of the coefficient of White on the critical hydraulic head is also investigated. An increase in the coefficient of White (an increase in the drag factor) results in an increase in the hydraulic head.

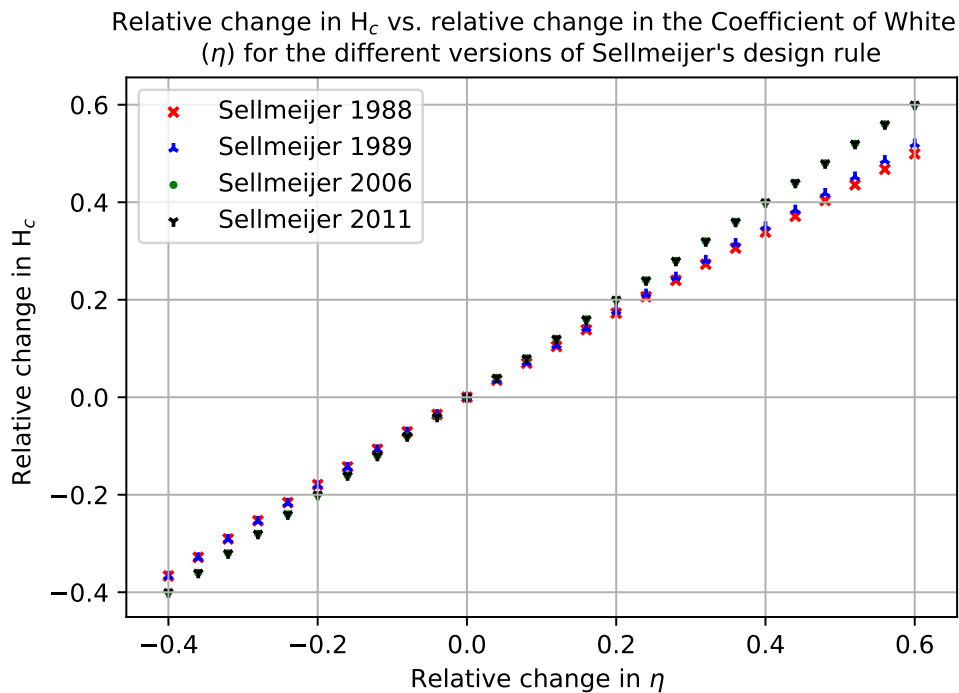


Figure 4.6: Relative change in the critical hydraulic head calculations for varying values for the Coefficient of White

All of the versions have a similar pattern, however the main difference which can be observed is between the four-force equilibrium and the two-force equilibrium acting on the sand grains. This can be seen in the difference in the results between the earlier two versions (1988 and 1989) with the later two versions (2006 and 2011)

4.7. Conclusions

There are four parameters which significantly effect the critical hydraulic head. They are; the seepage length, the thickness of the aquifer, the characteristic grain size and the hydraulic conductivity. A change in the seepage length resulted in the largest change in the critical hydraulic gradient.

As was mentioned earlier, the hydraulic conductivity and the characteristic grain size both significantly effect the critical hydraulic head. However, these two factors are coupled, and increase in the grain size will likely result in an increase in the hydraulic conductivity. However, an increase in the grain size will positively influence the critical gradient. While an increase in the hydraulic conductivity will negatively influence the critical gradient. How this coupling of the parameters effects the critical hydraulic gradient will not be studied.

Of the six studied parameters, only one of them can be impacted directly by mitigation measures. This is the seepage length, increasing the seepage length is relatively easy compared to changing the thickness of the aquifer or the characteristics of the sand. Therefore by slightly increasing the seepage length, depending on the D/L ratio, a large impact can be made in increasing the critical hydraulic gradient for pipe progression.

5

Simulations vs. Experimental data

In this chapter, a comparison will be made between the results of the large scale piping experiments done by Silvis, the results of simulations done in MSeep (2D groundwater model) and the results of the 2006 version of Sellmeijer's design rule. This is done to determine, how the results of both the MSeep simulations and the design rule compare to the experimental results.

Over the years, a number of different small, medium and large-scale experiments have been done to investigate the piping phenomenon. However, only one large scale piping experiment (Silvis, 1991) uses MSeep in predicting the expected critical hydraulic head. MSeep is a two dimensional groundwater model, in which an erosion tool has been included which uses the 2006 version of Sellmeijer's design rule. Further information on MSeep can be found in Appendix A.

First the results of the Delta Flume experiments done by Silvis in 1991 will be discussed. Next an attempt will be made to replicate the MSeep model results. Followed by an analysis of the design rule and the MSeep simulations in predicting the experiments done by Silvis.

5.1. Delta Flume experiments: Silvis (1991)

In 1991, large-scale experiments were done in the Delta Flume. These experiments were done to validate the adapted Sellmeijer design rule (Sellmeijer 1989). Three different experiments were done. Each of these three experiments had different seepage lengths; 6 metres (test T4), 9 metres (test T2) and 12 metres (test T3). For all three of the experiments, the thickness of the sand layer is assumed to be constant. The foundation of the dike was partly constructed out of perspex, so that processes underneath the foundation could be monitored. A ditch was created in the perspex, this was the location of the exit hole. A more elaborate description of the set-up can be found in Appendix B

In order to simulate a finely packed sand layer, the six meter thick sand was placed in six steps, after every step, the soil was compacted. The top 0.5 metres of the sand layer (the piping sensitive layer) consisted of a well mixed combination of sand. In order to determine the hydraulic conductivity of the sandy layer, a number of different samples of the sand mixture were taken. Based on these samples, the hydraulic conductivity of the sand layer was taken to be $1.5E-4$ m/s (this was the value used in MSeep). However, before the piping test was initiated, the discharge through the sand layer was first determined, this resulted in a different value for the hydraulic conductivity. According to this test, the hydraulic conductivity was $5.11E-5$ m/s.

During the tests, the water level was increased in small increments. As the head increased, turbid water as a result of fine particles in suspension were observed. Followed by the formation of sand boils, in these boils, no sand transport was observed. Eventually sand transport in the boils were observed, resulting in the formation of a crater. Overtime, the process stopped, since an equilibrium was formed. However when the head was increased further, the piping process started up again. Lastly, it was observed that with an increasing head, an increase in the size of the boils was seen as well as an increase in the length of the pipe. The experiments in the Delta Flume were stopped once the pipe length reached half the seepage length, because, according to Sellmeijer, if $l/L > 0.5$, a

further increase in water level would result in a shortening of the slit, this is physically impossible. Therefore, according to Sellmeijer, the critical hydraulic head is reached once the slit has reached half of the structure/seepage length (Sellmeijer and Koenders, 1991). The results of the piping experiments can be seen in Table 5.1.

Table 5.1: Overview of the experimental results of the Delta Flume experiments (Silvis et al., 1991)

Test no.	Sand	L [m]	D[m]	W [m]	W_{ditch} [m]	RD[-]	n[-]	k [m/s]	Hc [m]
T4	Marsdiep sand	6	6	5	0.5	0.65	0.38	0.000051	1.05
T2	Marsdiep sand	9	6	5	0.5	0.65	0.38	0.000051	1.69
T3	Marsdiep sand	12	6	5	0.5	0.65	0.38	0.000051	2.16

5.2. MSeep

Before the experiments were initiated a number of MSeep calculations were done. The following characteristics of the soil were used as input:

Table 5.2: Overview of the soil characteristic used in the mathematical model (Silvis et al., 1991)

Parameter	d_{70}	ρ'_p	ρ_{op}	θ	η
Value:	246 μm	1529 kg/m^3	1000 kg/m^3	51°	0.3

MSeep calculations were done by Silvis in 1991 using the 1989 version of the design rule. Both the results of the experiment and the MSeep calculations are found in Table 5.3. For all of the three experiments, the results of the piping experiment are significantly lower than the results of the MSeep calculation (Table 5.3). One of the main reasons for this is, that in the MSeep calculations done by Silvis, the hydraulic conductivity based on soil samples was used ($1.5E-4$) instead of the value determined by the discharge through the sand layer ($5.11E-5$).

Table 5.3: Overview of the experimental and analytical results of the Delta Flume experiments (Silvis et al., 1991)

Test no.	Sand	L [m]	D[m]	W [m]	k_{exp} [m/s]	Hc [m]	k_{MSeep} [m/s]	$H_{c,MSeep}$ [m]
T4	Marsdiep sand	6	6	5	0.0000511	1.05	0.00015	1.79
T2	Marsdiep sand	9	6	5	0.0000511	1.69	0.00015	2.51
T3	Marsdiep sand	12	6	5	0.0000511	2.16	0.00015	3.22

Replication of Silvis' MSeep calculations

Before, model runs could be done to determine the influence of leakage, first an attempt was made to replicate the MSeep results of Silvis. The previously mentioned input parameters were used in the MSeep calculations. Table 5.4 shows the results of the repeated experiments done by Silvis. In the table it can be seen that very similar values were obtained. Small differences are most likely due to the sensitivity of the model to a specific mesh size, since the refinement of the mesh was not specified. Since, it has been found that the results of the piping calculation in MSeep are very sensitive to the chosen mesh size(Appendix A).

Table 5.4: Overview of the results of the Delta Flume experiments (Silvis et al., 1991) as well as the MSeep simulations done by Silvis and the replicated MSeep calculations.

Test no.	L [m]	D[m]	W [m]	Hc [m]	$H_{c,MSeep,Silvis}$ [m]	$H_{c,MSeep,Lot}$ [m]
T4	6	6	5	1.05	1.79	1.81
T2	9	6	5	1.69	2.51	2.52
T3	12	6	5	2.16	3.22	3.22

MSeep runs using a hydraulic conductivity of $5.11E-5$

Next some model runs are done, to determine if the design rule implemented in MSeep is able to predict the critical hydraulic head measured in the piping experiments. In order to do this, all of the

input parameters used for the previous calculations are used, only the hydraulic conductivity of the sand layer is changed.

Table 5.5: Overview of the analytical results using MSeep for two different hydraulic conductivities.

Test no.	L [m]	D[m]	k_{MSeep} [m/s]	$H_{c,MSeep}$ [m]	k_{exp} [m/s]	$H_{c,MSeep,exp}$ [m]
T4	6	6	0.00015	1.81	0.0000511	1.31
T2	9	6	0.00015	2.52	0.0000511	1.83
T3	12	6	0.00015	3.22	0.0000511	2.35

This decrease in hydraulic conductivity, resulted in a decrease in the critical hydraulic head (Table 5.5). The results of the MSeep simulations using the actual value for the hydraulic conductivity are much closer to the results of the experiment. However, the difference between the two is still significant. According to Silvis et al. (1991), this uncertainty is most likely due to the uncertainty with respect to the parameters which describe the initiation of motion of a sand grain (the coefficient of White, η and the bedding angle, θ). Since, the other soil parameter were thoroughly examined and determined (Silvis et al., 1991). Another reason why there was a difference between the MSeep calculation and the experiments is because, the analytical model accounts for groundwater flow in two dimensions, and according to experimental results, the pipe path is clearly three-dimensional. As a result, the discharge increases, resulting in more transport of sand grains resulting in a lower critical hydraulic heads for piping progression (Silvis et al., 1991). Based on the above mentioned arguments, Silvis et al. (1991) proposes a correction factor for the design rule by Sellmeijer, which also accounts for the uncertainty in the bedding angle and the coefficient of White.

5.3. Design rule

In this section a comparison is made between the design rules and the results of the experiments. Two different combinations of parameters are modelled, the first set is the exact conditions of the experiment as mentioned in Table 5.2. The second combination of parameters uses a bedding angle of 37° , a smaller drag coefficient ($\eta = 0.25$) and a smaller hydraulic conductivity of the sand.

The results of the first situation can be seen in Figure 5.1. Both the 1988 and 2006 versions of the design rule over estimate the critical hydraulic gradient. For the larger seepage lengths, the difference is larger between the results of the experiments and the design rule. For all three simulations, the MSeep simulations over estimate the critical hydraulic gradient.

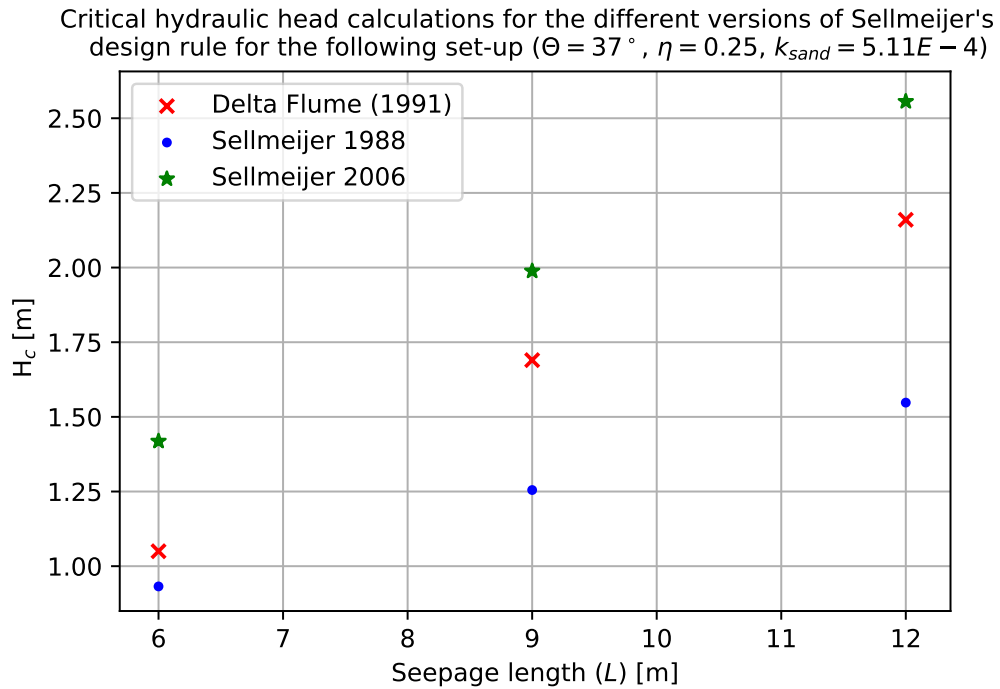


Figure 5.1: Critical hydraulic head calculated using the following input: $\Theta = 0.51$, $\eta = 0.3$, $k_{sand} = 1.5E - 4$.

Figure 5.2 shows the results of the design rule using slightly different input parameters. As can be seen, for these parameters, the 1988 version of Sellmeijer's design rule significantly underestimates the critical hydraulic head. While the results of the 2006 version of the design rule overestimate the result. For a seepage length of 9 meters, the difference between the calculated and observed critical hydraulic gradient is smallest.

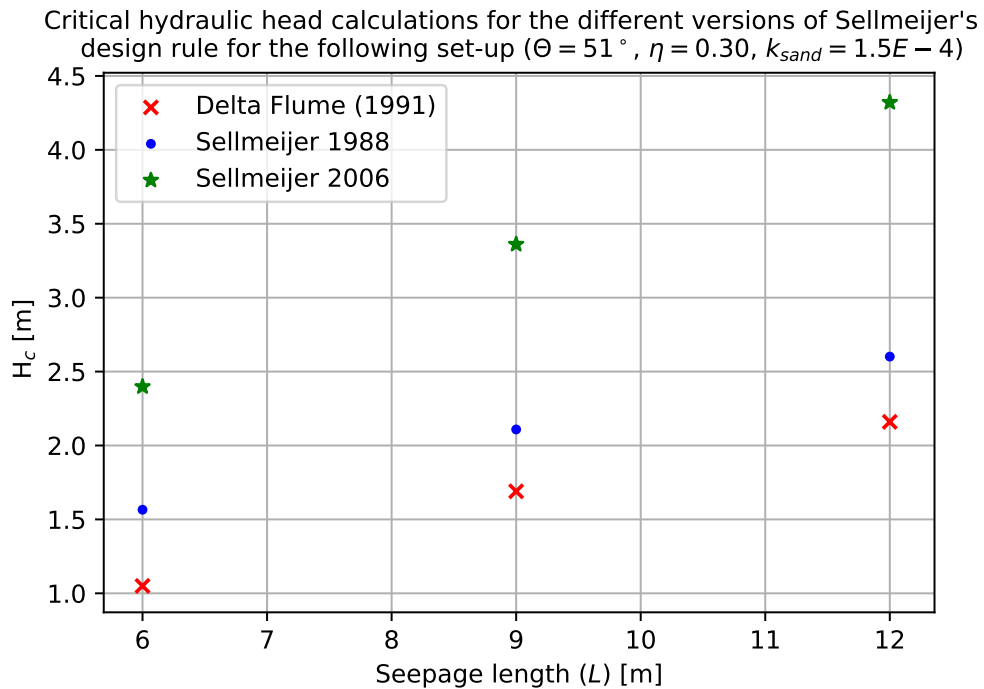


Figure 5.2: Critical hydraulic head calculated using the following input: $\Theta = 0.37$, $\eta = 0.25$, $k_{sand} = 5.11E - 5$.

5.4. Conclusion

In this chapter, the results of both the design rules and the MSeep simulations have been compared to the results of the Delta Flume experiments. Yet, the results of the MSeep simulations and the results of the design rule calculations have not been compared. In Figure 5.3, the results of the different simulations can be seen.

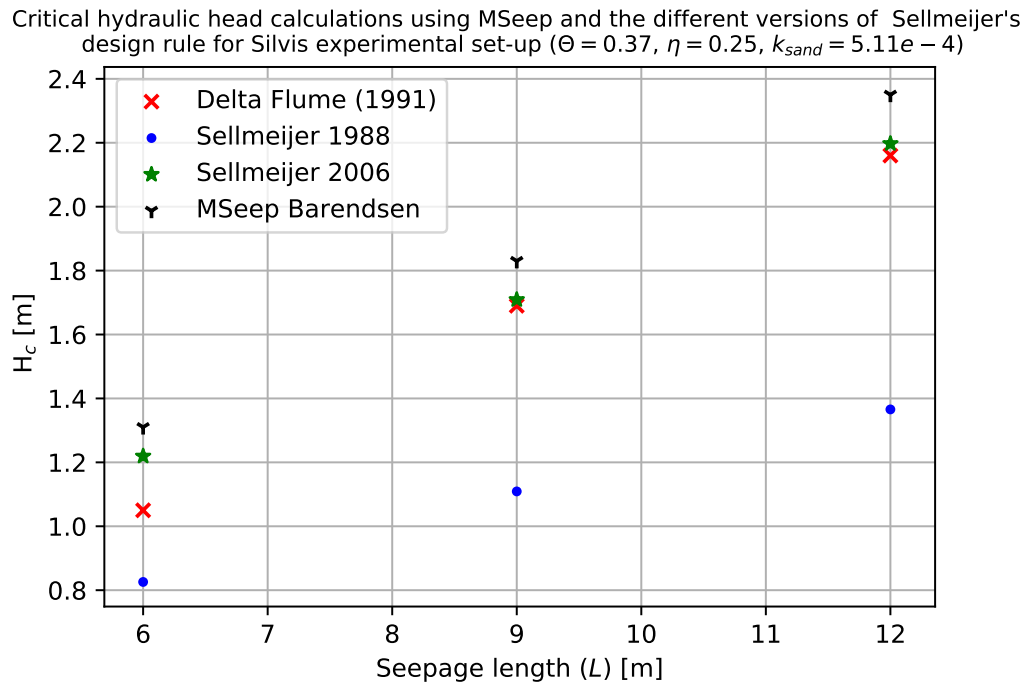


Figure 5.3: Critical hydraulic heads calculated using the 1988 and 2006 versions of the design rule as well as the results of MSeep calculations and the Delta Flume experiments.

In Figure 5.3 it can be seen that the original version of Sellmeijer's design rule significantly under predict the critical hydraulic head for pipe progression. The results of the 2006 version of Sellmeijer's design rule and the Delta Flume experiments are most similar. This is mainly because the Delta Flume experiments were used to calibrate this version of Sellmeijer's design rule. Next it can be seen that the critical hydraulic head computed using MSeep are slightly larger than the results of the experiments. From this it can be concluded that the MSeep simulations slightly over estimate the critical hydraulic head for pipe progression and that caution should be taken when using MSeep to calculate the critical hydraulic head for pipe progression.

II

Leakage and Piping

6

The effect of leakage on piping

In this chapter, leakage is explained with respect to the failure mechanism piping. Two different methods which are used to determine the influence of leakage on the potential in the aquifer are discussed. Lastly, how leakage effects the critical hydraulic head for pipe progression is discussed.

6.1. What is leakage?

In order for piping to occur a cohesive top layer needs to be placed on top of a sandy/silty foundation (?). Leakage occurs as a result of a difference in potential between a aquifer and a confining layer. It is a result of a difference in hydraulic conductivities of these layers. Since for more permeable layers, the change in potential is more rapid than for less permeable layers since water can flow more rapidly. As a result, water flows from an area of high potential to an area of low potential. The rate at which this occurs is dependent on the resistance of the layer through which it flows. For soil, this resistance is dependent on the hydraulic conductivity of this layer and the thickness of this layer. In the Netherlands, leakage is described using a leakage factor (λ)(Equation 6.1) and is defined as *"a measure of the spatial distribution of leakage through one or two aquitards into a leaky layer"* (Bezuijen, 2017).

$$\lambda = \sqrt{k_{sand} D_{sand} \frac{d_{clay}}{k_{clay}}} \quad (6.1)$$

Figure 6.1 gives an overview of the groundwater potentials in an aquifer under a impermeable dike with a cover layer that has a relatively high hydraulic conductivity. In the figure, groundwater flow towards the exit hole/ pipe location can be observed. Directly downstream of the exit point, seepage through the cover layer can also be observed. Lastly, at a larger depth, it can be observed that the groundwater potentials are completely vertical and that a portion of the groundwater flows towards the hinterland. Further downstream, a bend in these potentials can be seen as a result of more vertical seepage through the leaky layer.

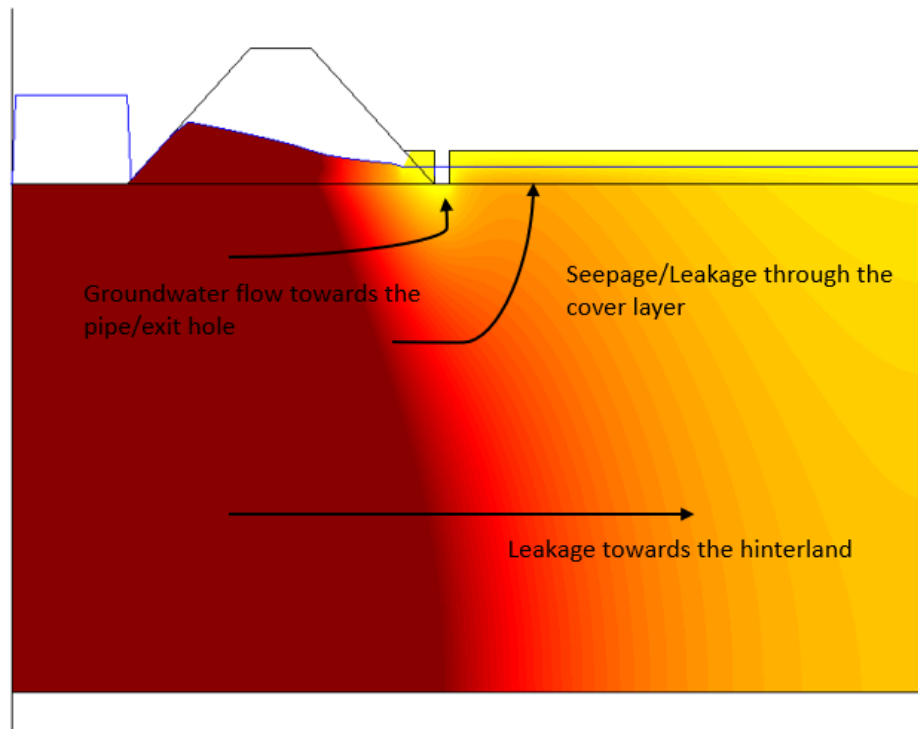


Figure 6.1: Cross-section of groundwater flow under a dike, flow towards the pipe can be observed, seepage due to a permeable cover layer is observed and leakage towards the hinterland is observed at larger depths in the aquifer. (MSeep output, x and z axis not scaled)

Leakage significantly effects the piping process. Leakage can occur both in the foreshore or hinterland, and depends on the hydraulic conductivity of the cover layer. Large leakage factors in the foreshore are beneficial for piping decreasing the potential in the aquifer at the outer toe of the dike, which causes the hydraulic gradient over the dike to decrease.

In the hinterland, short leakage lengths positively effect the probability of uplift since the difference in potential over the clay layer is smaller. However, if uplift does occur, these larger gradients in potential negatively affect the piping process. Since, these gradients are one of the main driving forces of the piping process. As can be seen in `autorefeq:leakagefactor`, the thickness of the aquifer/leaky layer also impacts the leakage factor. The leakage factor increases if the thickness of aquifer or cover layer increases, and decreases if the hydraulic conductivity of the clay increases.

Currently there are two different methods, which are used to determine the influence on leakage on the potential in the sand layer. The first method is used in the Netherlands to account for leakage and is based on the theory by Mazure (1936) and the formula by Verruijt (1970). This method can be found in the technical report for water pressure in dikes (translated: *Technisch Rapport Waterspanning bij dijken*). It is based on theory by Mazure and Verruijt and has been slightly adjusted to account for the difference in potential over the dike. The second method is mostly used in the United States of America where it has been derived by the Army Corps of Engineers. In the Netherlands, this method is referred to as the Blanket Theory. It is used to describe the natural seepage per unit length of the dike. These two methods will be explained briefly in the next two sections.

6.1.1. Leakage in The Netherlands

In the Technical report for water pressure in dikes (TRWD), leakage is described as being both seepage into and out of the aquifer through a leaky layer. Figure 6.2 shows how leakage through a leaky layer can effect the hydraulic head in the aquifer. If a semi-permeable layer is located upstream of the dike, depending on the permeability of this layer, the potential in the aquifer is lower than the water level in the river. This occurs, because the hydraulic conductivity of the cover layer limits the discharge through the layer and therefore also the potential in the aquifer.

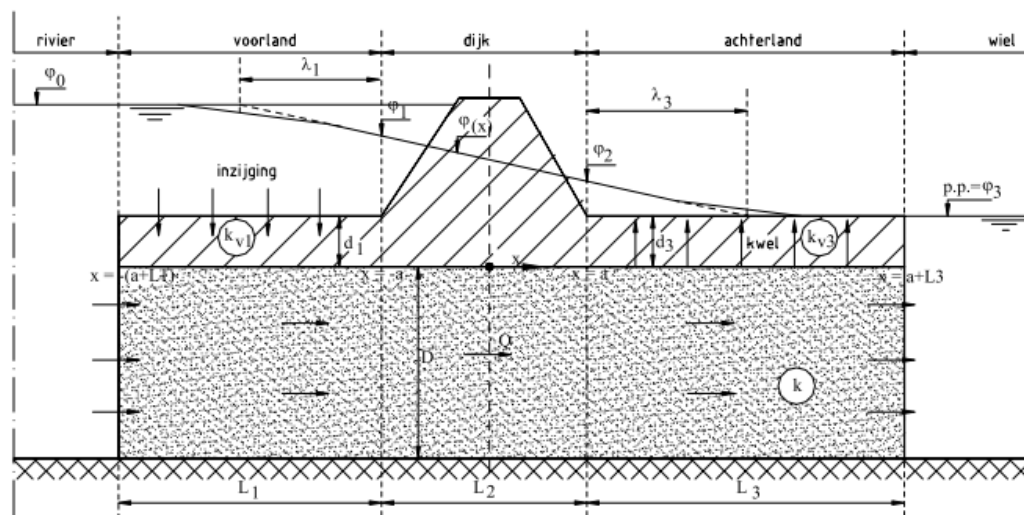


Figure 6.2: Schematization of groundwater flow under a clay dike with a cover layer (TAW, 2004).

If a leaky layer is present downstream of the dike, the potential in the aquifer is lower, that if an impermeable layer is present. Large leaky layers positively effect the critical hydraulic gradient, by increasing the distance over which the gradient changes. In this specific case (Figure 6.2), the leakage length in the hinterland (λ_3) is longer than in the foreshore (λ_1) and both positively effect the piping process. Further information and an overview of the different equations used in the TRWD can be found in Appendix C

Since Sellmeijer's design rule does not account for piping, in order to include the effect of the leakage factor in the piping calculation, the leakage factors (of both the foreshore and hinterland) are added to the structure length. Together these three components make up the new seepage length used in Sellmeijer's design rule.

6.1.2. Leakage in the Unites States of America

In the United States of America, the Army Corps of Engineers use a different method to determine the potential in the sand layer, this is referred to as the Blanket Theory by the Dutch. The Blanket theory is used to describe the natural seepage per unit length of the dike. The Blanket equations can be used to describe a number of different seepage conditions. According to Lam (2019), the Blanket equations used in case 4 and case 6 were able to accurately compute the potential in the aquifer as compared to the groundwater model D-GeoFlow. An overview of these specific cases and others can be found in Appendix D.

6.2. The effect of leakage on piping

Throughout the years, a number of different attempts have been made to determine the effect of leakage on the critical hydraulic head for pipe progression. The most recent being the report by Lam (2019). In this section a summary of the study and conclusions by Lam (2019) is given as well as some preliminary findings of the MSeep simulations.

6.2.1. Lam (2019)

Lam (2019) investigated the effect of a semi-permeable layer located downstream of the exit point on the critical hydraulic head for pipe progression. Lam (2019) used a groundwater model known as D-GeoFlow and modelled a number of different scenarios. For each scenario a number of different parameters were varied ($k_{clay}, k_{sand}, D, d, d_{70}$) to determine their influence on the critical hydraulic head for pipe progression.

For all of the simulations, Lam (2019) concluded that the presence of a leaky cover layer, had a positive effect on the critical hydraulic head for piping. An increase of the critical hydraulic head by 1 - 10 %

was observed in the simulations done by Lam (2019). Appendix E gives a more detailed description of the report by Lam (2019).

6.2.2. MSeep simulations

A similar investigation is carried out using MSeep. MSeep is used, since this was the original model which was used by Sellmeijer himself in the past to calibrate his design rules. In this section, some of the preliminary findings of the MSeep simulations are discussed. A detailed analysis as well as a description of the model set-up can be found in (chapter 7).

Figure 6.3 shows the difference in critical hydraulic head for a scenario with a leaky cover layer and for a scenarios with an impermeable cover layer. Figure 6.3 shows that leakage causes an increase in the critical hydraulic head for pipe progression. The magnitude of this increase is dependent on the hydraulic conductivity of the cover layer and the thickness of this layer. From these two sets of simulations, it can also be observed that leakage has a negligible effect on small aquifer depths ($D/L < 0.2$). The effect becomes more and more apparent as the aquifer depth increases ($D/L > 0.2$).

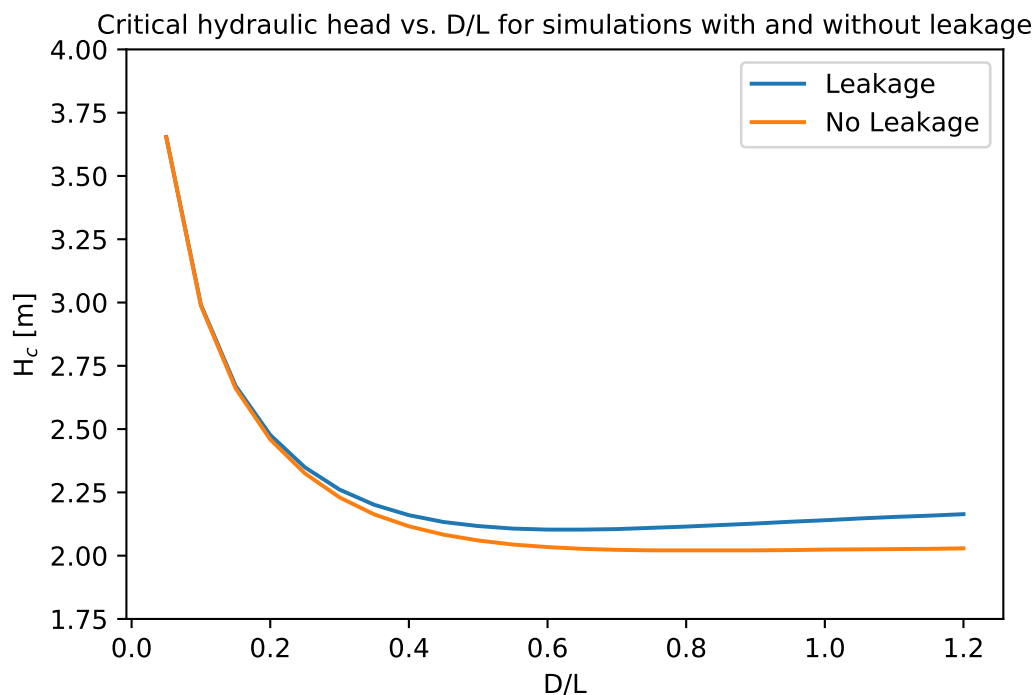


Figure 6.3: Plot showing the difference in critical hydraulic head for a scenario with and without leakage.

Originally, the objective of this research was to determine if leakage effects the critical hydraulic gradient for pipe progression. However, due the recent findings in the report by Lam (2019), this research question has already been answered for the most part. As a result, the focus of this thesis has shifted slightly to determining what we can do with the findings of these analysis. In Figure 6.4 an overview is given of the two different approaches used.

On the one hand, an attempt is made to determine how leakage can be included in Sellmeijer's design rule. In order to do this, the results of the MSeep simulations are analyzed. The goal here is to determine if a factor of method can be followed so that a leakage term can be included in Sellmeijer's design rule. From now on this is referred to as the **Engineering Approach**. Here only the results of the MSeep simulations are used in the analysis. This is because Sellmeijer uses a 2D approach to simulate backwards erosion piping. Secondly, no 3D model currently exists which can accurately simulate a pipe and accounts for a backwards erosion tool.

During the analysis of the MSeep simulations, it was observed that the presence of a leaky layer significantly impacts the streamlines and groundwater flow in the aquifer. As a result, an attempt is made to simulate the effect of a leaky layer in a groundwater model (iMOD) for both a quasi 3D and full 3D model set-up. In Figure 6.4 this analysis is referred to with the name: **Physics Approach**. It can also be seen that the analysis of the physics approach consists of both simulation in MSeep (2D) and iMOD (quasi 3D & 3D). First the results of the MSeep simulations are discussed (??) followed by the analysis and results of the iMOD simulations (chapter 8)

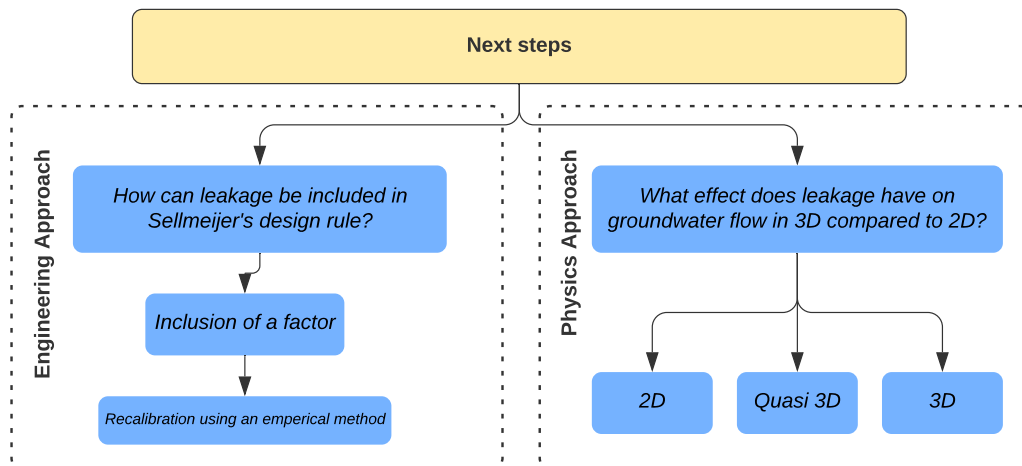


Figure 6.4: Overview of the next steps and how this is sub-divided into an Engineering Approach and a Physics Approach.

7

Leakage: 2D

In this chapter, the effects of leakage are studied for a two-dimensional groundwater model. First a brief description of the model set-up is given followed by a set of scenarios which will be modelled. The results of these simulations are then discussed. Lastly, the results of the two different approaches are discussed.

7.1. General model description

In order to determine the effects of leakage, first a simple model needed to be constructed. Figure 7.1 gives an overview of the model set-up. For each simulation, an impermeable clay dike was simulated on top of a permeable aquifer. Downstream of the dike (on the right hand side) a cover layer of a constant thickness is present. Upstream of the dike, the river is in direct contact with the aquifer, meaning that no foreshore is present. At the inner toe (directly downstream of the dike), an exit point is located. A more detailed overview of the relevant boundary conditions and model set-up can be found in Appendix F.

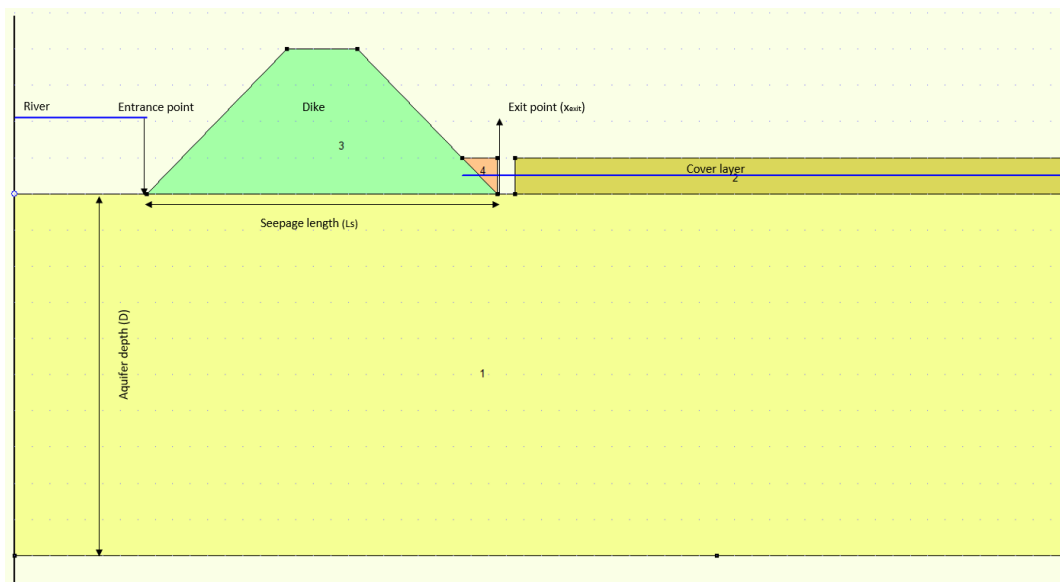


Figure 7.1: Schematization of the simulation set-up (MSeep, x- and z-axis not to scale)

Table 7.1 gives an overview of the parameters and values implemented. These parameters remained constant for all of the simulations.

Table 7.1: Input parameters for the different MSeep simulations

Parameter	d_{70}	L_s	H_{dike}	k_{sand}	n	θ	η	d_{clay}
Value:	200 μm	20 m	4 m	1.5E-4 m/s	0.4	37°	0.25	1 m

In order to study the effect of leakage, six different scenarios are modelled. In each scenario, the hydraulic conductivity of the cover layer is varied. Table 7.2 gives an overview of different hydraulic conductivities simulated. For each scenario, the thickness of the aquifer is also varied between 1 and 24 meters.

Table 7.2: Overview of the hydraulic conductivities implemented in each scenario

Parameter	Scenario 1	Scenario 2	Scenario 3	Scenario 4	Scenario 5	Scenario 6
k_{clay}	6.480 m/day	1.30 m/day	0.648 m/day	0.130 m/day	0.065 m/day	0.013 m/day

A second set of simulations was also done where the seepage length of the aquifer is increased to 40 metres and the thickness of the aquifer is varied between 2 and 48 metres so that similar D/L ratios are obtained. The results of these simulations can be found in Appendix F.

7.2. Six scenarios

In this section, the results of the six scenarios are given. For each scenario the critical hydraulic head is computed using MSeep as well as the geometry factor. Figure 7.2 shows the critical hydraulic head according to MSeep for the different scenarios and the different aquifer depths expressed in D/L ratios. These results are compared to both the 2006 and 2011 versions of Sellmeijer's design rule. A second set of simulations for slightly different dimension can be found in Appendix F. The second set of simulations were done to check if MSeep behaved similarly for a different set of input parameters.

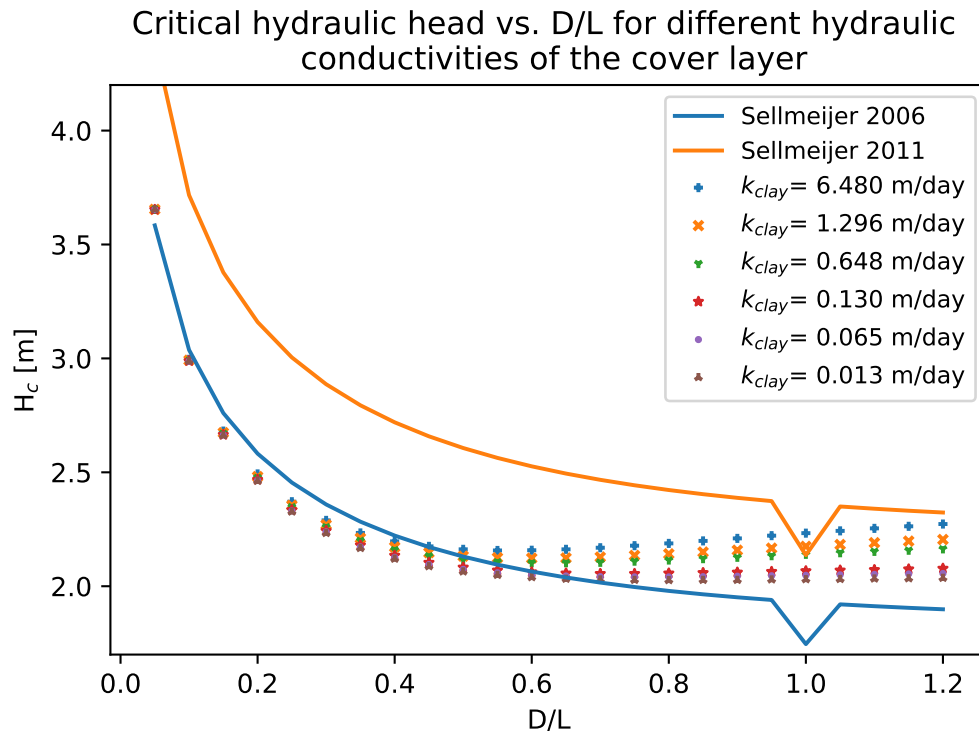


Figure 7.2: Plot showing H_c vs. D/L for the different scenarios as well as the results of the 2006 and 2011 versions of Sellmeijer's design rule.

In Figure 7.2 an overview of the critical hydraulic head is shown for a number of different scenarios and aquifer thickness (D/L ratio). From the results, it can be observed, that for small D/L (D/L

< 0.2) ratios, there is little difference between the results of the different MSeep simulations. As the aquifer thickness increases, the effect of leakage on the critical hydraulic head becomes more and more apparent.

From the figure, it can also be observed that for small D/L ratios, The results of the Sellmeijer 2006 design rule predict larger critical hydraulic heads compared to the results of the simulations. For larger D/L ratios (D/L > 0.5) the opposite is observed. The critical hydraulic head computed using the 2011 version of Sellmeijer’s design rule, is larger than the results of both the MSeep simulations and the 2006 version of Sellmeijer’s design rule. The general trend of results for both versions of Sellmeijer’s design rule are of an exponent tending towards a minimum value. With the exception of the results for a D/L ratio of 1. At this location, in the geometry factor, the D/L ratio is to the power of zero, resulting in a smaller value for the critical hydraulic gradient compared to other D/L ratios(computed in python). For the simulations, this is not the case, after a minimum value has been reached the critical hydraulic head starts to increase again. The results of these simulations are also not effected by a D/L ratio of 1.

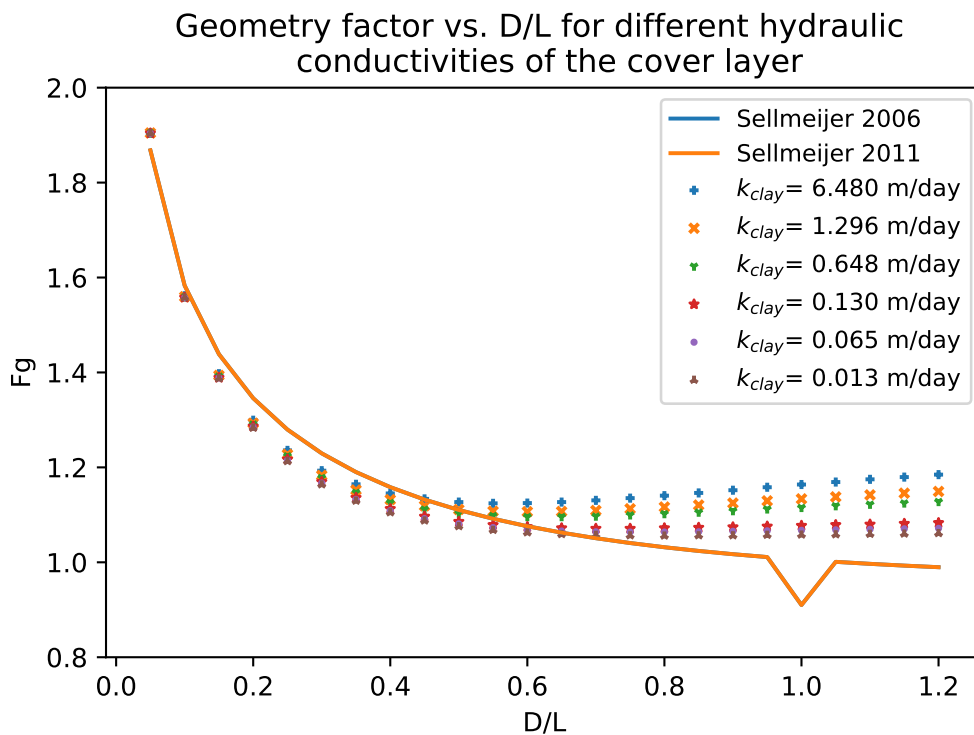


Figure 7.3: Plots showing F_g vs. D/L for the different scenarios as well as the results of the 2006 and 2011 versions of the geometry factor.

In part I of this thesis, it was concluded that Sellmeijer accounts for the influence of the geometry (aquifer thickness, hydraulic conductivity and the presence of an impermeable cover layer) in the geometry factor. In each scenario, the thickness of the aquifer was the only variable. Meaning that the critical hydraulic gradient computed is directly dependent on the geometry factor. Figure 7.3 shows the geometry factor (F_g) versus the ratio of aquifer thickness for both the results of the simulations and for Sellmeijers design rule.

Similar trends can be observed for the geometry factor as observed for the critical hydraulic head, with the exception of the results of the 2011 version of Sellmeijer’s design rule. From this it can be argued that the inclusion of the characteristics of the grain size has also resulted in a vertical shift in the critical hydraulic gradient, and that this shift is not a result of the difference in the geometry factor(hydraulic conductivity of the cover layer) but a result of including the characteristics of the grains.

7.3. Engineering approach

As was mentioned in the chapter before, an analysis of the results is done using two different approaches. In this section an engineering approach is used to determine the effect of leakage on the critical hydraulic head. The goal is to determine a method or factor, which can be included to Sellmeijer's design rule that is based on an analysis of the results of many different simulations. In Sellmeijer's design rule, the dimensions and characteristics of the cover layer are not included. However, according to the leakage factor, these terms are just as important in determining the amount of leakage which can occur.

In this section, the effect of the hydraulic conductivity is studied. Two different comparisons are made; the first focuses directly on effect of a change in the hydraulic conductivity on the geometry factor. Next, the leakage factor (λ) is computed and plotted against the critical hydraulic head to determine if a clear relation can be seen.

Geometry factor vs. D/L

In these simulations, the critical hydraulic head is directly dependent on the geometry factor. Therefore, the focus is on the geometry factor and the relative change in this factor as a result of different hydraulic conductivities of the cover layer. The six different scenarios are all compared to a reference case with an impermeable cover layer.

The change in the geometry can be seen in Figure 7.4. A linear trend can be observed for all of the simulations. For larger D/L ratios, it can be observed that there is a larger variation in the geometry factor. Next, Figure 7.4 shows that for larger hydraulic conductivities (more permeable cover layers), there is an increase of more than 4% in the geometry factor.

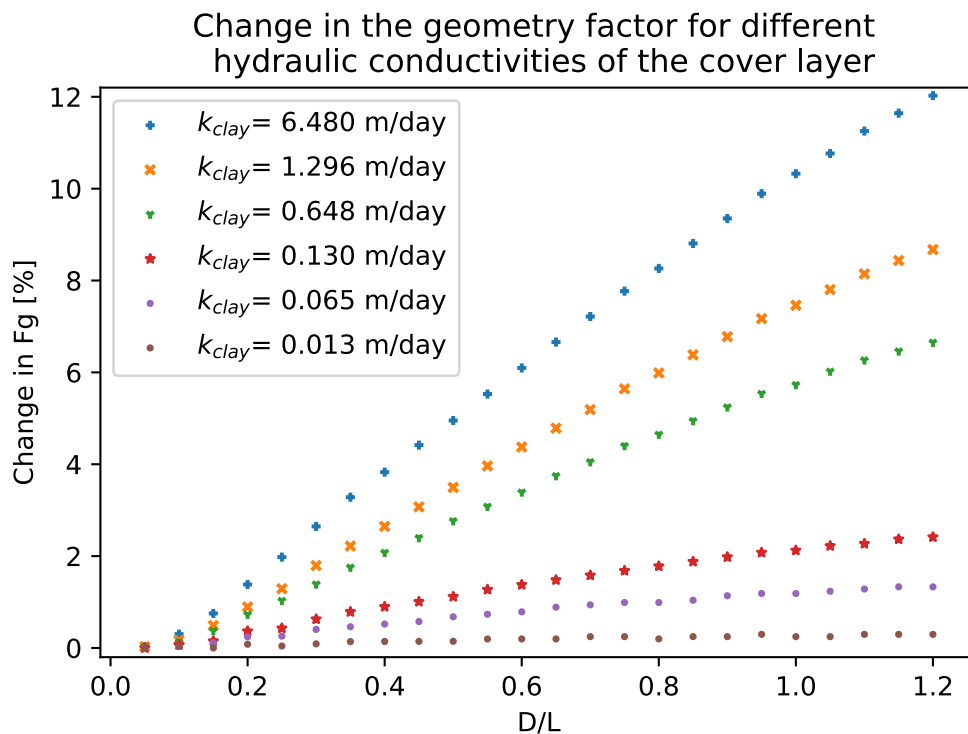


Figure 7.4: Plot showing relative change in F_g for the six different scenarios.

Leakage factor vs. Critical hydraulic head

Next, a comparison is made between two accepted design rules in the Netherlands; Sellmeijer's design rule and the leakage factor (Equation 6.1). In Figure 7.5 it can be seen that for smaller hydraulic conductivities of the cover layer, the leakage factor increases. For all of the six simulations, a similar

pattern can be observed. The results for smaller hydraulic conductivities are shifted down slightly and shifted towards the right.

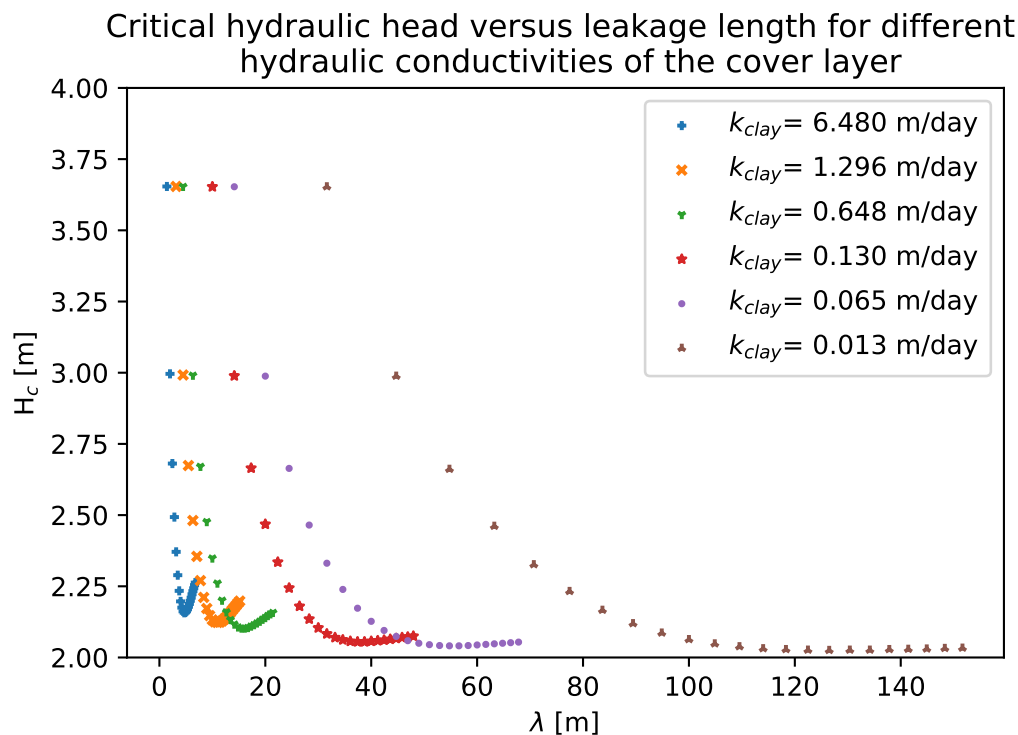


Figure 7.5: The critical hydraulic head computed using MSeep are plotted against the leakage length.

7.3.1. Discussion

For both comparisons, it can be seen that the relation between the leakage and the critical hydraulic head is important. However, these figures also show that the results are very case specific.

Geometry factor vs. D/L

In Figure 7.4 it can be seen that leakage effects the geometry factor and therefore also the critical hydraulic head. For these six scenarios, only the hydraulic conductivity was varied. From Figure 7.6 it can be seen that the relation is linear and that an increase in hydraulic conductivity of the cover layer (more leakage) results in a steeper gradient of the line. From this it can be argued that if a leakage term is included, for these six scenarios this term is wholly dependent on the hydraulic conductivity of the cover layer and this relation should be linear.

Unfortunately, six scenarios are not sufficient to determine this factor, in order to derive a factor which can account for leakage, a larger number of simulations first need to be done and analysed. In these additional simulations, both the hydraulic conductivity of the aquifer and the thickness of the cover layer should also be varied.

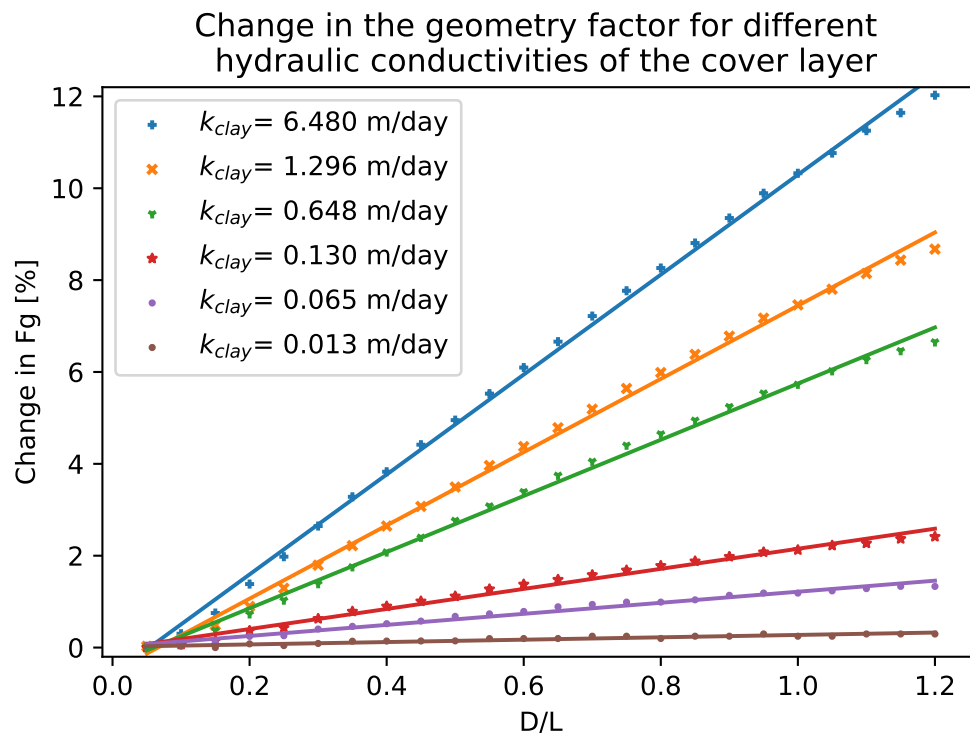


Figure 7.6: Plot showing relative change in F_g for the different scenarios, with a linear curve fit.

Leakage factor vs Critical hydraulic head

Currently, no leakage factor is included in Sellmeijer's design rule. However, from Figure 7.5 it can be seen that similar critical hydraulic heads can be observed for different leakage factors. This means that the critical hydraulic head, is therefore not explicitly dependent on the leakage factor. But more specifically on the combinations of the terms in the leakage factor; for these set of simulations only the hydraulic conductivity of the cover layer and the thickness of the aquifer was varied. However, the thickness of the cover layer and the hydraulic conductivity is also important in calculating the leakage factor.

Curve fitting of these lines proved to be difficult and no 'simple' relation can be determined. However, if the choice is done for a further analysis using the leakage factor a large number of additional scenarios should be simulated. Instead of just six simple scenarios where only a limited number of parameters were varied.

7.4. Physics approach

In this approach, the focus is predominantly on the effect of leakage on the groundwater flow. Hence the name Physics Approach. In this section, the focus is on the results of the 2D groundwater model. In the next chapter, some quasi 3D and full 3D simulations are analyzed.

In Sellmeijer's design rule, a geometry factor is included which accounts for the influence of an aquifer thickness on backwards erosion piping. As is mentioned earlier, one of the reasons for the transition from an infinitely deep aquifer to an aquifer with a finite depth is, that, by restricting the aquifer depth, the flow pattern in the aquifer is also restricted. The aquifer depth significantly affects the flow pattern in the aquifer, which, in turn affects the flow towards the pipe and therefore also the development of the pipe.

In this section, an attempt is made to determine if groundwater flow under the dike is affected by the presence of a leaky layer. In order to determine if this is indeed the case, the streamlines under the dike are studied for both a impermeable cover layer and a leaky cover layer.

In Figure 7.7a, the streamlines under a dike can be seen for a situation without a leaky cover layer. Two sets of streamlines can be distinguished, flow directly under the dike towards the exit point and

deeper streamlines. Here it can be seen that all of the streamlines converge towards the exit point, meaning that all of the streamlines under the dike will eventually reach the exit point.

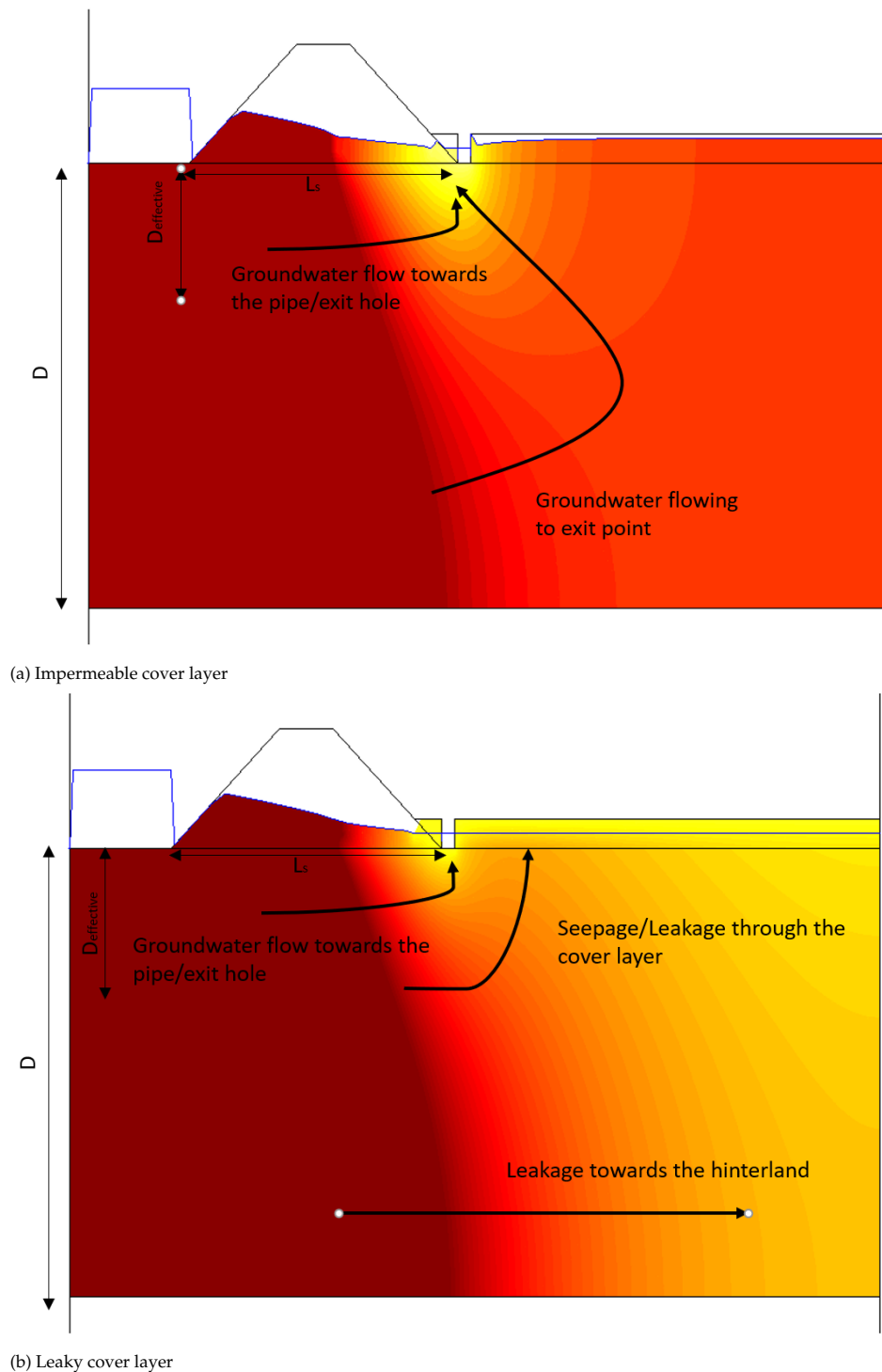


Figure 7.7: Overview of the groundwater potentials under a dike (MSeep output, x and z axis not scaled)

In Figure 7.7b, three different sets of streamlines can be distinguished. Directly under the dike, water flows towards the pipe/exit location. At a small depth under dike, it can be seen that a portion of the streamlines flow horizontally, until they bend towards the leaky cover layer, passing directly under the pipe and the exit point. Lastly, at a larger depth under the dike, it can be seen that the groundwater

flow is completely horizontal. This exact distribution in streamlines varied for different hydraulic conductivities of the cover layer, however, for relatively leaky layers similar configurations are found.

Based on these different sets of streamlines, a distinction has been made in the portion of the aquifer that supplies water to the pipe and the exit hole and a portion of the aquifer that supplies water towards the hinterland. The portion of the aquifer that acts as a driving force will be referred to as the **effective depth** ($D_{effective}$). For each scenario, the effective depth is determined. Figure 7.8 gives an overview of the effective depth for the different scenarios.

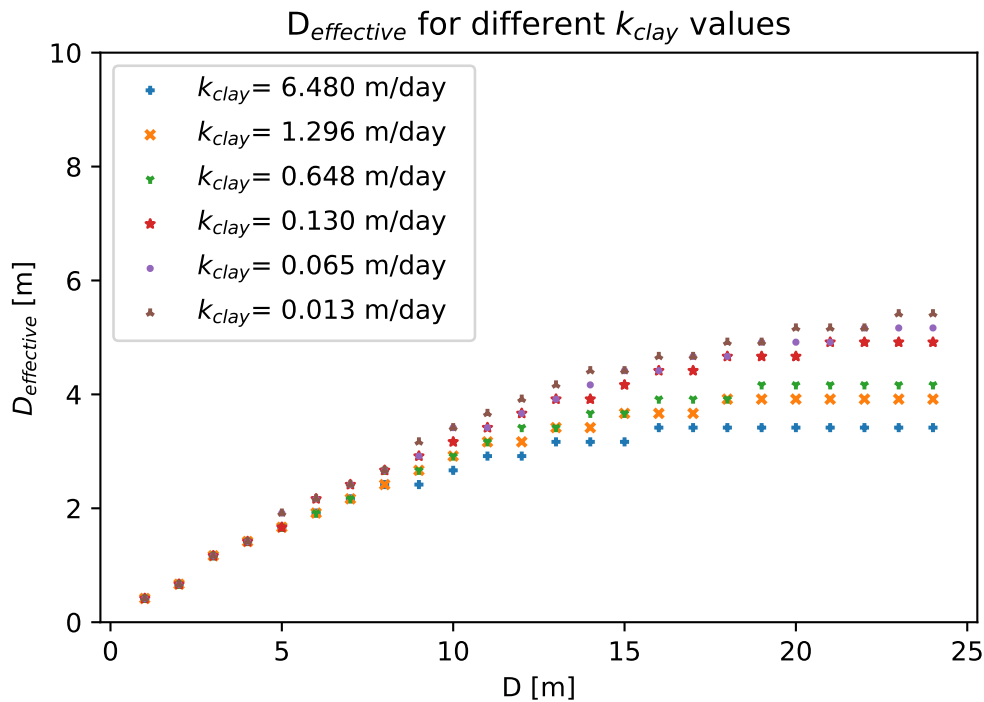


Figure 7.8: Graph showing the difference in effective depth for the different hydraulic conductivities of the cover layer (k_{clay}).

For relatively thin aquifers ($D < 5$), variations in hydraulic conductivity of the cover layer have no effect on the effective depth. For thicker aquifers ($D > 5$), leakage does play a role in determining the effective thickness of the aquifer which supplies water towards the pipe. The effect of leakage on the effective depth becomes more and more apparent for larger aquifer depths.

Figure 7.8, also shows that for the more permeable cover layers, the effective depth has reached a maximum. The smallest effective depths are observed for the most permeable cover layers. From Figure 7.8 and Figure 7.2 it can be seen that smaller effective depths, result in a smaller portion of the groundwater flowing towards the pipe. Which in turn results in a smaller discharges through the well, less erosion and therefore the critical hydraulic head for pipe progression increases. The maximum effective depth for the less permeable cover layers has not yet been reached, more simulations for larger aquifer thickness need to be done to be sure what the maximum effective depth is for these scenarios.

7.5. Conclusions

From the simulations it can be concluded that leakage positively affects the critical hydraulic head for pipe progression. The magnitude of this effect is largely dependent on the aquifer depth and the hydraulic conductivity of the cover layer. For the six simulations, a clear linear relation between the scenarios can be seen. From these results it can be concluded that a term can be included in the geometry factor and that this factor should include the hydraulic conductivity of the cover layer. In

order to derive this term additional simulations should be done where the hydraulic conductivity of the aquifer and thickness of the cover layer are also varied.

From the Phycis Approach it was observed that leakage affects the groundwater flow under a dike and that only a small portion of the aquifer depth acts as a driving force for the piping mechanism. Implicitly Sellmeijer already accounts for an effective depth in his design rule. However, Sellmeijer's design rule was derived for a situation where the cover layer is impermeable. Therefore, in order to include the effect of leakage in Sellmeijer's current design rule a recalibration of his design rule should be done where leaky layers have been included.

In order to determine the effect of leakage on the groundwater flow for piping situations, an further analysis is done in iMOD. An analysis of these results and the drawn conclusions will be elaborated in the next chapter.

8

Leakage: 3D

In this chapter, a further analysis is done using the Physics Approach. The effects of leakage on groundwater flow are studied using a three dimensional groundwater model (iMOD). First a general description of the model set-up is given, followed by a comparison of the groundwater flow in MSeep and iMOD for a situation without a pipe. Next, quasi 3D and 3D simulations are done for different hydraulic conductivities of the cover layer. Lastly, a comparison is made between a set of MSeep simulations, and iMOD simulations for an aquifer thickness of 10 meters. In which the iMOD simulations use the exact input from the MSeep simulations.

8.1. General model description

In all of the simulations, a simplified cross section is used (similar to the cross section implemented in MSeep), consisting of an impermeable dike located on a sandy aquifer. Directly downstream of the dike, the location of the exit point is assumed. Upstream of the dike, the river is located. The bottom of the river is in direct contact with the sandy aquifer, here no cover layer is present. A overview of this cross section is given in Figure 8.1.

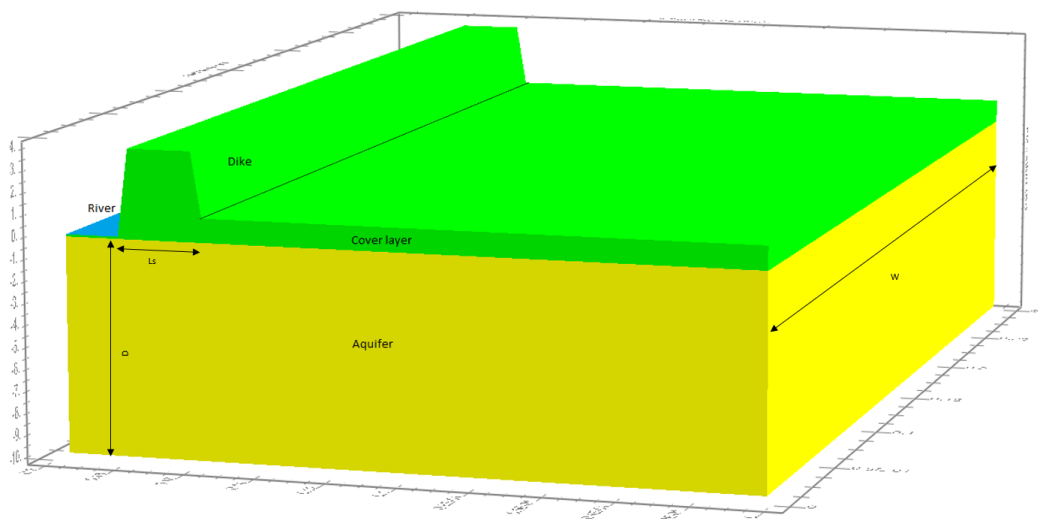


Figure 8.1: Three-dimensional view of the geometry implemented in iMOD.

An overview of the values used as input in the model can be found in Table 8.1. These values will remain constant, throughout the model simulations. Before any further simulations were done, a

check was done for the base set-up. This check was done to determine if the model behaved according to what was expected as well as to determine if the correct boundary conditions were implemented.

Table 8.1: Input parameters for the different MSeep simulations

Parameter	L	k_{sand}	k_{dike}	n	d_{sand}	d_{clay}	$Stage_{river}$
Value:	20 m	13 m/day	1.3E-05 m/day	0.4	10 m	1 m	2.1 m

Using the input values from the base case which were mentioned above, five different sets of simulations are done. They are:

1. A set of simulations where the hydraulic conductivity of the cover layer is constant throughout the model domain but has been varied according to the six different scenarios (Figure 8.1).
2. A set of simulations where the hydraulic conductivity is varied and a very permeable strip of 1 meter long by 1 meter deep is placed directly behind the dike along the whole model width (quasi 3D, Figure 8.2a).
3. A set of simulations where the hydraulic conductivity is varied and a very permeable strip of 1 meter long by 1 meter deep is placed directly behind the dike along the whole model width (quasi 3D, Figure 8.2b) together with a very permeable 'pipe' of 10 meters long and 0.1 meters deep along the whole model width.
4. A set of simulations where the hydraulic conductivity is varied and a very permeable strip of 1 meter long by 1 meter deep and 1 meter wide is placed directly behind the dike in the center of the model(3D, Figure 8.3a).
5. A set of simulations where the hydraulic conductivity is varied and a very permeable strip of 1 meter long by 1 meter deep and 1 meter wide is placed directly behind the dike in the center of the model(3D, Figure 8.3b). Together with a pipe of 10 meter longs and 0.1 meters deep and 0.1 meter wide.

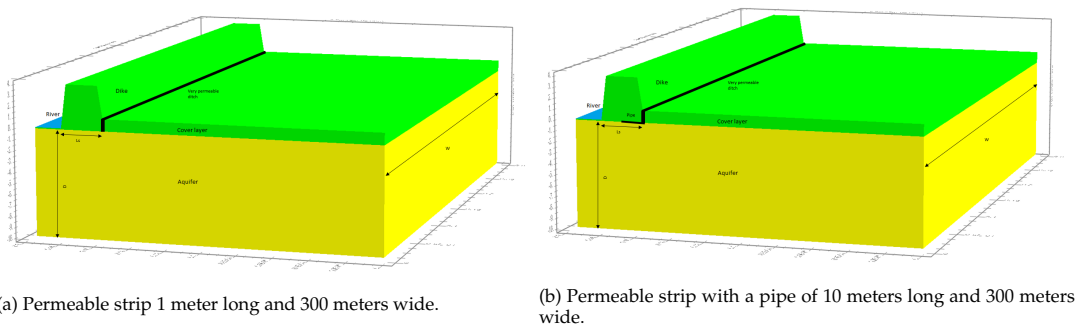


Figure 8.2: Quasi 3D schematization of an exit point and a pipe.

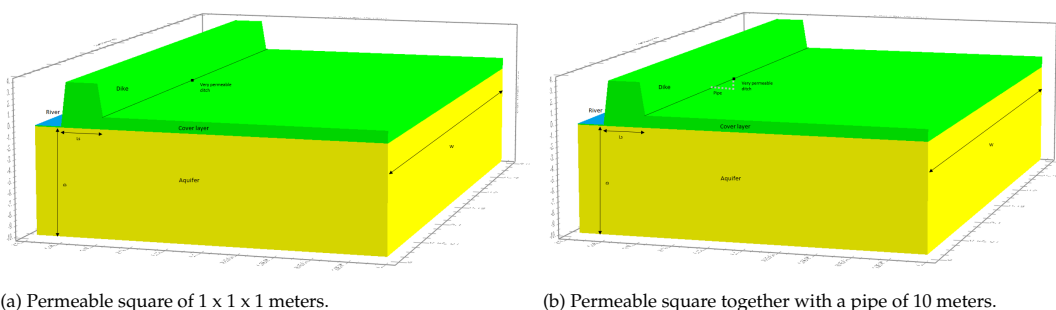


Figure 8.3: 3D schematization of an exit point and a pipe.

For each simulation, six different scenarios are modelled. In each scenario, the hydraulic conductivity of the cover layer is varied. Table 8.2 gives an overview of the values implemented.

Table 8.2: Overview of the parameters varied in the six different scenarios.

Parameter	Scenario 1	Scenario 2	Scenario 3	Scenario 4	Scenario 5	Scenario 6
k_{clay}	6.480 m/day	1.296 m/day	0.648 m/day	0.130 m/day	0.065 m/day	0.013 m/day

In order to compare the results of the MSeep simulations with the iMOD. Two additional sets of simulations (quasi 3D and full 3D) are done using the computed critical hydraulic head from the MSeep simulations. In these simulations, a pipe has been included with a length of 10 meters (equal to half the seepage length). An overview of the implemented river water level for the six different scenarios is found in Table 8.3.

Table 8.3: Overview of the critical hydraulic heads computed in MSeep for the six different scenarios.

Model	Hydraulic conductivity (k_{clay}) [m/day]					
	6.480	1.296	0.648	0.130	0.065	0.013
H_c [m]	2.16	2.13	2.12	2.08	2.07	2.06

Pipe dimensions

For the simulations done with a pipe, a fixed pipe length of 10 meters (half of the structure length) is included. This choice is based on the fact that the critical hydraulic head is often reached when the pipe length is equal to half the seepage length (Sellmeijer, 1988). The pipe has a height of 0.1 meters, this is equal to the dimensions of one cell. For the full 3D simulation, the pipe also had a width equal to one cell, while for the quasi 3D simulations, the width of the pipe was equal to the width of the model. In order to simulate the effect of a pipe on the groundwater flow, the pipe needed to become quite permeable. Therefore, the hydraulic conductivity in the pipe was assumed to be equal to 1000 m/day.

For each set of simulations, the effective depth, the effective width (only for the 3D simulations) and the discharge is determined. How these parameters are derived is explained briefly below.

8.1.1. Effective depth ($D_{effective}$) & Effective width ($W_{effective}$)

In order to determine both the effective depth and the effective width, a particle tracking tool was used. The effective depth was estimated by determining the largest depth from which streamlines originate that directly contribute to the flow in the pipe or in the uplift channel. An example of this can be seen in Figure 8.4a. The effective width is also determined in a similar manner. Where it has been defined as the width, from which the streamlines originate that directly contribute to the flow in the pipe or in the uplift channel (Figure 8.4b). The effective width is smaller than the total width of the that is influence by the presence of a uplift channel. Where the total width influenced by the uplift channel is defined as the influence width ($W_{influence}$).

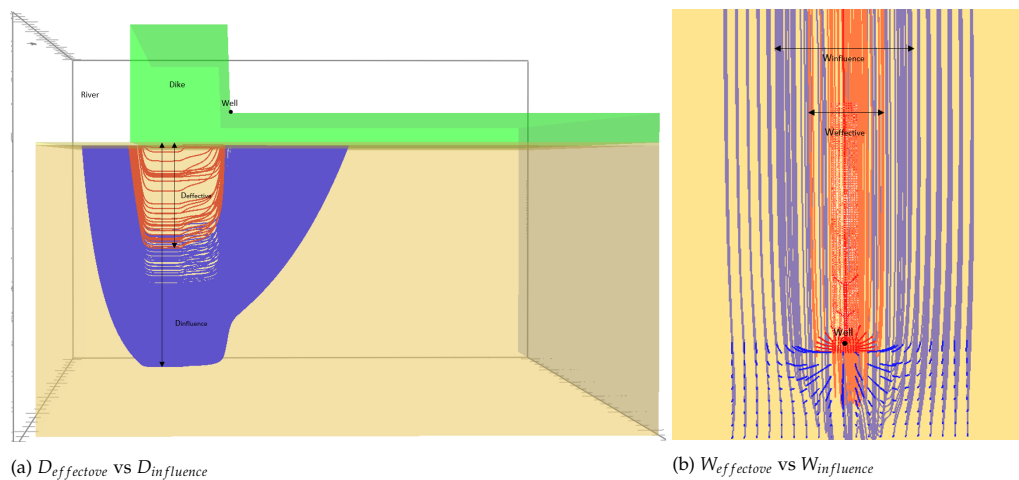


Figure 8.4: Difference in effective depth, effective width and total depth and total width.

Discharge ($Q_{exitpoint}$)

The Water Balance tool is used to calculate the discharge through the very permeable ditch. For each simulation, the discharge is computed.

8.2. Simple groundwater models

First a comparison is made between the two different groundwater models; a MSeep model without a pipe, and an iMOD model without a pipe for both a quasi 3D and 3D model. In all of the simulations, the water level in the river is equal to 2.1 meters and the potential in the clay layer is equal to 0.5 meters. First the groundwater flow potentials in MSeep are compared to the streamlines of a quasi 3D iMOD simulation. This comparison can be made because the streamlines in MSeep are directly perpendicular to the contour potentials. An overview of the potentials and streamlines can be found in Figure 8.5.

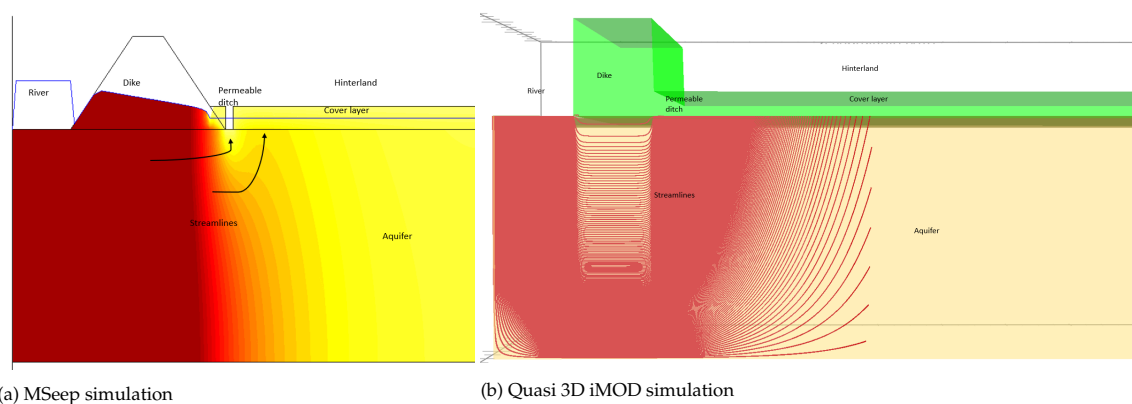


Figure 8.5: Comparison of streamlines for an MSeep simulation and a Quasi 3D iMOD simulation

Similar streamlines can be observed for both the 2D MSeep simulation and the quasi 3D iMOD simulation. For a further comparison, the discharge through the ditch (MSeep), permeable strip (iMOD quasi 3D) and permeable patch (iMOD 3D) are determined. Table 8.4 gives an overview of the results for the six different scenarios.

Table 8.4: Discharge through the ditch (MSeep) and the very permeable strip and patch (iMOD).

Model	Discharge (Q_{ditch}) [m^2/day]					
	Hydraulic conductivity (k_{clay}) [m/day]					
	6.480	1.296	0.648	0.130	0.065	0.013
MSeep (2D)	3.72	4.45	4.83	5.70	5.98	6.29
iMOD (Quasi 3D)	1.52	1.89	2.13	2.81	3.09	3.60
iMOD(3D)	2.48	3.99	5.02	8.24	9.82	13.11

It can be observed that there is a difference in magnitude (a factor 2) between the MSeep model and the quasi 3D iMOD model. One of the reasons for this difference is that, in MSeep the discharge is computed at the nodes of the cells (Figure 8.6a). While in iMOD the discharge is calculated at the center of the cells (Figure 8.6b).

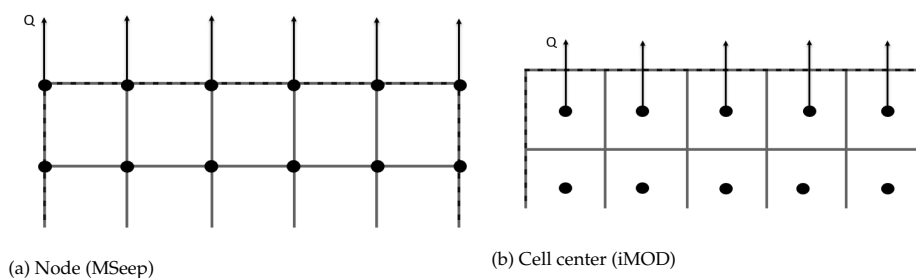


Figure 8.6: Discharge is computed in MSeep in the nodes while in iMOD in the cell centres.

Lastly, similar trends can be observed for all three models. A decrease in the hydraulic conductivity of the cover layer results in an increase in flow towards the ditch and therefore also an increase in discharge through the ditch.

8.3. Phycis Approach: Effect of leakage

Here, the two quasi 3D and the two full 3D simulations are compared. For each simulation, the six different scenarios are modelled (Table 8.2). For these simulations, both the effective depth, the effective width (in the case of 3D) and the discharge through the permeable patch in the cover layer is determined.

For all of the simulations, the effective depth was determined and an overview is given in Table 8.5. For all simulations, it can be observed that the effective depth increases for less leaky layers. For the quasi 3D simulations, the presence of a pipe results in smaller effective depths the simulaitons without a pipe. While for the full 3D simulation, the presence of a pipe results in a larger effective depth. From Table 8.5 it can be observed that the effective depth is smaller for the quasi 3D simulations. This is because for these simulations, the effective width also becomes important since water can now also be supplied from a lateral direction instead of only in the vertical. The effective width for these two simulations are given in Table 8.6.

Table 8.5: Effective depth for the four different simulations(iMOD).

Model	Effective depth ($D_{effective}$) [m]					
	Hydraulic conductivity (k_{clay}) [m/day]					
	6.480	1.296	0.648	0.130	0.065	0.013
iMOD (Quasi 3D)	5.43	5.68	5.88	6.44	6.67	7.05
iMOD (3D)	1.47	1.79	2.07	3.27	4.05	6.08
iMOD (Quasi 3D) pipe	1.52	1.76	1.96	2.65	3.00	3.72
iMOD (3D) pipe	1.99	2.38	2.74	4.21	5.10	7.28

The presence of a pipe also effects the streamlines under the aquifer. The difference in streamlines as a result of a dike can be seen in Figure 8.7. At the location of the pipe, there is a vertical bend in the streamlines. This is the result of the pipe attracting water.

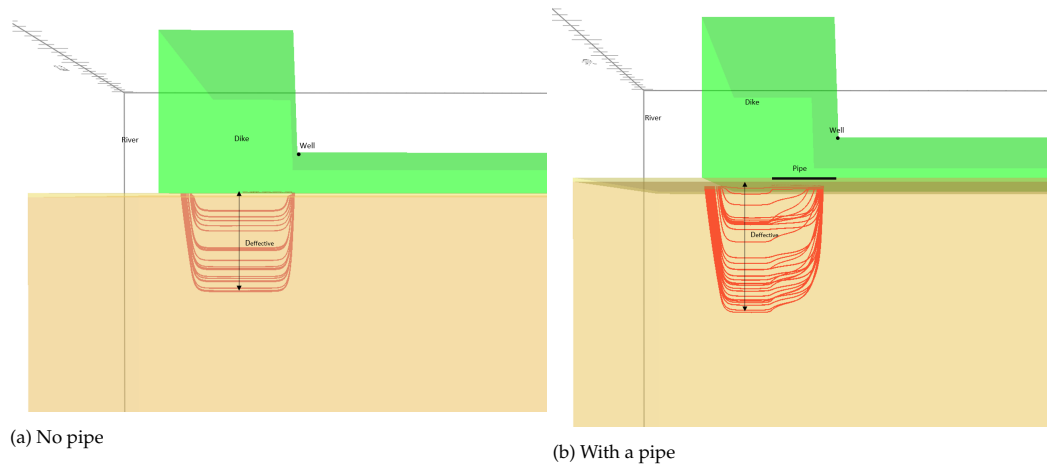


Figure 8.7: Difference in streamlines under the dike for 3D simulations with and without a pipe.

For the 3D simulations, the effective width is also computed (Table 8.6). For these simulations, the effective width increases as the hydraulic conductivity of the cover layer decreases, regardless of the presence of a pipe. Next, it can also be observed that the effective width is slightly larger for the set of simulations with a pipe. This is because as a result of the pipe, more lateral groundwater is attracted towards the location of the pipe, than is the case for the simulations without a pipe.

Table 8.6: Effective width for the fully three dimensional simulations(iMOD).

Model	Effective width ($W_{effective}$) [m]					
	Hydraulic conductivity (k_{clay}) [m/day]					
	6.480	1.296	0.648	0.130	0.065	0.013
iMOD(3D)	1.40	1.90	2.22	2.97	3.37	4.67
iMOD(3D) pipe	1.34	2.04	2.35	3.17	3.67	5.20

For these four sets of simulations, the effective area is also calculated. For the 3D simulations, this was done by multiplying the effective width by the effective depth. For the quasi 3D simulations, this was done by multiplying the effective depth by the width of one cell which is equal to 0.1 meters. The results of these calculations can be found in Table 8.7. The results show that the effective area is significantly larger for the full 3D simulations compared to the 2D simulation. It can also be seen that the presence of a pipe also results in a larger effective area.

Table 8.7: Effective area for the four different simulations(iMOD)

Model	Effective area ($A_{effective}$) [m^3/day]					
	Hydraulic conductivity (k_{clay}) [m/day]					
	6.480	1.296	0.648	0.130	0.065	0.013
iMOD (Quasi 3D)	0.54	0.57	0.59	0.64	0.67	0.70
iMOD (3D)	2.06	3.40	4.59	9.73	13.63	28.41
iMOD (Quasi 3D) pipe	0.15	0.18	0.20	0.26	0.30	0.37
iMOD (3D) pipe	2.67	4.85	6.44	13.35	18.71	37.88

Finally, the discharge through the permeable cover layer was also determined. Table 8.8, gives an overview of the computed discharge through the ditch/permeable patch. Here it can also be observed that an increase in discharge is paired with a decrease in the hydraulic conductivity of the cover layer. Secondly, for the simulations in which a pipe has been modelled, larger discharges through the ditch are observed.

Table 8.8: Discharge through the very permeable patch in the cover layer for the four different simulations(iMOD).

Model	Discharge (Q_{ditch}) [m^2/day]					
	Hydraulic conductivity (k_{clay}) [m/day]					
	6.480	1.296	0.648	0.130	0.065	0.013
iMOD (Quasi 3D)	1.52	1.89	2.13	2.81	3.09	3.60
iMOD (3D)	2.48	3.99	5.02	8.24	9.82	13.11
iMOD (Quasi 3D) pipe	5.44	5.75	5.98	6.56	6.78	7.14
iMOD (3D) pipe	3.15	4.75	5.85	9.35	11.07	14.68

8.4. Comparison of MSeep and iMOD modules

In this section a comparison is made between two sets of simulations. A set of simulations done in MSeep for an aquifer depth of 10 meters with the piping module for the six scenarios and two sets of iMOD simulations (quasi 3D and 3D). The results and output of these simulations are implemented in iMOD. An overview of the results of the MSeep simulations is given in Table 8.9. The critical hydraulic head computed in MSeep is implemented in iMOD.

Table 8.9: Overview of the results of the MSeep simulations for the six different scenarios.

Model	Hydraulic conductivity (k_{clay}) [m/day]					
	6.480	1.296	0.648	0.130	0.065	0.013
H_c [m]	2.16	2.13	2.12	2.08	2.07	2.06
$D_{effective}$ [m]	2.42	2.92	2.92	3.17	3.42	3.42
Q_{pipe} [m^3/s]	8.74	9.01	9.15	9.48	9.58	9.69

In each iMOD simulation a constant pipe length was used of 10 meters. Since this is in accordance with Sellmeijer's design rule which assumes that the critical hydraulic head is reached at a pipe length of half the structure length. The hydraulic conductivities were varied in accordance with the six different scenarios.

As was mentioned two sets of iMOD simulations are done, quasi 3D and 3D. For these simulations, first the effective depth was determined. The results of these simulations can be seen in Table 8.10. Here it can be seen that the effective depth of the MSeep simulations are smaller than for the quasi 3D iMOD simulations. While for the fully 3D simulations, the effective depth for the more permeable cover layers ($k_{clay} > 0.65$) is first smaller than for the MSeep simulations. However, for the less permeable cover layers ($k_{clay} < 0.65$), the effective depth is larger in 3D than in 2D.

Table 8.10: Effective depth for the results of the MSeep simulations in iMOD.

Model	Effective depth ($D_{effective}$) [m]					
	Hydraulic conductivity (k_{clay}) [m/day]					
	6.480	1.296	0.648	0.130	0.065	0.013
MSeep (2D)	2.42	2.92	2.92	3.17	3.42	3.42
iMOD (Quasi 3D) pipe	5.43	5.68	5.88	6.44	6.67	7.04
iMOD (3D) pipe	2.00	2.38	2.74	4.21	5.10	7.27

The effective width was also calculated an overview can be found in Table 8.11). The same trend in effective width can be observed as for the effective depth. The effective width also increases as the hydraulic conductivity of the cover layer decreases.

Table 8.11: Effective width for the results of the MSeep simulations in iMOD.

Model	Effective width ($W_{effective}$) [m]					
	Hydraulic conductivity (k_{clay}) [m/day]					
	6.480	1.296	0.648	0.130	0.065	0.013
iMOD(3D) pipe	3.45	3.74	3.97	4.81	5.29	6.70

Lastly, the discharge (Table 8.12) through the permeable patch layer was also computed for both the quasi 3D and 3D simulations. The results of the quasi 3D iMOD simulations are quite similar in magnitude to the discharges computed in MSeep. From this it can be assumed that the models behave similarly. However, for the fully 3D simulations, the discharge through the permeable ditch is smaller for the more permeable cover layers ($k_{clay} > 0.648$) and larger for the less permeable cover layers ($k_{clay} < 0.648$).

Table 8.12: Discharge through the very permeable patch in the cover layer for the results of the MSeep simulations in iMOD

Model	Discharge(Q_{ditch}) [m^3/day]					
	Hydraulic conductivity (k_{clay}) [m/day]					
	6.480	1.296	0.648	0.130	0.065	0.013
MSeep (2D)	8.74	9.01	9.15	9.48	9.58	9.69
iMOD (Quasi 3D) pipe	7.34	7.65	7.92	8.52	8.77	9.20
iMOD (3D) pipe	4.25	6.32	7.75	12.16	14.32	18.90

8.5. Conclusions

For all simulations, the results of the quasi 3D and full 3D simulations follow the trends found in the 2D MSeep simulations: an increase in the hydraulic conductivity results in a decrease in the effective depth and discharge. However, in the full 3D simulations, smaller effective depths are observed for simulations without a pipe. This is because now water is also attracted from the lateral direction instead of just the vertical. For the simulations with a pipe a different trend is observed. This very permeable slit now also attracts water from both a larger width and depth, resulting in larger well discharges.

Lastly, the simulations also show that the range in the results (effective depth, effective width and discharge) between the most permeable and least permeable cover layer is much larger than in the 2D and quasi 3D simulations. The discharge varies between 4.25 and 18.90 m^2/day , while in the quasi 3D the discharge varies between 5.44 and 7.14 m^2/day . From these results it can be concluded that the effect of leakage is larger on the groundwater flow in the full 3D simulations compared to the 2D/Quasi 3D simulations currently used. Use of a 2D model for the prediction of groundwater flow should be done with caution.

9

Discussion

In this thesis, the effect of leakage on backwards erosion piping has been studied. In order to study the effect of leakage on Sellmeijer's design rule as well as on the groundwater flow. In this chapter, the results of the two different groundwater simulations are discussed. Next, the limitations of the research are discussed together with the assumption that were made.

9.1. Model results

The results of both the MSeep simulations and iMOD simulations will be discussed separately in this chapter. Starting with the results of the MSeep simulations. In each section the results of the models are discussed and how these results influence the research.

9.1.1. MSeep simulations

In the MSeep simulations, it was observed that leakage effects the critical hydraulic gradient for pipe progression. One of the goals of this thesis was to determine how leakage can be included in Sellmeijer's design rule. How this can be done was studied in the Engineering approach. From the Engineering Approach, it was observed that the effect of leakage on the critical hydraulic head is largely dependent on the hydraulic conductivity of the cover layer. Therefore, the leakage factor should include this term. Unfortunately only six scenarios were studied. In order to derive this term, additional simulations should be done where the hydraulic conductivity of the aquifer and the thickness of the cover layer are also varied.

For each piping simulation, MSeep also computes the contour potentials and the streamlines. From these figures it was observed that the presence of a leaky layer has a significant impact on the groundwater flow under the dike. It was observed that only a small portion of the aquifer thickness ($D_{effective}$) acts as a driving force for piping. From the analysis done in the Physics Approach, it was observed that the effective depth is a useful tool in determining the impact of leakage on the groundwater flow. Since, smaller effective depths were observed for more permeable cover layers.

From the analysis done in the Physics Approach, it can be argued that the effective depth ($D_{effective}$) should be used in the piping calculations instead of the aquifer depth (D). However, due to the way in which the design rule by Sellmeijer has been derived and calibrated/validated, calculating the H_c using the effective depth will result in values which significantly overestimate the critical hydraulic gradient. Therefore, ideally a new curve fit of his design rule should be done on MSeep simulations where the effective depth is used instead of the aquifer depth. So that the effect of leakage can be included in his design rule.

If $D_{effective}$ were to be implemented in Sellmeijer's design rule, the next problem arises; determining what the effective depth is. In real life situations this will be difficult to determine. So a rule of thumb or graph should be derived based on the results of thousands of different groundwater simulations for which the effective depth has been determined for different combinations of leaky layers (hydraulic conductivity of the aquifer and cover layer, and the thickness of both of these layers).

9.1.2. iMOD simulations

Currently, no three dimensional model exists which accounts for backwards erosion piping or includes Sellmeijer's design rule. Therefore, some basic quasi 3D and 3D simulations were done to study the effect of leakage on the groundwater flow surrounding an uplift channel. Simulations were done, for a number of difference scenarios both with and without a 'pipe'. Where a pipe has been simulated by a horizontal strip consisting of very permeable cells.

Before any simulations were done, first a check was done to determine if the used input parameters and boundary conditions resulted in similar potentials and streamlines in the aquifer for both the 3D MSeep model and the quasi 3D iMOD model. From Figure 8.5, it can be seen that similar streamlines are observed in both models. Unfortunately, in iMOD it is not possible to view the potentials in the aquifer and therefore be able to compare the two situations more easily. However, from Figure 8.5b, the streamlines in the aquifer are similar to the streamlines in MSeep.

Next, the discharge through the exit ditch was also determined. The MSeep discharges are all approximately a factor two larger than for the quasi 3D simulations. By calculating the discharge at the nodes, not only the flow through the cell is accounted for but also a portion of the flow from the left and right of the node. This difference can result in a slight overestimation of the discharge. Lastly, full 3D simulations were also done for this base case. From these simulations, it was observed that the discharge was significantly higher for the less permeable cover layers ($k_{clay} > 0.65$). For these simulations, the effective width becomes more and more important since less water can leak through these layers, resulting in larger discharges through the permeable patch.

Next, a comparison was made between the four different iMOD set-ups: a quasi 3D set-up, a quasi 3D set-up with a pipe, a 3D set-up and lastly a 3D set-up with a pipe. From these simulations, it was observed that the effective depth is smaller for the 3D simulations without a pipe. For the 3D simulations with a pipe, the effective depth is larger compared to the quasi 3D simulations. The effective width increased slightly for the simulations with a pipe. This increase in effective width occurs since, the pipe behaves similarly to a drain, attracting the lateral groundwater towards the pipe.

Larger effective depths and effective widths result in larger effective areas. As a result, according to Darcy's law, an increase in discharge should be observed. Since the gradient ($\partial h / \partial x$) and hydraulic conductivity (k) remain constant. This is indeed the case, for the simulations with a pipe (for both the quasi 3D and the fully 3D simulations). From these simulations, it can be observed, that by approaching piping as a 3D/quasi 3D problem, a portion of the groundwater flowing towards the exit point is unaccounted for. The impact of this has becomes more important for situations where the hydraulic conductivity of the cover layer is very small.

In the last set of iMOD simulations, a comparison was made between MSeep simulations and iMOD simulations with the presence of a pipe. Where the input of the iMOD models were determined by the results of the MSeep simulations. From these simulations, it was observed that there is still a difference between the two models. One of the main reasons is that in MSeep the erosion tool has been included and in iMOD this has been accounted for by creating a very permeable ditch and a pipe under the dike. Secondly, this difference is also as a result of the way in which the two models calculate the discharge (MSeep at the nodes, and iMOD in the center of the cell).

The difference in effective depth between MSeep and the quasi 3D iMOD model seem to have little influence on the discharge through the well as a result of the implemented water levels. Similar values for the discharge were observed for these two simulations.

The largest difference in both the effective depth and discharge was observed for the full 3D simulations. For these simulations, the range in the effective depth for the most and least permeable cover layer was largest. A large difference was also observed in the effective width for these simulations. Which in turn also resulted in a larger difference in the discharge. For these simulations, a slightly different river water level was implemented. Resulting in a small difference in the hydraulic gradient ($\partial h / \partial x$). The effect of this is negligible compared to the change in effective area, for these six different scenarios.

From the model results, it has become clear that accounting for leakage in the piping calculation would positively affect the critical hydraulic gradient for pipe progression. However, in this thesis the limitations of 2D modelling and Sellmeijer's design rule have also become more apparent. The question

arises whether further energy should be spent on determining a way in which leakage can be included in Sellmeijer's design rule. Or that this energy is better spent on deriving a new design rule which is more transparent, and can account for the effect of both leakage and groundwater flow in the third dimension.

For a short term quick fix, it is recommended to derive a leakage term which can be included in Sellmeijer's design rule. However, with the continuing developments in 3D modelling, energy should also be spent on deriving a new design rule which accounts for not only the effect of leaky layers, but, also accounts for lateral groundwater flow.

9.2. Limitations of the research

In this section the main limitations of the study are discussed, together with the assumptions made.

Model accuracy

In order to determine the effect of leakage on the critical hydraulic gradient, a large number of model simulations needed to be done in MSeep. A choice had to be made in achieving the required refinement, limiting the computation time and accounting for a significantly large model domain. In order to limit the computation time, a model domain of 100 meters was used, resulting in a hinterland length of 60 meters.

For the piping calculations a hinterland of 60 meters was sufficient. Since the effect of larger model domains on the critical hydraulic gradient was negligible ($< 2\%$). However, the effect of the right boundary (length of the hinterland) on the groundwater flow (effective depth) should still be evaluated, especially for the more impermeable layers. For these cases, a hinterland of at least 3 times the leakage factor should be simulated.

In the iMOD simulations, a much larger model domain was simulated. This was done to ensure that the boundaries did not effect the groundwater flow in the aquifer. A model domain of 300 meters wide and 200 meters long with a mesh refinement of 0.1 by 0.1 by 0.1 meters was used. Ideally, both models should have had similar model dimensions to remove the uncertainty that the model dimensions affect the results. For future studies, case should be taken in ensuring that identical models are constructed.

Comparison of models

Two different types of groundwater models were used: MSeep which is a finite element model and iMOD which is a finite difference model. As a result, there are slight difference in implementable geometry. The mesh in MSeep consists of a number of triangles which can be easily adapted to sloping boundaries. While the mesh in iMOD consists of squares, make it difficult to simulate a sloping boundary. This difference in mesh size and format can also effect the results of the simulations.

Model sensitivity

It was also found that the results of the MSeep simulations were sensitive to the size of the ditch in which the uplift channel was located. Larger critical hydraulic gradients are observed for simulations with smaller ditch sizes. However, this specific effect was limited in the simulations since in all simulations, the size of the ditch remained constant and was equal to 1 meter.

Modelling of the pipe

In all of the simulations (also in MSeep), the assumption is made that the path progresses horizontally; directly under the dike. While in actuality, the path of the pipe is largely dependent on the local subsoil conditions and is therefore very difficult to predict. From experiments it has been observed that the pipe behaves more like a meandering river with a larger number of branches. Unfortunately, no model exists which is capable of simulating the pipe path in 3D.

In Sellmeijer's design rule he assumes that the pipe is straight and progresses horizontally. This assumption is also used in the iMOD models. This difference in behaviour of a pipe can result in different flow patterns in the aquifer and as a result different effective depth's, effective width's and well discharges. This meandering nature will likely result in a decrease in the effective depth, but an increase in the effective width. If a meandering pipe system of 10 meters long is modelled, it is expected that

larger well discharges will also be observed. However, this exact distribution is again strongly dependent on the local subsoil conditions (hydraulic conductivity of the layers, porosity, grain size and aquifer depth).

Simplified model

In all of the simulations, a very simplified schematization of reality was modelled, this is often the case in modelling studies. However, in this thesis only one simple schematization was studied. A scenario where a impermeable dike located on a homogeneous sandy layer, downstream of the dike a cover layer was present. No foreshore was present and the river was in direct contact with the aquifer. In the simulations it was assumed that the hydraulic conductivity of the cover layer and aquifer was constant. Spatial variation in these soil parameters are not accounted for.

For further research it is recommended that a larger variation of scenarios are studied. So that the effect of for more complex (and realistic) geometries can be determined.

III

Conclusions

10

Conclusion

In the Netherlands, dikes are the most commonly used structures to retain water and provide safety against flooding. In order to ensure the safety of these dikes against a number of different failure mechanisms, such as backwards erosion piping, wave overtopping and macro stability, a detailed safety assessment has been created. The focus of this thesis is on the failure mechanism known as piping and consists of three different sub-mechanisms: uplift, heave and backwards erosion piping.

In order to assess the effect of leakage on groundwater flow, and how this affects the critical hydraulic gradient for which a pipe progresses three different research questions were determined. Each research question and the associated conclusions will first be discussed followed by a general conclusion of the whole thesis.

10.1. What assumptions were used in the derivation of Sellmeijer's design rule?

A number of different assumptions and simplifications were made by Sellmeijer before he was able to derive his design rule. The most significant being, simplifying the three-dimensionality of the piping process to a two-dimensional process. By doing this, Sellmeijer, does not account for the meandering nature of the pipe and excludes the effect of the lateral groundwater flow on the pipe progression. By limiting the problem to a two-dimensions, Sellmeijer derived a mathematical model on which his design rule was based.

In Sellmeijer's mathematical model, three different processes are described analytically. The groundwater flow towards the lee side of the dike and to the slit. The flow of groundwater through that slit and the analytical description of the stability of the grains in the bottom of the slit (pipe). Over the years, Sellmeijer's design rule has been adapted three times. Each adaptation resulting in a more accurate design rule by including the effect of more and more parameters. However, with each adaptation, Sellmeijer's design rule did not become more transparent. The first adaptation was the most significant and resulted in the inclusion of a finite aquifer depth and an impermeable cover layer downstream of the dike. The remaining two adaptations resulted in the inclusion of new fitting parameters. The 2006 version of Sellmeijer's design rule was a result of a transition from a four-force equilibrium acting on the sand grains to a two-force equilibrium. The last adaptation accounted for the effect of the characteristics of the grain size on the critical hydraulic gradient. Neither adaptation accounted for the effect of leakage on backwards erosion piping.

Of particular interest, in this thesis, was to determine if leakage is included in Sellmeijer's design rule. In retracing the steps done by Sellmeijer in deriving his design rule, it can be concluded that the effect of leakage and therefore the presence of a leaky cover layer is not included in Sellmeijer's design rule. The only mention of a cover layer is of an impermeable cover layer. Meaning that there can be no vertical flow (leakage) through this layer. The effect of this has been included in the geometry factor of Sellmeijer's design rule. In addition, based on the sensitivity analysis, it can also be concluded that the two terms of the geometry factor (aquifer thickness and seepage length) have the largest impact on

the critical hydraulic head. From these findings it was assumed that leakage is indeed important and further investigation should be done on the effect of leakage on the critical hydraulic head for pipe progression.

10.2. How does leakage effect the critical hydraulic head for pipe progression?

Leakage occurs as a result of a difference in hydraulic conductivity between an aquifer and a leaky cover layer and the difference in thickness of these layers. It is expressed using a leakage factor. Currently, the effect of leakage is not included in Sellmeijer's design rule. From results of the MSeep simulations and the report by Lam (2019) it can be concluded that leakage effects the critical hydraulic head for pipe progression. Leakage increases the critical hydraulic head for pipe progression. The greatest increase in critical hydraulic head was observed for very permeable cover layers.

From the analysis, it was observed that the magnitude of the effect of leakage on increasing the critical hydraulic head for pipe progression is largely dependent on the thickness of the aquifer. For relatively shallow aquifers ($D < 5$ m), the effect of leakage on increasing the critical hydraulic head for pipe progression was negligible. However, as the thickness of the aquifer increased, the effect became more apparent increasing with a maximum of 12 % for the studied scenarios.

10.2.1. How does leakage effect the groundwater flow in 3D compared to 2D?

As mentioned earlier, one of the main limitations of Sellmeijer's design rule is that it assumes that piping is a two-dimensional problem. However, from the iMOD simulations and previous literature, it can be concluded that this is indeed not the case. Lateral groundwater flow also acts as a driving force for piping. Therefore both an effective depth, as well as an effective width need to be determined in order to capture the effect of leakage in 3D. Since, according to Darcy's Law the discharge through the aquifer is directly dependent on: the cross sectional area (effective depth and effective width), the hydraulic conductivity of the aquifer and the hydraulic gradient.

It was also observed that for very leaky cover layers, the effective depth and effective width are substantially smaller (approximately 3 to 4 times smaller) than the set of simulations with an almost impermeable cover layer. This decrease in effective area directly effects the discharge through the uplift channel/exit and therefore also the flow velocity in the pipe, positively effecting the piping process.

Next, from the comparison of the quasi 3D and 3D simulations it can be concluded that leakage clearly affects the groundwater flow. The full 3D simulations show a larger range in the well discharge than compared to the quasi 3D simulations. In the full 3D simulations (with a pipe), the discharge varies between 3.15 and 14.68 m²/day, while in the quasi 3D (with a pipe) simulations the discharge varies between 5.44 and 7.14 m²/day. From these results it can be concluded that the effect of leakage is larger on the groundwater flow in the full 3D simulations compared to the quasi 3D simulations currently used.

Lastly, a comparison was made between the 2D, quasi 3D and 3D simulations. From these simulations similar trends were observed in the discharge for the 2D and quasi 3D simulation. The discharge computed for the full 3D simulations differed considerably. The variation of these discharges can be seen in Figure 10.1. From these results it can be argued that the impact of leakage might be considerably larger in 3D (in reality) than computed using a 2D or quasi 3D model.

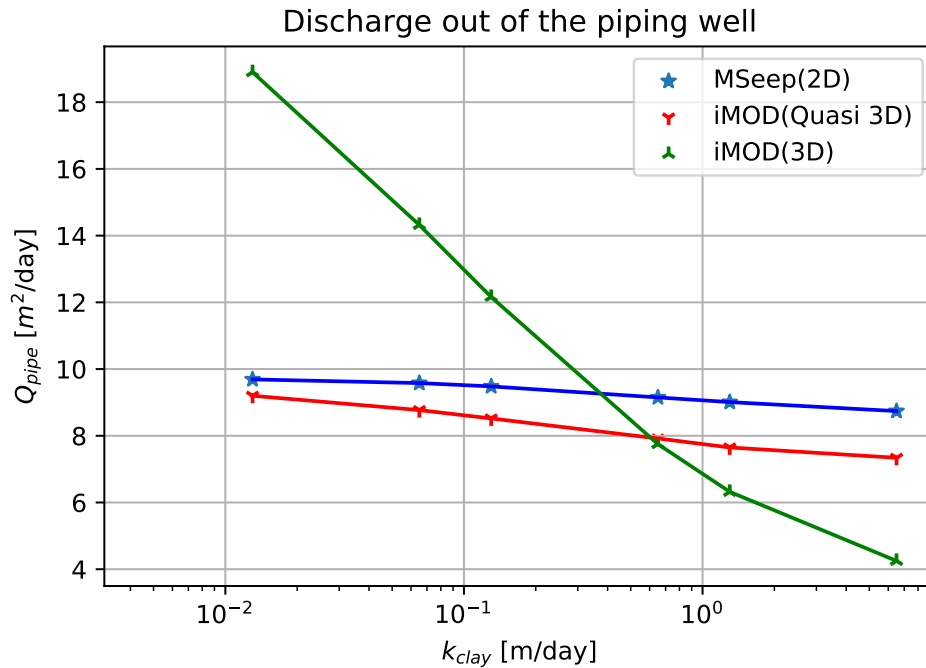


Figure 10.1: Discharge through the well for the 3 different models (2D, quasi 3D and 3D)

10.3. How can leakage be included in Sellemeijer's design rule?

In order to answer this question, the focus will be on the results and the analysis of the MSeep simulations. Since this model has also been used by Sellmeijer himself during calibration of his model.

In the Engineering Approach, the goal was to determine if leakage can be included in Sellmeijer's design rule. In order to do this, the focus was on the results of the geometry factor. From the analysis it can be concluded that there is a linear relation between the results of the six scenarios and that this linear relation is largely dependent on the hydraulic conductivity of the cover layer. In order to derive this term additional simulations should be done where the hydraulic conductivity of the aquifer and the thickness of the cover layer are also varied.

From the analysis done in the Physics Approach, it can be concluded that the effect of leakage on groundwater flow can be captured by determining the effective depth. However, implementation of this in Sellmeijer's design rule would be very difficult. Since, Sellmeijer's design rule is fit on simulations without leakage and for a total aquifer thickness. Implicitly Sellmeijer already accounts for an effective depth in his design rule. Unfortunately Sellmeijer's design rule is derived for a situation where the cover layer is impermeable. Therefore, in order for leakage to be included in his design rule thousands more MSeep simulations need to be done to which the new geometry factor (design rule) needs to be fit.

10.4. Concluding remarks

In this report, it was found that leakage has a positive effect on the critical hydraulic gradient for pipe progression. From the analysis of groundwater, both in 2D and 3D, it was observed that leakage effects the streamlines in the aquifer. This change in streamlines is quantified with the use of an effective depth in 2D and an effective depth and width in 3D.

In the full 3D simulations it was observed that the difference in discharge between the most leaky scenario and the least leaky scenario was substantially larger than the difference in discharge for the 2D simulations. Furthermore, it can be argued that the increase in the critical hydraulic head as a result of a leaky layer, in actuality, may be larger than computed using the 2D model. Meaning that a larger increase in the critical hydraulic gradient for pipe progression due to leaky layers can be expected.

11

Recommendations

From the 3D simulations, it has been observed that by accounting for the effect of the hydraulic conductivity of the cover layer on the groundwater flow, it appears that not only favourable scenarios arise but also unfavourable scenarios (Figure 11.1). Further research is recommended in order to determine if these unfavourable scenarios impact the piping process or if these scenarios have already been included in the calibration of Sellmeijer's design rule.

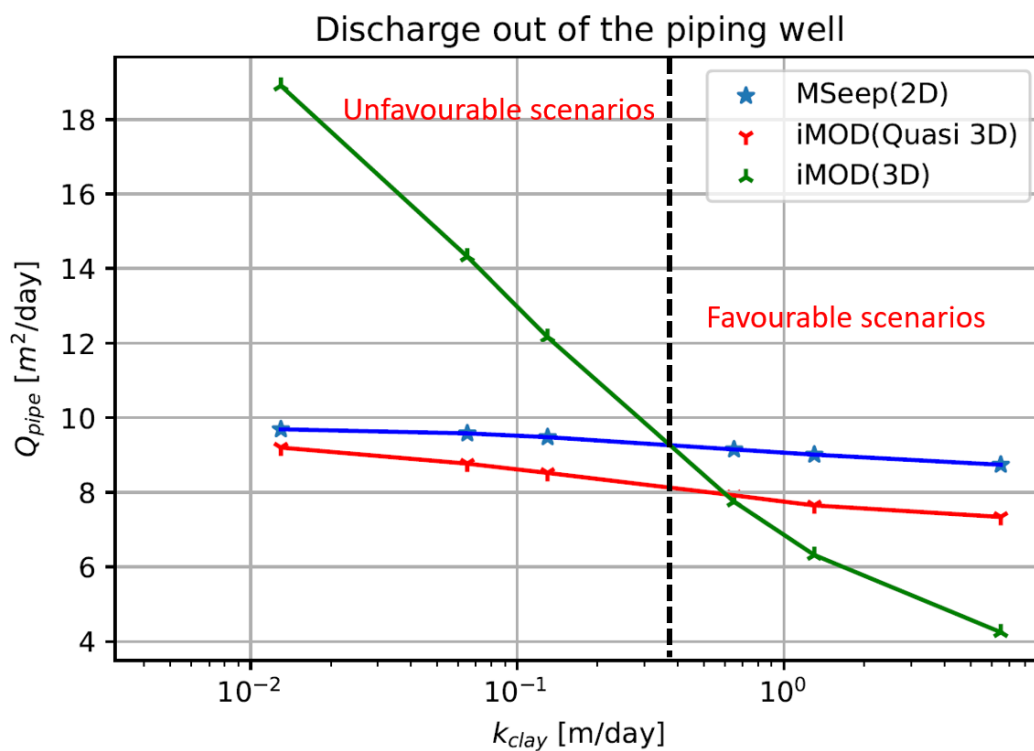


Figure 11.1: Discharge through the well for the 3 different models (2D, quasi 3D and 3D)

Next, it is recommended to determine if these favourable scenarios indeed represent realistic cases. Since in this thesis a relatively large range in hydraulic conductivities of the cover layer were used. Ranging from clay soils, to loamy soils and finally to fine grained sand.

In this thesis, a simple configuration for a pipe was implemented. A pipe was modelled using a number of cells placed horizontally with a fixed height, width, length and constant hydraulic conductivity. An analysis on a number of different pipe configurations is recommended, where the dimensions of the pipe are also varied as well as the hydraulic conductivity of the pipe.

Bibliography

- Adam Bezuijen. The influence of the leakage length on the initiation of backward erosion piping. In *25th Meeting of the European Working Group on Internal Erosion*, pages 88–96, Delft, 2017.
- W. G. Bligh. Dams, barages and weirs on porous foundations. *Engineering News*, 64(26):708—710, 1910.
- E. O. F. Calle, H. Best, J. B. Sellmeijer, and J. B. A. Weijers. Probabilistic analysis of piping underneath water retaining structures. Technical report, 1989.
- Henry Philibert Gaspard Darcy. *Les Fontaines publiques de la ville de Dijon. Exposition et application des principes à suivre et des formules à employer dans les questions de distribution d'eau*. V. Dalamont, Paris, 1856.
- H. T. J. de Bruijn. Het pipingproces in stripvorm. page 26, 2013.
- J. M. de Wit, J. B. Sellmeijer, and A Penning. Laboratory testing on piping. *Soil mechanics and foundation engineering*, pages 517–520, 1981.
- Deltares. Dijkontwerp tegen Sijperosie met MSeep Versie 7, 2005.
- Deltares. WTI 2017 Toetsregels Kunstwerken. Technical report, Deltares, 2017a.
- Deltares. MSeep Two dimensional stationary groundwater flow. Technical report, Delft, 2017b.
- Deltares. D-Geo Flow, 2018.
- Jules Étienne Juvénal Dupuit. *Études Théoriques et Pratiques sur le Mouvement des Eaux dans les Canaux Découverts et à Travers les Terrains Perméables*. Paris, 1863.
- Ulrich Förster, Geeralt van den Ham, Ed Calle, and Gerard Kruse. Onderzoeksrapport Zandmeevorende Wellen. Technical report, Deltares, Rijkswaterstaat, 2012.
- Ullrich Karl Hanses. *Zur Mechanik der Entwicklung von Erosionskanälen in geschichtetem Untergrund unter Stauanlagen*. Technical University of Berlin, Berlin, 1985.
- G. J. C. M. Hoffmans. Shields-Darcy model. Alternative piping model? Technical report, 2014.
- G. J. C. M. Hoffmans and Leo Van Rijn. Hydraulic approach for predicting piping in dikes. *Journal of Hydraulic Research*, 56(2):268–281, 2018. ISSN 00221686. doi: 10.1080/00221686.2017.1315747.
- S. B. Hooghoudt. Bijdragen tot de kennis van eenige natuurkundige grootheden van den grond: Algemeene beschouwing van het probleem van de detailontwatering en de infiltratie door middel van parallel loopende drains, greppels, slooten en kanalen. Technical report, Algemeene Landsdrukkerij, 1940.
- Han Knoeff, J. B. Sellmeijer, J. Lopez, and S. Luijendijk. SBW Piping - Hervalidatie piping. 2009.
- K. S. Lam. KPP Piping - doorlatendheid deklaag: eindrapport. Technical report, 2019.
- Emory Wilson Lane. Security from under seepage masonry dams on earth foundations. *Transactions of ASCE*, 100:1234–1351, 1935.
- David Lonsdale. *Spatial Variability in the Piping Failure Mechanism of Dikes*, volume 64. 2001. ISBN 9789461860880.

- J.P. Mazure. Kwel en chloor beheer in de Wieringermeer. *Geo-hydrologische gesteldheid van de Wieringermeer (Seepage and chlorine issues in the Wieringermeer. Geo-hydrological condition of the Wieringermeer), Rapporten en Mededeelingen betreffende de Zuiderzeewerken. Algemeene Landsdrukkerij, Den Haag, The Neth*, page 131, 1936.
- D Miesel. Rückschreitende erosie unter bindiger Deckschicht. *Baugrundtagung Berlin*, 1978.
- H Müller-Kirchenbauer, M Rankl, and C Schlötzer. Mechanism for regressive erosion beneath dams and barrages. In *Proceedings of the First International Conference on Filters in Geotechnical and Hydraulic Engineering*, pages 369–376. 1993.
- Bryant A. Robbins and Vera M. van Beek. Backward erosion piping: A historical review and discussion of influential factors. *Association of State Dam Safety Officials, Dam Safety 2015*, (June 2017), 2015.
- J. B. Sellmeijer. On the mechanism of piping under impervious structures. Technical report, 1988. URL [http://repository.tudelft.nl/assets/uuid:7f3c5919-1b37-4de9-a552-1f6e900eeaad/TRdiss1670\(1\).pdf](http://repository.tudelft.nl/assets/uuid:7f3c5919-1b37-4de9-a552-1f6e900eeaad/TRdiss1670(1).pdf).
- J. B. Sellmeijer. Numerical computation of seepage erosion below dams (piping). *Proceedings Third International Conference on Scour and Erosion*, pages 596–601, 2006. ISSN 2049-0992. doi: 10.1352/1934-9556-50.3.243.
- J. B. Sellmeijer and M. A. Koenders. A mathematical model for piping. *Topics in Catalysis*, 15(11-12): 646–651, 1991. ISSN 0307904x. doi: 10.1016/S0307-904X(09)81011-1. URL [http://dx.doi.org/10.1016/S0307-904X\(09\)81011-1](http://dx.doi.org/10.1016/S0307-904X(09)81011-1).
- J. B. Sellmeijer, E. O. F. Calle, and J. W. Sip. Influence of Aquifer thickness on piping below dikes and dams. In *International Symposium on Analytical Evaluation of dam related safety problems*, pages 357–366, Copenhagen, 1989.
- J.B. Sellmeijer, Juliana López de la Cruz, Vera M. van Beek, and Han Knoeff. Fine-tuning of the backward erosion piping model through small-scale, medium-scale and ijkdiik experiments. *European Journal of Environmental and Civil Engineering*, 15(8):1139–1154, 2011. ISSN 19648189. doi: 10.1080/19648189.2011.9714845.
- F. Silvis, J. B. Sellmeijer, and P. Lubking. Verificatie piping model Proeven in de Deltagoot. Technical report, 1991.
- TAW. Technisch Rapport Waterspanningen bij dijken. Technical Report september, 2004.
- Karl Terzaghi. Der grundbruch an stauwerken und seine verhutung. *Wasserkraft*, 17:445–449, 1922.
- USACE. Design and Construction of Levees, EM 1110-2-1913. (March 1978):164, 2000. URL http://www.publications.usace.army.mil/Portals/76/Publications/EngineerManuals/EM_{ }1110-2-1913.pdf.
- Vera van Beek, H. M. van Essen, Kristine Vandenboer, and Adam Bezuijen. Developments in modelling of backward erosion piping. *Géotechnique*, 65(9):740–754, 2015.
- Vera M. van Beek and G. J. C. M. Hoffmans. Evaluation of Dutch backward erosion piping models and a future perspective Evaluation of Dutch backward erosion piping models and a future. *European Working Group on Internal Erosion*, pages 97–113, 2017.
- Vera M. van Beek, Han Knoeff, and Timo Schweckendiek. Piping: Over 100 years of experience. Technical report, 2011a.
- Vera M. van Beek, Han Knoeff, and J. B. Sellmeijer. Observations on the process of backward erosion piping in small-, medium- and full-scale experiments. *European Journal of Environmental and Civil Engineering*, 15(8):1115–1137, 2011b. ISSN 19648189. doi: 10.1080/19648189.2011.9714844.
- Vera M. van Beek, Adam Bezuijen, and J. B. Sellmeijer. Backward Erosion Piping. *Erosion in Geomechanics Applied to Dams and Levees*, pages 193–269, 2013. doi: 10.1002/9781118577165.ch3.

- J. M. van Esch. WTI 2017 : Toetsregel piping Validation piping module DgFlow. Technical report, Deltares, 2015.
- J. M. van Esch, J. B. Sellmeijer, and D. Stolle. Modelling transient Groundwater Flow and Piping under Dikes and Dams. *Comgeo Iii*, (1):1–27, 2012.
- H. M. van Essen, W Canning, and Vera M. van Beek. Research and Development of Flood Defense Assessment Tools for Piping in WTI 2017 - Report 12. Heterogeneity. Technical report, Deltares, 2014.
- K. Vandenboer, V. M. van Beek, and A. Bezuijen. 3D character of backward erosion piping. *Geotechnique*, 68(1):86–90, 2018. ISSN 17517656. doi: 10.1680/jgeot.16.P.091.
- Kristine Vandenboer, Vera M. van Beek, and Adam Bezuijen. 3D finite element method (FEM) simulation of groundwater flow during backward erosion piping. *Frontiers of Structural and Civil Engineering*, 8(2):160–166, 2014. ISSN 20952449. doi: 10.1007/s11709-014-0257-7.
- P.T.M Vermeulen, F.J. Roelofsen, L.M.T Burgering, and J Verkaik. iMOD User Manual. 3304(January): 1–148, 2012.
- A. Verruijt. *Theory of Groundwater Flow*. Macmillan, New York, 1970.
- J. K. Vrijling, M. Kok, E. O. F. Calle, W. G. Epema, M. T. van der Meer, P. van den Berg, and T. Schweckendiek. Realiteit of Rekenfout ? 2010.
- J B A Weijers and J.B. Sellmeijer. A new model to deal with the piping mechanism. *Filters in Geotechnical and Hydraulic Engineering: proceedings of the first international conference "Geo-Filters"*, pages 349–355, 1993.
- C. M. White. The equilibrium of grains on the bed of a stream. *Proceedings of the Royal Society of London. Series A. Mathematical and Physical Sciences*, 174:322–338, 1940.

List of symbols

Symbol	Unit	Description
γ	-	safety factor
γ'_p	kN/m ³	volumetric weight of the sand grains
γ'_w	kN/m ³	volumetric weight of water
γ'_{wet}	kN/m ³	volumetric weight of the wetted sand grains
η	-	coefficient of White
θ/θ'	°	bedding angle
κ	m ²	intrinsic permeability of the piping sensitive sand layer
μ	Pa · s	dynamic viscosity
ν	m ² /s	kinematic viscosity
ρ_s	kg/m ³	density of the soil particles
ρ_w	kg/m ³	density of the water
τ_c	N/m ²	critical shear stress
ϕ_z	m	piezometric head directly under the cover layer
$\phi_{z,g}$	m	critical potential for which uplift can occur
ϕ_0	m	piezometric head at the bottom of the seepage screen
Φ	m	piezometric head in the slit
c	-	cluster of soil parameters
c_v	m ² /s	consolidation coefficient
C	-	surface factor
C_{creep}	-	creep factor
$C_{w,creep}$	-	weighted creep factor
D	m	thickness of the sandy aquifer
d_{cover}	m	thickness of the cover layer
d_{70}	m	particle diameter for which 70% passes through a sieve
d_{70m}	m	mean d_{70} in the small scale tests
d_c	m	is the characteristic grain size
g	m/s ²	gravitational acceleration
h_p	m	head in the polder
H	m	hydraulic head
H_c	m	critical hydraulic head
K	m/s	hydraulic conductivity
ℓ_c	m	critical length of the pipe
L	m	minimum seepage length
L_h	m	horizontal seepage length
L_v	m	vertical seepage length
m_v	m ² /kN	compression coefficient
n	-	porosity
RD	-	relative density
RD_m	-	average relative density in small scale tests (0.725)
$S_{pipe,c}$	-	hydraulic pipe gradient
$S_{sand,c}$	-	hydraulic sand gradient
t_h	s	hydrodynamic period
x_{exit}	m	exit point

A

MSeep

In this chapter, background information on a two-dimensional groundwater model known as MSeep will be given. First a general description of the model will be given, followed by the required input parameters need by the model as well as an explanation of the implemented erosion module.

A.1. General model description

The program MSeep is a model which can analyse stationary two-dimensional groundwater flow for either a cross-section in layered soil structures or for phreatic aquifers. In the *cross-section method*, an analysis is done of vertical two dimensional stationary groundwater flow in layered soil structures, accounting for all kinds of different boundary conditions; a phreatic surface and internal wells or pumps. While the *phreatic aquifer method*, assumes that the flow in the aquifer is essentially horizontal and that therefore, equipotential surfaces are vertical. For this method many different types of boundary conditions can be used.

In this thesis, the cross-section model will be used, therefore the explanation will only be given for this method. For the cross-section model, MSeep uses the Finite Element Method (FEM) to solve Laplace's differential equations for stationary ground water flow (Equation A.3). The Laplace equation for steady two-dimensional flow are based on the continuity equation and Darcy's law (Equation A.1).

$$q = -k \frac{d\phi}{dx} \quad (\text{A.1})$$

Darcy's law is valid for laminar flow (small values of the Reynolds number).

$$Re = q \frac{D}{\nu} \quad (\text{A.2})$$

$$\frac{\partial}{\partial x} \left(-k_x \frac{\partial \phi}{\partial x} \right) + \frac{\partial}{\partial y} \left(-k_y \frac{\partial \phi}{\partial y} \right) = Q \quad (\text{A.3})$$

Where:

- ϕ is the hydraulic head [m]
- ν is the kinematic viscosity of water [m^2/s]
- D is the mean particle diameter [m]
- k_x, k_y are the hydraulic conductivities in x- and y- directions [m/s]
- q is the specific discharge [m^2/s]
- Q is the discharge along the boundaries or the discharge of internal sources [m^3/s]

The positions of the phreatic surface in the cross section is unknown beforehand. MSeep iteratively calculates the phreatic surface, using two boundary conditions along the surface. The first boundary conditions is that the phreatic surface is a streamline and the second boundary condition is that the pressure is equal to the atmospheric pressure. During these iterations, for each node on the phreatic surface or seepage face, the quantity and direction of the specific discharge will be determined.

A.2. Input

MSeep has a number of basic dike configurations which can be loaded into the model. For these dike configurations, the number of different soil layers can be adjusted. For each soil layer present in the dike profile (Figure A.1), the characteristics of the soil need to be given (soil type, hydraulic permeability in both the x and y direction, the porosity, the grain size and the bedding angle) or else the model will use standard values.

Table A.1: Standard soil permeabilities in MSeep (Deltares, 2017b)

Soil type	Permeability [m/s]
gravel	0.1 - 0.01
gravel sand	0.01 - 1.0E-5
fine sand/silt	1.0E-5 - 1.0E-8
peat	0.001 - 1.0E-6
layered clay	1.0E-6 - 1.0E-9
fine clay	1.0E-8 - 1.0E-10

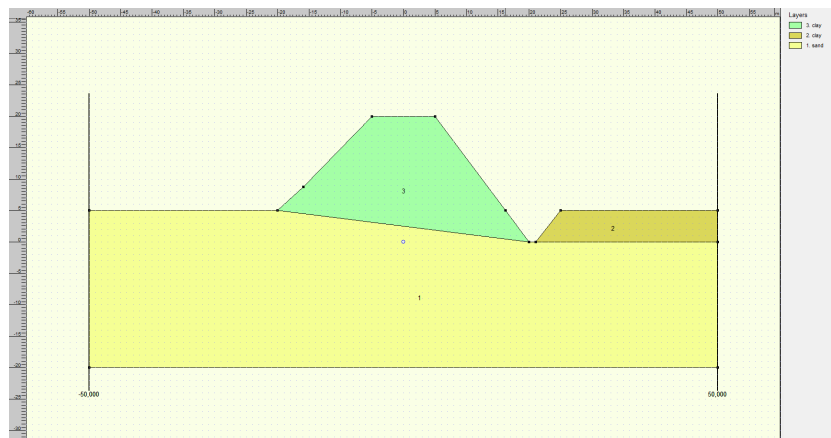


Figure A.1: Example of a dike configuration in MSeep (Source: MSeep)

For all of the different boundaries located on the edge of the construction boundary conditions need to be given. MSeep has the following different boundary condition settings:

- a *discharge boundary*
A constant discharge will be divided over all the nodes of this boundary. A positive discharge is defined as an injection well and a negative discharge as an extraction well.
- a *boundary with a potential*
Along this boundary, a fixed potential will be applied to all the nodes.
- a *phreatic or seepage boundary*
The position of the nodes will be adapted until the potential is greater than or equal to the elevation head. If the potential is less than the elevation head, the position of the node will be changed until the potential is equal to the elevation head.
- a *phreatic/closed boundary*
When the potential is greater than the elevation head, there will no seepage, in other words there can be overpressure on that boundary.
- an *overtopping boundary*
Along this boundary, all nodes get a potential equal to the elevation head.

Unfortunately, one of the main limitations of the MSeep module, is that the phreatic surface can never drop through a boundary layer as a result, of the mesh being adapted (Deltares, 2017b).

A.3. Grid

Once the cross-section has been generated, the grid needs to be formed. For horizontal layers, MSeep generates a rectangular grid (with nodes). This rectangular grid is further refined into a number of triangular elements. When flow velocity calculations are done, this is done for each (triangular) cell. Therefore the flow velocity is calculated at the center of gravity of the cell. For a triangle this is located at 2/3 of the height of the triangle and 1/3 of the base of the triangle.

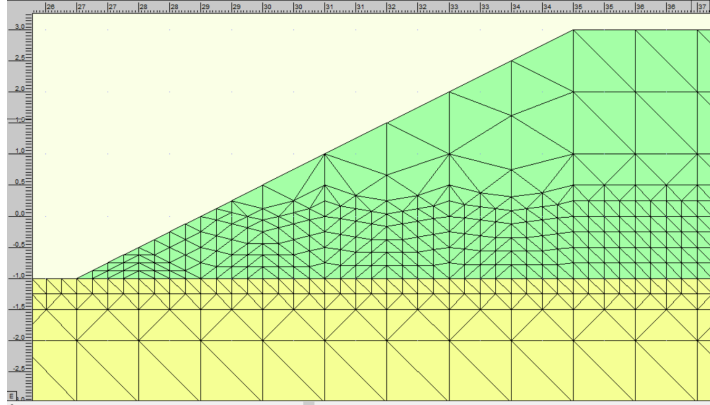


Figure A.2: Refinement of the grid near to the piping sensitive layer

For the piping calculations, a refinement of the grid has been done (Figure A.5), an extra node has been added (-1.25 m) between -1.0 and -1.5 meters. In this grid, discharges will be calculated at the nodes and flow velocities will be calculated at the centres of gravity of the cells (-1.1667 m, 2/3 between -1.0 m and -1.25 m)

A.4. Erosion module

In the erosion module, the critical hydraulic gradient for pipe progression can be calculated. Here the boundary condition for the erosion of grain is calculated. In the erosion module both a heave and piping input can be given. In the model, it has been assumed that the pipe progresses horizontally along the sand clay boundary.

MSeep uses the 2006 version of the design rule by Sellmeijer (Equation A.5, Equation A.6, Equation A.7).

$$\frac{H_c}{L} = F_R F_S F_G \quad (\text{A.4})$$

$$F_R = \eta \frac{\gamma'_p}{\gamma_w} \tan \theta \quad (\text{A.5})$$

$$F_S = \frac{d_{70}}{\sqrt[3]{\kappa L}} \quad (\text{A.6})$$

$$F_G = 0.91 \left(\frac{D}{L} \right)^{\frac{0.28}{2.8} + 0.04} \quad (\text{A.7})$$

Before the piping calculation can be done, the model requires a few extra input parameters of the sandy aquifer; the porosity, the characteristic grain size and the volumetric weight of the sand. Next both the exit point and entrance point need to be determined. Lastly a safety factor for the heave gradient needs to be supplied (a value of 0.5 is often used because this is stated in the Leidraad Rivierdijken). Once all of the input parameters have included, the calculation can start. MSeep calculates both the hydraulic head as well as the pipe length. However, currently only the hydraulic head has been validated. While the length of the pipe corresponding to a specific hydraulic head has not been validated.

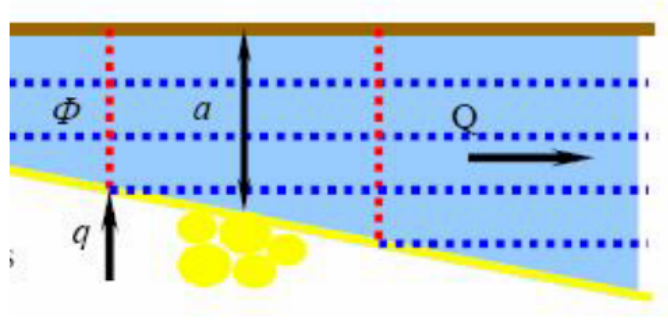


Figure A.3: Flow in the erosion channel (Deltares, 2005)

In the erosion channel of the pipe, the flow is assumed to be viscous. In the channel, the height of the channel changes over the length of the pipe. From the base of the channel water flows into the pipe, resulting in a larger discharge through the pipe. The flow of water through the pipe is assumed to be laminar (since the Reynolds number is still significantly small) and as a result, the laminar stationary Navier-Stokes equations can be used (Equation A.8). Once these equations are solved for a channel with a small height, the solutions is similar to the Poisseuille formula.

$$\begin{aligned}\frac{\partial \phi}{\partial x} &= \frac{\nu}{g} \left(\frac{\partial^2 u}{\partial x^2} + \frac{\partial^2 u}{\partial y^2} \right) \\ \frac{\partial \phi}{\partial y} &= \frac{\nu}{g} \left(\frac{\partial^2 v}{\partial x^2} + \frac{\partial^2 v}{\partial y^2} \right)\end{aligned}\tag{A.8}$$

Where:

- ν is the kinematic viscosity [m²/s]
- u, v are flow velocities in x and y direction [m/s]

In the Poisseuille formula, two quantities are of importance, the continuity of the discharge and the drag force along the bottom of the channel.

The erosion module in MSeep follows the two-force equilibrium for the sand grains. The two-force assumption has been used to calculate the limit equilibrium of the sand grains. In MSeep, the preference for grain movement is by rolling, this means that a Coulumb type condition is used:

$$\frac{H}{V} = \frac{\sin(\theta + \alpha)}{\cos(\theta)}\tag{A.9}$$

Where:

- H is the force in the direction of the erosion channel
- V is the force perpendicular to the erosion channel
- Θ is the material parameter

If $H/V \sin(\theta + \alpha) / \cos(\theta)$ then the sand grain rolls away. If $H/V \sin(\theta + \alpha) / \cos(\theta)$ the grain remains stuck in the bed (Deltares, 2005).

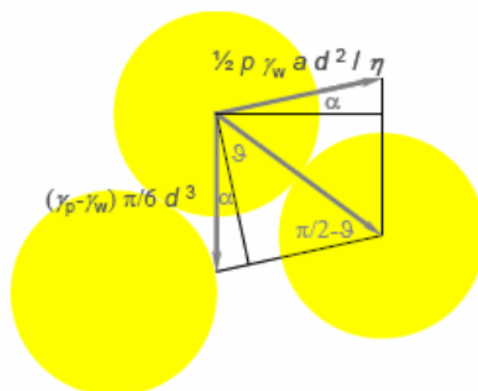


Figure A.4: Limit equilibrium of the sand grains (Deltares, 2005)

A.5. Model sensitivity

In this section the effect of the mesh size and the width ditch on the critical hydraulic head are studied.

A.5.1. Mesh size

The implemented mesh significantly affects the computational results as can be seen in Figure A.5. The finer the mesh the higher the critical hydraulic gradient (more detailed). Finer mesh sizes results in larger computations times, the user should account

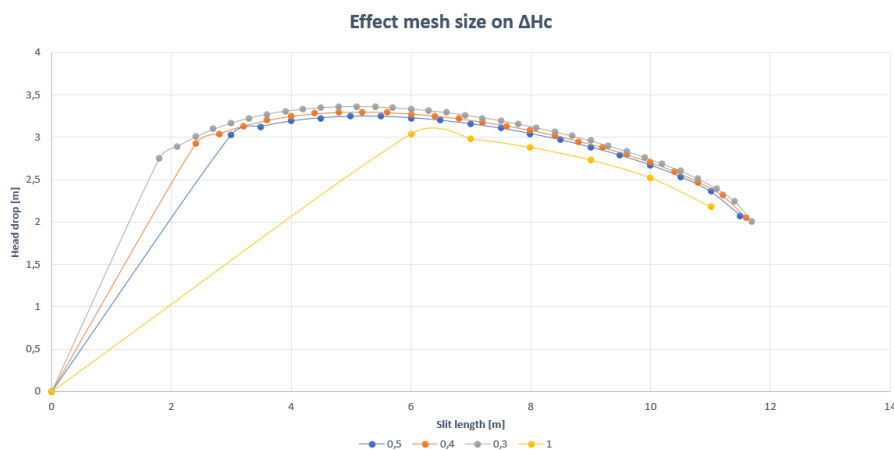


Figure A.5: Influence of the mesh size on the critical hydraulic gradient

A.5.2. Width ditch

A number of additional simulations were done where the width of the ditch was varied, to determine if this had effect on determining the effective depth. In Table A.2 the results clearly show that the side of the ditch effect the critical hydraulic head and therefore also the effective depth.

Table A.2: Effect of the ditch width on both the critical hydraulic gradient and on the effective depth

Width ditch	H_c	$D_{effective}$
1.0 m	2.135	-2.67
0.5 m	2.219	-2.83
0.1 m	2.203	-2.92

B

Delta Flume experiments: Silvis (1991)

In 1991, large-scale experiments were done in the Delta Flume. These experiments were done to validate the adapted Sellmeijer design rule (Sellmeijer 1989). Three different experiments were done. Each of these three experiments had different seepage lengths; 6 metres (test T4), 9 metres (test T2) and 12 metres (test T3). For all three of the experiments, the thickness of the sand layer is assumed to be constant. The foundation of the dike was partly constructed out of perspex, so that processes underneath the foundation could be monitored. Underneath the perspex a waterproof camera was placed, this camera was used to monitor the progress of the pipe. The water retaining structure was constructed using steel. The perspex was connected to the walls and the barrier with a water tight sheet. A ditch was created in the perspex, this was the location of the exit hole (Weijers and Sellmeijer, 1993). An overview of the experimental set-up is given in Figure B.1.

In order to simulate a finely packed sand layer, the six meter thick sand was placed in six steps, after every step, the soil was compacted. The top 0.5 metres of the sand layer (the piping sensitive layer) consisted of a well mixed combination of sand. In order to determine the hydraulic conductivity of the sandy layer, a number of different samples of the sand mixture were taken. Based on these samples, the hydraulic conductivity of the sand layer was taken to be $1.5E-4$ m/s (this was the value used in MSeep). However, before the piping test was initiated, the discharge through the sand layer was first determined, this resulted in a different value for the hydraulic conductivity. According to this test, the hydraulic conductivity was $5.11E-5$ m/s.

During the tests, the water level was increased in small increments. As the head increased, turbid water as a result of fine particles in suspension were observed. Followed by the formation of sand boils, in these boils, no sand transport was observed. Eventually sand transport in the boils were observed, resulting in the formation of a crater. Overtime, the process stopped, since an equilibrium was formed. However when the head was increased further, the piping process started up again. Lastly, it was observed that with an increasing head, an increase in the size of the boils was seen as well as an increase in the length of the pipe. The experiments in the Delta Flume were stopped once the pipe length reached half the seepage length, because, according to Sellmeijer, if $l/L > 0.5$, a further increase in water level would result in a shortening of the slit, this is physically impossible. Therefore, according to Sellmeijer, the critical hydraulic head is reached once the slit has reached half of the structure/seepage length (Sellmeijer and Koenders, 1991). The results of the piping experiments can be seen in Table B.1.

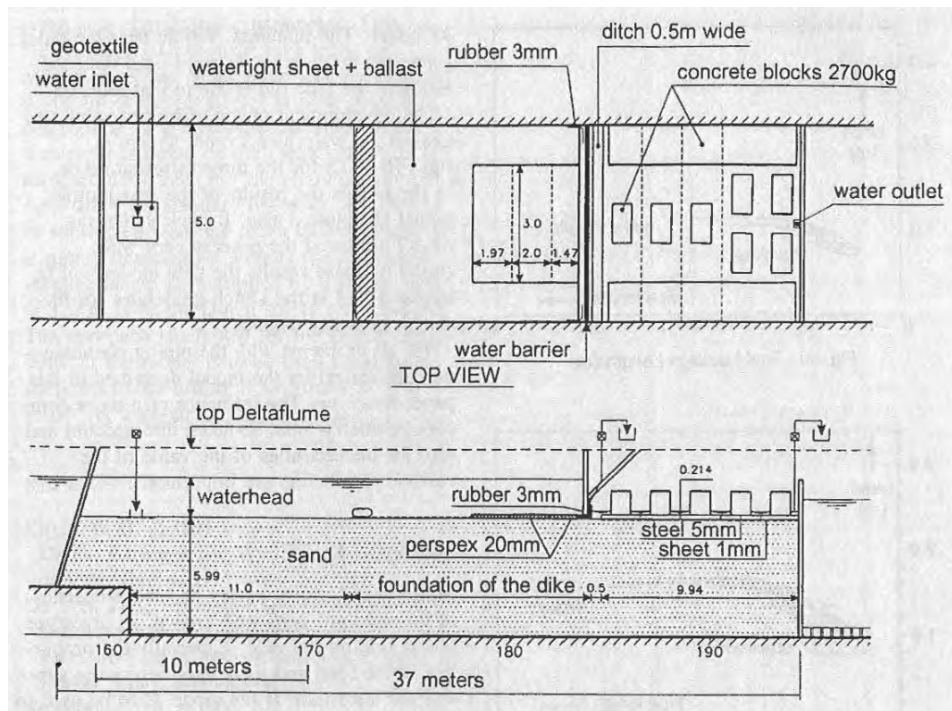


Figure B.1: Set-up of the experiments done by Silvis in the Delta Flume (Silvis et al., 1991).

Table B.1: Overview of the experimental results of the Delta Flume experiments (Silvis et al., 1991)

Test no.	Sand	L [m]	D[m]	W [m]	s[m]	RD[-]	n[-]	k [m/s]	Hi [m]	Hc [m]
T4	Marsdiep sand	6	6	5	0.5	0.65	0.38	0.000051	0.4	1.05
T2	Marsdiep sand	9	6	5	0.5	0.65	0.38	0.000051	0.8	1.69
T3	Marsdiep sand	12	6	5	0.5	0.65	0.38	0.000051	0.7	2.16

Before the piping test was initiated, the discharge through the sand layer was first determined, this resulted in a actual hydraulic conductivity of $5.11E-5$ m/s.

The results of the critical hydraulic head of the piping experiments are about a factor of 1/3 lower than the predicted critical hydraulic head according to Sellmeijers analytical model (Table B.2). According to Silvis et al. (1991), two different aspects were of importance. The first was, were the values implemented in the design rule correct. The second aspect was, whether or not the design rule was correct.

Table B.2: Overview of the experimental and analytical results of the Delta Flume experiments (Silvis et al., 1991)

Test no.	Sand	L [m]	D[m]	W [m]	H _c [m]	H _{c,MSleep} [m]
T4	Marsdiep sand	6	6	5	1.05	1.79
T2	Marsdiep sand	9	6	5	1.69	2.51
T3	Marsdiep sand	12	6	5	2.16	3.22

Most of the input parameters were thoroughly examined and determined. However, according to Silvis et al. (1991), some uncertainty exists with respect to the parameters which describe the initiation of motion of a sand grain: the coefficient of White (η) and the bedding angle (θ). Secondly, the analytical model accounts for groundwater flow in two dimensions, and according to experimental results, the pipe path is clearly three-dimensional. As a result, the discharge increases, resulting in more transport of sand grains resulting in a lower critical head for piping progression (Silvis et al., 1991). Because of this, Silvis et al. (1991) proposes a correction factor of 0.64 for the design rule by Sellmeijer. This correction factor also accounts for the uncertainty of White's coefficient and the bedding angle.

C

Groundwater and leakage

In this chapter, first an overview of some basic groundwater flow principles will be given followed by the equations used in the technical report water pressures in dikes to account for leakage.

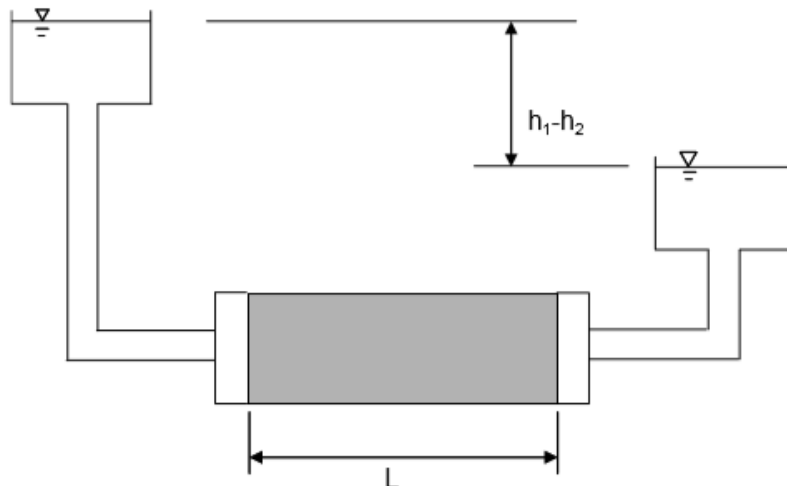


Figure C.1: Darcy's experimental set-up

Groundwater flows from areas of with high hydraulic heads to areas with lower hydraulic head. In 1856, Darcy did an experiment(Figure C.1) in which he showed that the groundwater flow is directly proportional to the difference in hydraulic head. He also observed, that the discharge though the porous medium was also proportional to the cross-sectional area of that medium. Lastly, he also observed that the discharge was inversely proportional to the length of the porous medium. As a result, Darcy (1856) came up with an empirical relation which is now referred to as Darcy's Law. This relation can be used to describe groundwater flow through a porous column (Equation C.1) and relates the specific discharge to a gradient in the piezometric head (Darcy, 1856).

$$Q_x = Dq_x = -kD \frac{\partial h}{\partial x}, \quad Q_y = Dq_y = -kD \frac{\partial h}{\partial y} \quad (C.1)$$

Where:

- A is the cross-sectional area [m²]
- h is the hydraulic head [m]
- k is the hydraulic conductivity [m/s]
- L is the length [m]

However, since the cross-section of the sub-surface is rarely known, the specific discharge (Equation C.2) is used to determine groundwater flow. Here the specific discharge is defined as the volume of water that passes through a unit surface per unit of time ([m/s]).

$$q = \frac{Q}{A} \quad (\text{C.2})$$

The specific discharge can be split up into three different vector components, q_x , q_y and q_z .

$$q_x = -k \frac{\partial h}{\partial x}, \quad q_y = -k \frac{\partial h}{\partial y}, \quad q_z = -k \frac{\partial h}{\partial z} \quad (\text{C.3})$$

If the vertical components of the flow are negligible or small, the assumptions by Dupuit can be used to simplify the solutions to the groundwater flow in aquifers. Dupuit (1863) assumes that the groundwater flow in aquifers is mainly horizontal and can be described as being a two-dimensional problem, where the piezometric head does not vary with the depth. However, in aquitards the groundwater flow is predominantly vertical, the groundwater flow between two aquifers through an aquitard can be described using Equation C.4

$$q_z = k \frac{h_2 - h_1}{H} \quad (\text{C.4})$$

Where:

- h_1 is the piezometric head in aquifer 1 [m]
- h_2 is the piezometric head in aquifer 2 [m]
- H is the thickness of the aquitard (clay) layer [m]
- k is the vertical hydraulic conductivity [m/s]
- q_z is the specific discharge in the vertical direction

Equation C.4 can be re-written as

$$q_z = \frac{h_2 - h_1}{c} \quad (\text{C.5})$$

Where, $c = H/k$ and is known as the resistance of the clay layer and has the unit time.

The equation for stationary one-dimensional groundwater flow can easily be derived by combining the continuity equation with Darcy's Law. Suppose a piece of aquifer has a length equal to Δx and a width equal to the unit width, and the groundwater recharge is equal to N (Figure C.2). According to the continuity equation for stationary groundwater flow, the volume of water leaving the cell is equal to the volume of water flowing into the cell.

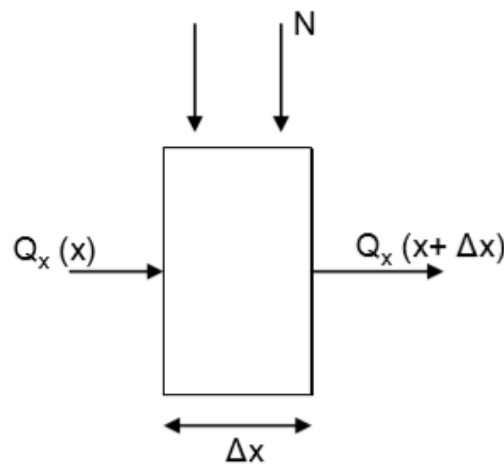


Figure C.2: Water balance for a piece of aquifer with length Δx and the width equal to the unit width

Equation C.6 shows the mass balance of the aquifer.

$$In - Uit = N\Delta x + Q_x(x) - Q_x(x + \Delta x) = 0 \quad (C.6)$$

If we divide the mass balance by Δx and take the limit of Δx as it approaches to zero, the following differential equation is left:

$$\frac{dQ_x}{dx} = N \quad (C.7)$$

If we substitute Equation C.1 into Equation C.7, we get the following differential equation:

$$\frac{d^2h}{dx^2} = -\frac{N}{kD} \quad (C.8)$$

If we assume that kD is constant, Equation C.8 becomes the Poisson equation. If the groundwater recharge is zero, then we get the Laplace equation. Which is a second order, linear ordinary differential equation. The Laplace equation is also homogeneous, and the general solution for one-dimensional groundwater flow can be written as seen in Equation C.9, where A and B are constants which needs to be determined using the boundary conditions.

$$h = Ax + B \quad (C.9)$$

C.1. Confined aquifer with no recharge

In this sections the groundwater flow for a confined aquifer will be derived. In this case, groundwater flow between two channels will be derived (Figure C.3), for a situations without groundwater recharge. The transmissivity ($T = kD$) is assumed to be constant. The following boundary conditions apply:

- $x = 0, h = h_1$
- $x = L, h = h_2$

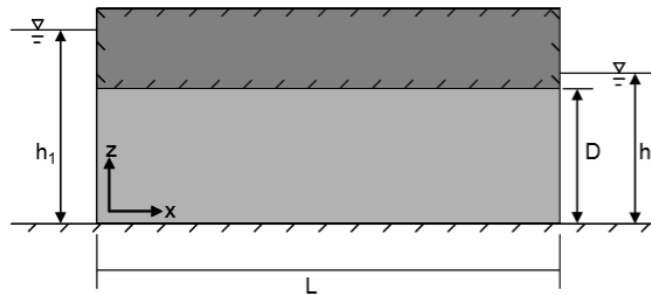


Figure C.3: Groundwater flow through a confined aquifer between two channels

By applying the above mentioned boundary conditions, the constants A and B of the homogeneous solutions can be solved resulting in a equation for the hydraulic head at a distance x from h_1 (Equation C.10). The hydraulic head will vary linearly between the two channels, since the discharge between the two channels needs to be constant.

$$h(x) = (h_2 - h_1)\frac{x}{L} + h_1 \quad (C.10)$$

The discharge through the aquifer can be determined by taking the derivative of Equation C.10 and substituting it into Equation C.1, so that :

$$Q_x = kD\frac{h_1 - h_2}{L} \quad (C.11)$$

C.2. Confined aquifer with recharge

Now a similar situation is assumed as above however, recharge does occur. Recharge is assumed to be constant and evenly distributed over the whole length. Now the Poisson equation needs to be solved. For the cases where the Poisson equation is no longer homogeneous, the particular solution needs to be found.

$$h(x) = -\frac{N}{2kD}x^2 \quad (C.12)$$

The particular solution can be added to the general solution which should be solved for the above mentioned boundary conditions resulting in Equation C.13, which is also known as the Hooghoudt equation (Hooghoudt, 1940).

$$h(x) = -\frac{N}{2kD}x^2 + \left(\frac{N}{2kD}L + \frac{h_2 - h_1}{L}\right)x + h_1 \quad (C.13)$$

According to the Hooghoudt (1940) equation, the piezometric head in the aquifer is parabolic between the two channels. If both channels have the same water level, halfway between the channels the water level in the polder is equal to $NL^2/(8kD)$ higher than the water level in the channel. For the previously mentioned situation that the water level in both channels is equal, half of the groundwater recharge will flow towards the left channel and half will flow towards the right channel. Resulting in a discharge equal to $NL/2$. However if the water level in both channels is not equal, the derivative of Equation C.13 should be substituted into Equation C.1, resulting in:

$$Q_x = N\left(x - \frac{L}{2}\right) + kD\frac{h_1 - h_2}{L} \quad (C.14)$$

C.3. Semi-confined aquifer with no recharge

In this section, a scenario which often occurs in The Netherlands will be discussed. A situation where a aquifer is covered with a semi-permeable cover layer often consisting of either peat or clay. As mentioned earlier, the specific discharge in the vertical direction through the semi-impermeable layer is described by:

$$q_z = \frac{h_2 - h_1}{c} = \frac{h - h^*}{c} \quad (C.15)$$

With:

h^* is the water level in the polder [m]

In this situation, the vertical flow through the clay layer behaves similarly to a recharge scenario. Therefore the recharge term N in Equation C.8 will be replaced with $(h - h^*)/c$, resulting in:

$$\frac{d^2h}{dx^2} = \frac{h - h^*}{kDc} \quad (C.16)$$

If the water level in the polder (h^*) is independent of x , then Equation C.16 can be re-written as:

$$\frac{d^2(h - h^*)}{dx^2} = \frac{h - h^*}{\lambda^2} \quad (C.17)$$

Where:

$$\lambda = \sqrt{kDc} \quad (C.18)$$

With:

λ is the leakage length [m]

The leakage length is defined as a "measure of the spatial distribution of leakage through one or two aquitards into a leaky layer" (Bezuijen, 2017). Now the second order linear, homogeneous differential equation is the well known Helmholtz equation. Where the general solution is:

$$h - h^* = Ae^{-x/\lambda} + Be^{x/\lambda} \quad (\text{C.19})$$

Here A and B are constant which can be solved by applying the specific boundary conditions.

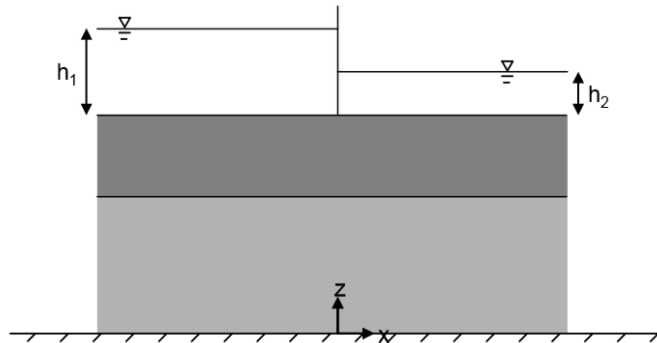


Figure C.4: Groundwater flow through a semi-confined aquifer with two different groundwater levels in the polder

For a situation as described by Figure C.4, with the origin of the axis being located in the middle between the two different polders. There is a different solution for the groundwater flow for the left polder compared to the right polder. The constants A_1 and B_1 will be used to describe the constants in the solution for the left side and A_2 and B_2 will be used for the right side. The following boundary conditions will apply:

- Far upstream (to the left) of the left polder the water level will be equal to h_1^*
- Far upstream (to the right) of the right polder the water level will be equal to h_2^*

Resulting in:

$$h(x) = h_1^* + B_1 e^{x/\lambda}, \quad x \leq 0 \quad (\text{C.20})$$

$$h(x) = h_2^* + A_2 e^{-x/\lambda}, \quad x \geq 0 \quad (\text{C.21})$$

In order to determine A_2 and B_1 , Equation C.20 should be equal to Equation C.21 at $x = 0$, resulting in Equation C.22 and Equation C.23. These equations are known as the Mazure equations.

$$h(x) = h_1^* - \frac{h_1^* - h_2^*}{2} e^{x/\lambda}, \quad x \leq 0 \quad (\text{C.22})$$

$$h(x) = h_2^* + \frac{h_1^* - h_2^*}{2} e^{-x/\lambda}, \quad x \geq 0 \quad (\text{C.23})$$

At $x = 0$, the seepage both into the clay layer and out of the clay layer is largest (kwel and wegzijging). Over a distance of three times the leakage length, less than 5 % of the maximum value (which occurs at $x = 0$) of seepage occurs.

$$q_z = \pm \frac{h_1^* - h_2^*}{2c} \quad (\text{C.24})$$

C.4. Technical report water pressures in dikes

In the technical report for water pressures in dikes (in dutch TRWD) a schematization is given on the effect of leakage on the potential in the aquifer (Figure C.5). For this situations a cover layer is located both in the foreshore and hinterland.

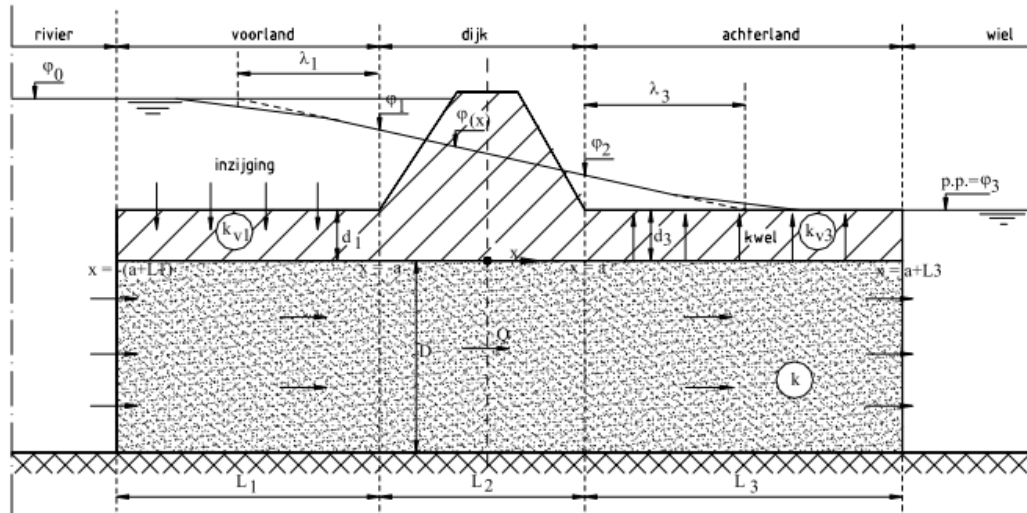


Figure C.5: Schematization of groundwater flow under a clay dike with a cover layer (TAW, 2004)

In Figure C.5 a distinction is made between the foreshore and hinterland. Both a leakage factor is determined in the fore shore and hinterland. According to the TRWD, in order to compute the potential in the aquifer at the outer toe of the dike (river side) the following equation should be used:

$$\varphi_2 = \varphi_3 + (\varphi_0 - \varphi_3) \frac{W_3}{\Sigma W} = \varphi_3 + (\varphi_0 - \varphi_3) \frac{\lambda_3 \tanh \frac{L_3}{\lambda_3}}{\lambda_1 \tanh \frac{L_1}{\lambda_1} + L_2 + \lambda_3 \tanh \frac{L_3}{\lambda_3}} \quad (C.25)$$

In order to compute the potential at the location of the inner toe, the following equation should be used:

$$\varphi_1 = \varphi_3 + (\varphi_0 - \varphi_3) \frac{W_2 + W_3}{\Sigma W} = \varphi_3 + (\varphi_0 - \varphi_3) \frac{L_2 + \lambda_3 \tanh \frac{L_3}{\lambda_3}}{\lambda_1 \tanh \frac{L_1}{\lambda_1} + L_2 + \lambda_3 \tanh \frac{L_3}{\lambda_3}} \quad (C.26)$$

With:

$$W_1 = \frac{\lambda_1}{kD} \tanh \frac{L_1}{\lambda_1} \quad (C.27)$$

$$W_3 = \frac{\lambda_3}{kD} \tanh \frac{L_3}{\lambda_3} \quad (C.28)$$

Where:

- φ is the potential at either in the foreshore or hinterland[m]
- λ is the leakage factor of the foreshore or hinterland [-]
- L is the length of the foreshore or hinterland [m]
- W is the resistance of the cover layers

D

Blanket layer theory

In the United States of America, leakage towards the hinterland is described by blanket layer theory (USACE, 2000). The seepage discharge (leakage) has been evaluated for seven different cases:

- Case 1 No cover layer
- Case 2 Impermeable cover layer both riverside and landside
- Case 3 Impermeable riverside top layer and no landside top layer
- Case 4 Impermeable landside top layer and no riverside top layer
- Case 5 Semi-permeable riverside top layer and no landside top layer
- Case 6 Semi-permeable landside top layer and no riverside top layer
- Case 7 Semi-permeable top layer both for the riverside and landside

For all of these cases, the natural seepage per unit length of the dike can be calculated using Equation D.1.

$$Q_s = \S k_f H \quad (D.1)$$

Where:

- \S is the shape factor
- k_f is the horizontal permeability of the permeable layer [m^2/d]
- H Critical head [m]

Next, the six different cases will be discussed briefly together.

Case 1: No cover layer

For this case as the name implies, the dike is located directly on top of a permeable sand layer. Both upstream and downstream of the dike a cover layer is not present. The seepage discharge can be calculated using Equation D.1 where the shape factor (\S) is:

$$\S = \frac{d}{L_2 + 0.86d} \quad (D.2)$$

Where:

- d is the thickness of the aquifer [m]
- L_2 is the width of the dike [m]

The hydraulic head landward of the dike is equal zero ($h_0 = h_x = 0$). For this case, the maximum allowable exit gradient should be 0.5.

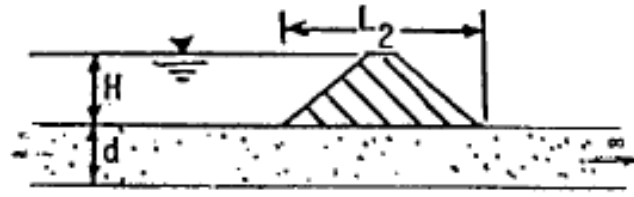


Figure D.1: Case 1:

Case 2: Impermeable cover layer both riverside and landside

This case describes a situations where a thick impermeable sub-layer ($d_{clay} > 4.58$) is present both upstream and downstream of the dike. For this situation, little or no seepage occurs through the cover layer at the land side of the dike. If the impermeable cover layer is blocked downstream of the dike, no seepage occurs under the dike and $Q_s = 0$. The potential under the dike, at the landside of the dike is equal to the net head at all points so that $H = h_0 = h_x$.

$$h_0 = H \left(\frac{L_3}{L_1 + L_2 + L_3} \right) \quad (D.3)$$

$$h_x = h_0 \left(\frac{L_3 - x}{L_3} \right) \text{ for } x \leq L_3 \quad (D.4)$$

$$h_x = 0 \text{ for } x \geq L_3 \quad (D.5)$$

However, if the cover layer in the foreland (L_1) is impermeable, and if an exit point is located landward of the dike at a distance L_3 . The distance from the landward toe of the dike towards the effective seepage entry (intrede punt) is $S = L_1 + L_2$.

$$\S = \frac{d}{L_1 + L_2 + L_3} \quad (D.6)$$

Where:

- d is the thickness of the sand layer [m]
- h_0 is the head in the sand layer at the downstream toe [m]
- h_x is the head in the sand layer at a distance x from the landward toe [m]
- L_1 is the distance from the river to the upstream toe of the dike [m]
- L_2 is the width of the base of the dike [m]
- L_3 is the length of the foundation and cover layer downstream of the inner dike toe [m]
- x_1 is the distance from the effective seepage entry to the riverside dike to [m]
- x_3 is the distance from the landward side of the dike to the effective seepage exit [m]

If the permeable sub-layer is blocked downstream of the river, no seepage occurs beneath the dike and $Q_s = 0$. The head beneath the dike and at the downstream side is equal to the net head at all points so that $H = h_0 = h_x$

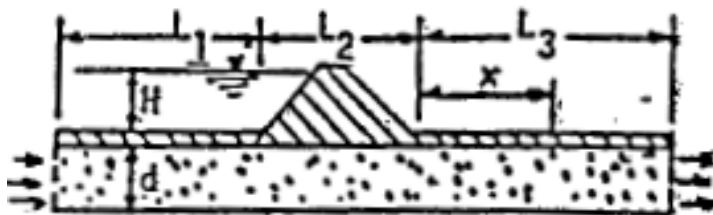


Figure D.2: Case 2:

Case 3: Impermeable riverside top layer and no landside top layer

This condition can occur naturally or due to human interventions; resulting in the removal of all impermeable material downstream of the dike for a considerable distance. Seepage can be computed using the following shape factor (Equation D.7) and Equation D.1.

$$S = \frac{d}{L_1 + L_2 + 0.43d} \quad (\text{D.7})$$

Downstream of the dike, the groundwater potential is equal to zero, and the danger from piping must be evaluated from the upward gradient determined using a flow net.

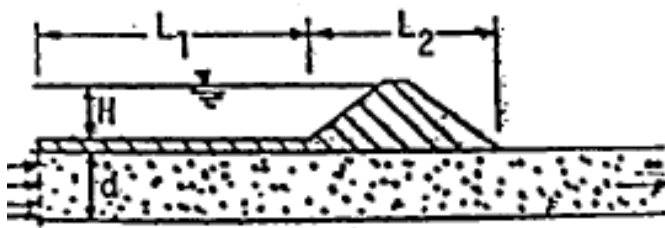


Figure D.3: Case 3:

Case 4: Impermeable landside top layer and no riverside top layer

This is a more common case than case 3, this can occur due to the erosive character of the river removing the cover layer upstream of the dike. While downstream the cover layer still exists. Seepage can be computed using the following shape factor (Equation D.8) and Equation D.1.

$$S = \frac{d}{0.43d + L_2 + L_3} \quad (\text{D.8})$$

The hydraulic heads are different and can be calculated using Equation D.9 Equation D.10.

$$h_0 = H \left(\frac{L_3}{0.43d + L_2 + L_3} \right) \quad (\text{D.9})$$

$$h_x = h_0 \left(\frac{L_3 - x}{L_3} \right) \quad (\text{D.10})$$

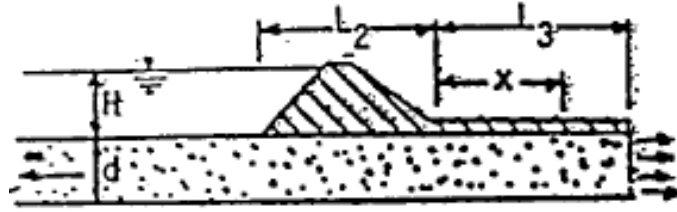


Figure D.4: Case 4:

Case 5: Semi-permeable riverside top layer and no landside top layer

For this case, the same shape factor can be used as in Case 3, provided x_1 is substituted for L_1 . Since no cover layer exists on the landward side of the dike $h_0 = h_x = 0$

$$S = \frac{d}{x_1 + L_2 + 0.43d} \tag{D.11}$$

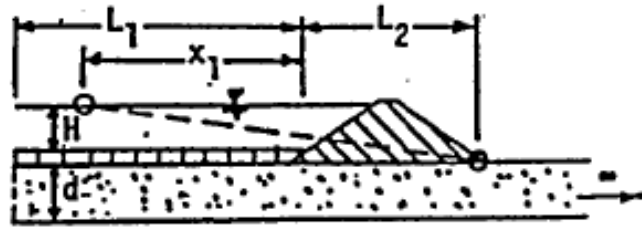


Figure D.5: Case 5:

Case 6: Semi-permeable landside top layer and no riverside top layer

The same equations can be used here as used for case 4, provided that x_3 is substituted for L_3 .

$$S = \frac{d}{0.43d + L_2 + x_3} \tag{D.12}$$

And:

$$h_0 = H \left(\frac{x_3}{0.43d + L_2 + x_3} \right) \tag{D.13}$$

$$h_x = h_0 \left(\frac{x_3 - x}{x_3} \right) \tag{D.14}$$

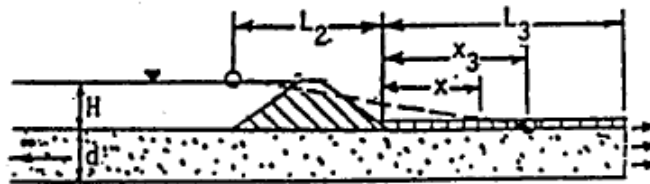


Figure D.6: Case 6:

Case 7: Semi-permeable top layer both for the river and land side

In this case, a cover layer is present both upstream and downstream of the dike. This cover layer is semipervious. The shape factor for this situation is:

$$\mathfrak{S} = \frac{d}{x_1 + L_2 + x_3} \quad (\text{D.15})$$

Where the head beneath the cover layer landward of the dike is expressed by:

$$h_0 = H \left(\frac{x_3}{x_1 + L_2 + x_3} \right) \quad (\text{D.16})$$

Landward boundary conditions

For all of the above mentioned cases where the cover layer landward of the dike is semipervious, the head (h_x) beneath the cover layer depends not only on the head h_0 , but also on conditions landward of the dike. Three of these conditions as mentioned in the USACE (2000) will be explained.

$$L_3 = \infty$$

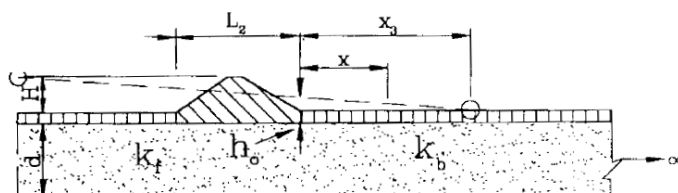


Figure D.7: Hinterland length is infinitely long

In this case, the downstream conditions are constant and enough seepage has occurred that the potential in the sand is equal to polder level (Figure D.7).

$$x_3 = \frac{1}{c \tanh(cL_3)} \quad (\text{D.17})$$

$$h_x = h_0 e^{-cx} \quad (\text{D.18})$$

$$h_x (\text{ for } x = L_y) = \frac{h_0}{\cosh cL_3} \quad (\text{D.19})$$

L_3 is finite to a seepage block

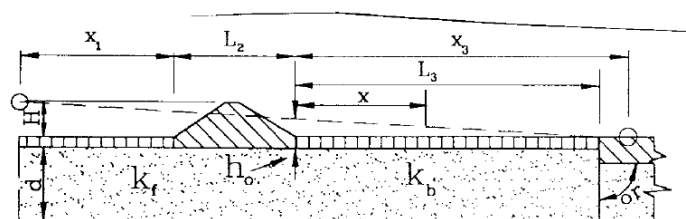


Figure D.8: Length is finite to a seepage block

In this case, downstream of the dike, over a large distance, the same cover layer is present. However, further downstream, the cover layer has become impermeable (a seepage block, Figure D.8). The hydraulic head at this location can be calculated using ??.

$$x_3 = \frac{1}{c \tanh(cL_3)} \quad (\text{D.20})$$

$$h_x = h_0 \frac{\cosh c(L_3 - x)}{\cosh cL_3} \quad (\text{D.21})$$

$$h_x \quad (\text{for } x = L_3) = \frac{h_0}{\cosh cL_3} \quad (\text{D.22})$$

L_3 is finite to an open seepage block

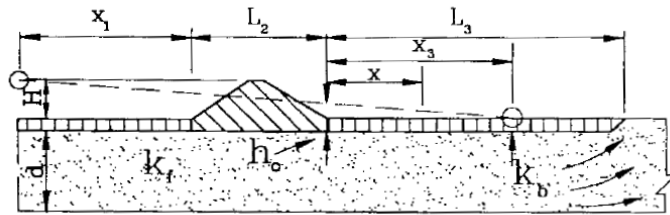


Figure D.9: Length is finite to an open seepage block

In this case, downstream of the dike, the clay cover layer does not continue over an infinite distance. Instead, the sandy aquifer is now the ground level (Figure D.9).

$$x_3 = \frac{\tanh(cL_3)}{c} \quad (\text{D.23})$$

$$h_x = h_0 \frac{\sinh c(L_3 - x)}{\sinh cL_3} \quad (\text{D.24})$$

$$h_x \quad (\text{for } x = L_3) = 0 \quad (\text{D.25})$$

E

Report: Lam (2019)

In this chapter a summary will be given of the research which has been done to determine the effect of leakage on the piping process. Recently in 2019 a report by Deltares was published which focuses on the effects of a leaky layer on the critical hydraulic head for pipe progression.

E.1. KPP Piping - permeability of the cover layer

Research has been done by Deltares, on the effect of leakage (vertical seepage; in Dutch kwel), through a cover layer on the critical hydraulic head for piping. In the report by (Lam, 2019), an comparison was made between the blanket equations used in the United States of America and the groundwater model D-GeoFlow (FEM model, with a piping module). The goal was to determine if the groundwater model, behaved similarly to the analytical equations described by the blanket theory, for specific seepage situations as well as determine if the critical hydraulic head for which piping occurs was influenced by the presence of a cover layer which was permeable. In order to do this, first two different scenarios where compared. The first scenario tested was the presence of an impermeable cover layer located downstream of the dike. The second scenario tested, was for a case where a semi-permeable cover layer is present downstream of the dike. An overview of the different scenarios which can be described by the blanket theory can be found in Appendix D. The two specific cases used in the report by Lam (2019) are Case 4 and Case 6.

These blanket equations were verified, with the use of D-GeoFlow. The groundwater potential in the aquifer was computed using D-GeoFlow and compared to the analytical solutions of the blanket equations for two basic geometries: an impermeable cover layer and a semi-permeable cover layer. The blanket equations are able to account for the presence of closed boundaries, as is used in D-GeoFlow. First the basic geometries were compared, then a number of different combinations for the basic geometry were analysed. The following variations were modelled:

- the permeability of the cover layer
- the permeability of the aquifer
- the thickness of the cover layer
- the thickness of the aquifer
- a combination of two cover layers on top of each other, the more permeable layer on top of the less permeable layer
- a combination of two cover layers on top of each other, the less permeable layer on top of the more permeable layer

According to Lam (2019), for all of the above mentioned scenarios, the blanket equations were more or less able to accurately compute the potential in the aquifer (as compared to D-GeoFlow computations). Therefore, according to Lam (2019), the blanket equations used for these two specific cases can be used to accurately determine the groundwater potential in the hinterland.

Next, the effects of a permeable cover layer on the backwards erosion process was studied. In order to do this, a situation was modelled for a uplift channel located directly downstream of the dike (at the

toe). This location was chosen, since this is the location where the highest potential in the sand layer is predicted.

The critical hydraulic head will be modelled for a situation accounting for a cover layer downstream of the ditch with a high permeability and for a situation where the cover layer is impermeable.

Next the following different variations in parameters (for standard geometries) will be modelled:

- the permeability of the cover layer
- the permeability of the aquifer
- the thickness of the cover layer
- the thickness of the aquifer
- the sediment size (d_{70})

According to (Lam, 2019), all of the model runs concluded that the presence of a cover layer with a large permeability, had a positive effect on the critical gradient for piping. This positive effect ranged between an increase of the critical hydraulic head by 1 - 10 %.

F

MSeep simulations

In this chapter, the results of the MSeep simulations can be found for the two different cases. The first case has been elaborated in the report, while the results of the second case will be given here. The second case will be used as a check with which the results of the first case can be compared to ensure that the model behaves similarly for a slightly different situation.

F.1. Case I

An analysis of the results of this case can be found in the report. In this section, an overview of the input parameters as well as the results of the MSeep simulation can be found. Table F.8 gives an overview of the input parameters for the six different scenarios simulated using MSeep.

F.1.1. Geometry

A very simplified cross-section of a dike is implemented in MSeep (Figure F.1). A dike of 20 meters wide and four meters high is placed directly on top of the aquifer. At the upstream side, the river is in direct contact with the aquifer. Downstream of the dike a cover layer consisting of permeable clay is present and has a constant thickness. A ditch of one meter wide is located at the outer toe of the dike. The exit point of the pipe is located here and it is assumed that the pipe progresses towards the river.

F.1.2. Input

Table F.1: Case I: Input parameters for the different MSeep simulations

Parameter	d_{70}	L	k_{sand}	n	θ	η	d_{clay}
Value:	200 μm	20 m	1.5E-4 m/s	0.4	37°	0.25	1 m

F.1.3. Boundary conditions

In the simulations three different sets of boundary conditions were used. Closed boundaries, phreatic/closed boundaries and boundaries with a potential. In Figure F.1 an overview is given of the different boundaries. In Table F.2 an overview is given of the boundary conditions applied at each boundary.

Table F.2: Overview of the different boundaries and their type

Boundary condition	Boundary	Color line
Closed boundary	1, 11 and 12	Black
Phreatic/closed boundary	3, 4, 5, 6 and 7	Purple
Boundary with a potential	2, 8, 9 and 10	Blue

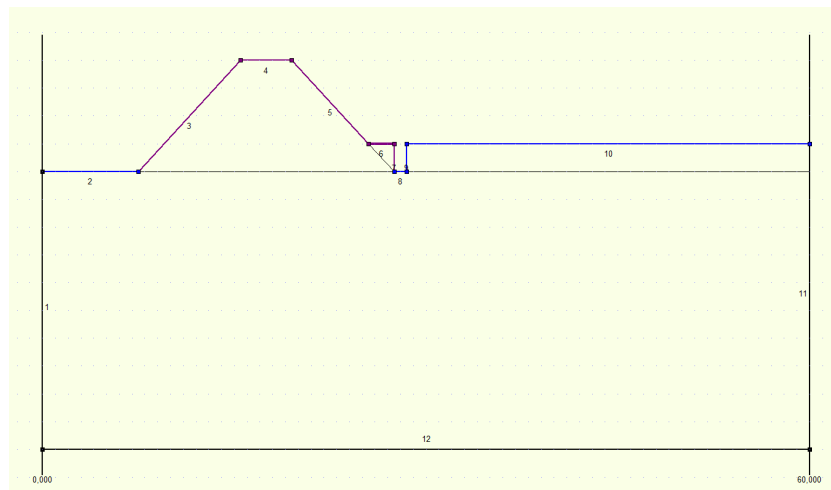


Figure F.1: Cross section of the dike showing the numbering of the different boundaries

F.1.4. Erosion

The erosion module was implemented in MSeep with a standard heave gradient of 0.5. The entrance point (intrede punt) was located directly at the inner toe of the dike. The exit point was located directly at the outer toe of the dike, resulting in a seepage length of 20 meters. The width of the ditch in which the exit point was located was equal to 1 meter.

F.1.5. Mesh size

The results of the piping simulations are dependent on the mesh size. The mesh size was chosen such that directly under the dike, the mesh is refined. At a larger depth, a more coarse mesh size was implemented. Such that the computation time of MSeep was limited. A refinement of 0.25 meters was chosen.

F.1.6. Results

Critical hydraulic head

For each scenario, twenty four different simulations have been run (for the different values of the aquifer thickness). Six different scenarios were simulated each having a different value for the hydraulic conductivity of the cover layer. The results of these simulations are summarized in Table F.3. The results are plotted in Figure F.2

Table F.3: Case I: Critical hydraulic gradient computed using MSeep for the various scenarios

D [m]	Critical hydraulic head (H_c) [m]						
	Hydraulic conductivity (k_{clay}) [m/day]						Sellmeijer DR
	0.013	0.065	0.130	0.648	1.296	6.480	2006
1	3.65	3.65	3.65	3.65	3.65	3.65	3.58
2	2.99	2.99	2.99	2.99	2.99	3.00	3.04
3	2.66	2.66	2.67	2.67	2.67	2.68	2.76
4	2.46	2.47	2.47	2.48	2.48	2.49	2.58
5	2.33	2.33	2.34	2.35	2.36	2.37	2.46
6	2.23	2.24	2.24	2.26	2.27	2.29	2.36
7	2.17	2.17	2.18	2.20	2.21	2.23	2.28
8	2.12	2.13	2.14	2.16	2.17	2.20	2.22
9	2.09	2.10	2.10	2.13	2.15	2.18	2.17
10	2.06	2.07	2.08	2.12	2.13	2.16	2.13
11	2.05	2.06	2.07	2.11	2.13	2.16	2.09
12	2.04	2.05	2.06	2.10	2.12	2.16	2.06
13	2.03	2.05	2.06	2.10	2.12	2.16	2.04
14	2.03	2.04	2.06	2.11	2.13	2.17	2.02
15	2.03	2.04	2.06	2.11	2.14	2.18	2.00
16	2.03	2.04	2.06	2.12	2.14	2.19	1.98
17	2.03	2.04	2.06	2.12	2.15	2.20	1.96
18	2.03	2.04	2.06	2.13	2.16	2.21	1.95
19	2.03	2.05	2.06	2.13	2.17	2.22	1.94
20	2.03	2.05	2.07	2.14	2.18	2.23	1.75
21	2.03	2.05	2.07	2.15	2.18	2.24	1.92
22	2.03	2.05	2.07	2.15	2.19	2.25	1.91
23	2.03	2.05	2.08	2.16	2.20	2.26	1.91
24	2.03	2.06	2.08	2.16	2.21	2.27	1.90

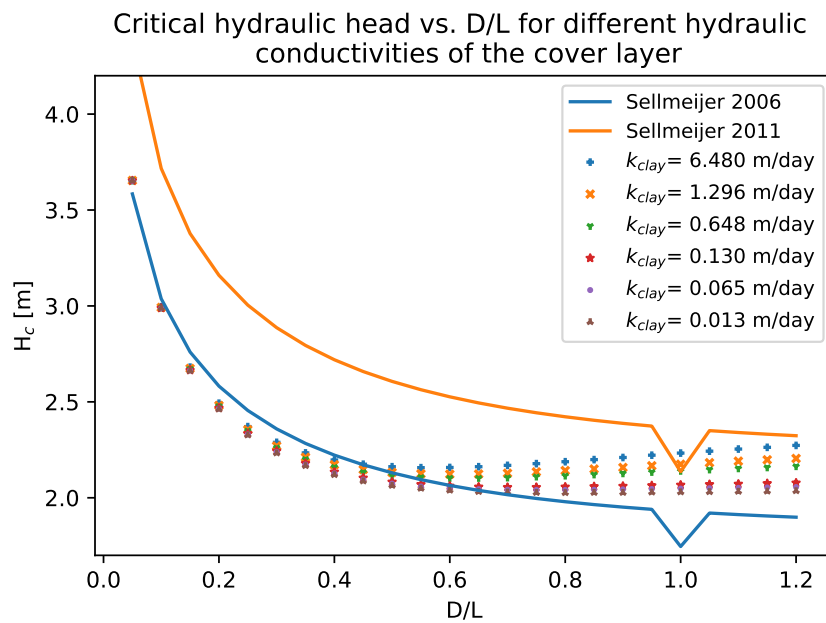


Figure F.2: Plot showing H_c vs. D/L for the different scenarios as well as the results of the 2006 version of Sellmeijer’s design rule.

Geometry factor

Table F.4 gives the results of the geometry factor computed from the MSeep simulations and using

Sellmeijer’s design rule. These results are plotted in Figure F.3.

Table F.4: Case I: Geometry factor for the computed critical hydraulic heads in MSeep for the various scenarios

D [m]	Geometry factor (F_g) [m]						Sellmeijer DR
	Hydraulic conductivity (k_{clay}) [m/day]						
	0.013	0.065	0.130	0.648	1.296	6.480	
1	1.90	1.90	1.90	1.90	1.90	1.90	1.87
2	1.56	1.56	1.56	1.56	1.56	1.56	1.58
3	1.39	1.39	1.39	1.39	1.39	1.40	1.44
4	1.28	1.28	1.29	1.29	1.29	1.30	1.35
5	1.21	1.21	1.22	1.22	1.23	1.24	1.28
6	1.16	1.17	1.17	1.18	1.18	1.19	1.23
7	1.13	1.13	1.14	1.15	1.15	1.16	1.19
8	1.10	1.11	1.11	1.13	1.13	1.15	1.16
9	1.09	1.09	1.10	1.11	1.12	1.13	1.13
10	1.08	1.08	1.09	1.10	1.11	1.13	1.11
11	1.07	1.07	1.08	1.10	1.11	1.12	1.09
12	1.06	1.07	1.07	1.10	1.11	1.12	1.08
13	1.06	1.07	1.07	1.10	1.11	1.13	1.06
14	1.06	1.06	1.07	1.10	1.11	1.13	1.05
15	1.06	1.06	1.07	1.10	1.11	1.14	1.04
16	1.06	1.06	1.07	1.10	1.12	1.14	1.03
17	1.06	1.06	1.07	1.11	1.12	1.15	1.02
18	1.06	1.07	1.07	1.11	1.12	1.15	1.02
19	1.06	1.07	1.08	1.11	1.13	1.16	1.01
20	1.06	1.07	1.08	1.12	1.13	1.16	0.91
21	1.06	1.07	1.08	1.12	1.14	1.17	1.00
22	1.06	1.07	1.08	1.12	1.14	1.17	1.00
23	1.06	1.07	1.08	1.12	1.15	1.18	0.99
24	1.06	1.07	1.08	1.13	1.15	1.18	0.99

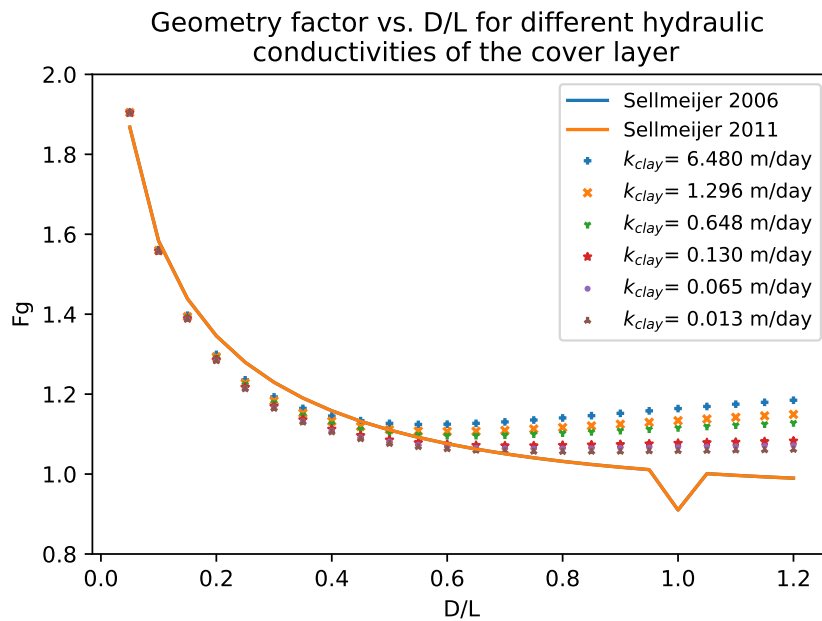


Figure F.3: Plot showing F_g vs. D/L for the different scenarios as well as the results of the 2006 version of Sellmeijer’s design rule.

Effective depth

Table F.5 gives shows the effective depths extracted from the MSeep simulations. The effective depth is plotted versus the aquifer depth in in Figure F.4.

Table F.5: Case I: Effective depth of the different simulations

D [m]	Effective depth ($D_{effective}$) [m]					
	Hydraulic conductivity (k_{clay}) [m/day]					
	6.480	1.296	0.648	0.130	0.065	0.013
1	-0.42	-0.42	-0.42	-0.42	-0.42	-0.42
2	-0.67	-0.67	-0.67	-0.67	-0.67	-0.67
3	-1.17	-1.17	-1.17	-1.17	-1.17	-1.17
4	-1.42	-1.42	-1.42	-1.42	-1.42	-1.42
5	-1.67	-1.67	-1.67	-1.67	-1.92	-1.92
6	-1.92	-1.92	-1.92	-2.17	-2.17	-2.17
7	-2.17	-2.17	-2.17	-2.42	-2.42	-2.42
8	-2.42	-2.42	-2.67	-2.67	-2.67	-2.67
9	-2.42	-2.67	-2.83	-2.92	-2.92	-3.17
10	-2.67	-2.92	-2.92	-3.17	-3.42	-3.42
11	-2.92	-3.17	-3.17	-3.42	-3.42	-3.67
12	-2.92	-3.17	-3.42	-3.67	-3.67	-3.92
13	-3.17	-3.42	-3.58	-3.92	-3.92	-4.17
14	-3.17	-3.42	-3.67	-4.08	-4.17	-4.42
15	-3.17	-3.67	-3.67	-4.17	-4.42	-4.42
16	-3.42	-3.67	-3.92	-4.42	-4.42	-4.67
17	-3.42	-3.67	-3.92	-4.42	-4.67	-4.67
18	-3.42	-3.92	-3.92	-4.67	-4.67	-4.92
19	-3.42	-3.92	-4.17	-4.67	-4.92	-4.92
20	-3.42	-3.92	-4.17	-4.67	-4.92	-5.17
21	-3.42	-3.92	-4.17	-4.92	-4.92	-5.17
22	-3.42	-3.92	-4.17	-4.92	-5.17	-5.17
23	-3.42	-3.92	-4.17	-4.92	-5.17	-5.42
24	-3.42	-3.92	-4.17	-4.92	-5.17	-5.42

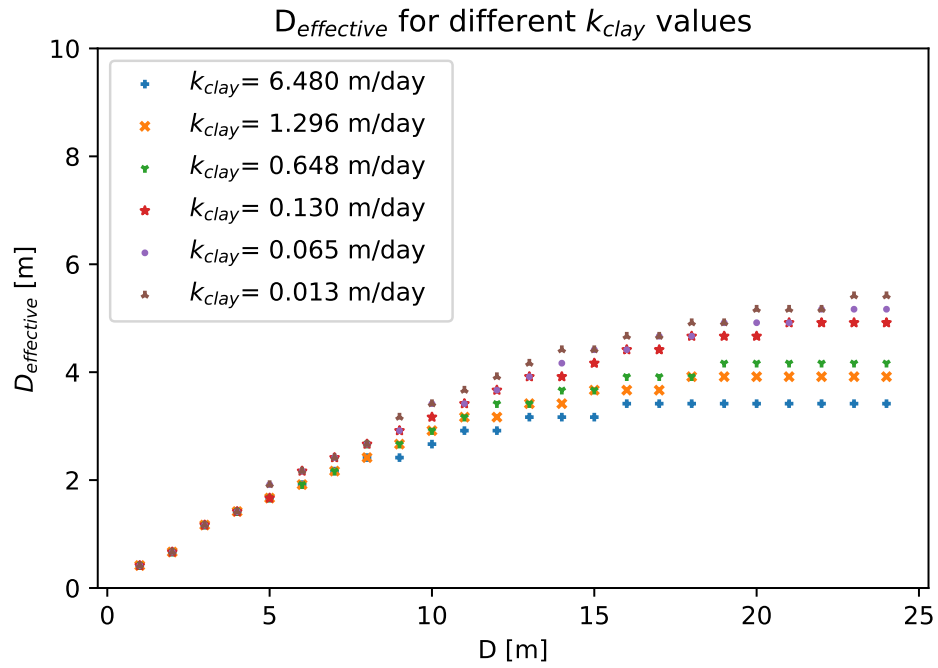


Figure F.4: Graph showing the difference in effective depth for the different scenarios(k_{clay}).

Discharge well for a pipe length of 1.5 meters

The discharge computed in MSeep for a pipe length of 1.5 meters is given in Table F.6.

Table F.6: Case I: Discharge of the well for a pipe of 1.5 meters for the various scenarios

D [m]	Discharge well (Q_{well}) [m^3/day]					
	Hydraulic conductivity (k_{clay}) [m/day]					
	6.480	1.296	0.648	0.130	0.065	0.013
1	1.88	1.88	1.88	1.88	1.88	1.88
2	2.44	2.44	2.44	2.42	2.42	2.40
3	2.72	2.71	2.70	2.68	2.66	2.63
4	2.88	2.87	2.86	2.82	2.80	2.75
5	3.00	2.98	2.96	2.92	2.89	2.83
6	3.08	3.05	3.04	2.98	2.95	2.89
7	3.14	3.11	3.09	3.03	3.00	2.92
8	3.18	3.16	3.14	3.07	3.04	2.95
9	3.22	3.20	3.18	3.10	3.06	2.98
10	3.25	3.23	3.20	3.13	3.09	3.00
11	3.28	3.25	3.23	3.15	3.10	3.01
12	3.30	3.27	3.25	3.16	3.12	3.02
13	3.31	3.29	3.27	3.18	3.13	3.03
14	3.33	3.31	3.28	3.19	3.15	3.04
15	3.34	3.32	3.30	3.20	3.15	3.05
16	3.35	3.33	3.31	3.21	3.16	3.06
17	3.36	3.34	3.32	3.22	3.17	3.06
18	3.37	3.35	3.33	3.23	3.18	3.07
19	3.38	3.36	3.33	3.23	3.18	3.07
20	3.39	3.36	3.34	3.24	3.19	3.07
21	3.39	3.37	3.34	3.25	3.19	3.08
22	3.40	3.37	3.35	3.25	3.19	3.08
23	3.40	3.38	3.35	3.25	3.20	3.08
24	3.40	3.38	3.36	3.26	3.20	3.08

Discharge well for a pipe length of 10 meters

The discharge computed in MSeep for a pipe length of 10 meters is given in Table F.7.

Table F.7: Case I: Discharge of the well for a pipe of 10 meters for the various scenarios

D [m]	Discharge well (Q_{well}) [m^3/day]					
	Hydraulic conductivity (k_{clay}) [m/day]					
	6.480	1.296	0.648	0.130	0.065	0.013
1	2.25	2.25	2.25	2.25	2.25	2.25
2	3.68	3.67	3.67	3.66	3.65	3.63
3	4.91	4.89	4.88	4.85	4.83	4.79
4	5.96	5.94	5.92	5.86	5.82	5.75
5	6.86	6.82	6.79	6.69	6.64	6.54
6	7.62	7.56	7.52	7.38	7.32	7.18
7	8.26	8.20	8.14	7.96	7.87	7.70
8	8.81	8.73	8.66	8.43	8.33	8.12
9	9.28	9.19	9.10	8.82	8.70	8.46
10	9.69	9.58	9.48	9.15	9.01	8.74
11	10.03	9.91	9.80	9.43	9.26	8.96
12	10.33	10.19	10.07	9.66	9.48	9.15
13	10.58	10.43	10.30	9.85	9.65	9.30
14	10.79	10.64	10.50	10.01	9.79	9.42
15	10.98	10.82	10.67	10.15	9.91	9.51
16	11.14	10.97	10.82	10.26	10.01	9.59
17	11.28	11.11	10.94	10.36	10.10	9.65
18	11.40	11.22	11.05	10.44	10.17	9.71
19	11.50	11.32	11.14	10.51	10.22	9.75
20	11.59	11.40	11.22	10.57	10.27	9.78
21	11.66	11.48	11.29	10.62	10.31	9.80
22	11.73	11.54	11.35	10.66	10.35	9.83
23	11.79	11.59	11.41	10.70	10.37	9.84
24	11.84	11.64	11.45	10.73	10.40	9.85

F.2. Case II

In this section, the model input and results of a second set of simulations is given.

F.2.1. Geometry

A very simplified cross-section of a dike is implemented in MSeep (Figure F.5). A dike of 40 meters wide and four meters high is placed directly on top of the aquifer. At the upstream side, the river is in direct contact with the aquifer. Downstream of the dike a cover layer consisting of permeable clay is present and has a constant thickness. A ditch of one meter wide is located at the outer toe of the dike. The exit point of the pipe is located here and it is assumed that the pipe progresses towards the river.

F.2.2. Input

Table F.8: Case I: Input parameters for the different MSeep simulations

Parameter	d_{70}	L	k_{sand}	n	θ	η	d_{clay}
Value:	200 μm	40 m	1.5E-4 m/s	0.4	37°	0.25	1 m

F.2.3. Boundary conditions

In the simulations three different sets of boundary conditions were used. Closed boundaries, phreatically closed boundaries and boundaries with a potential. In Figure F.5 an overview is given of the different boundaries. In Table F.9 an overview is given of the boundary conditions applied at each boundary

Table F.9: Overview of the different boundaries and their type

Boundary condition	Boundary	Color line
Closed boundary	1, 11 and 12	Black
Phreatic/closed boundary	3, 4, 5, 6 and 7	Purple
Boundary with a potential	2, 8, 9 and 10	Blue

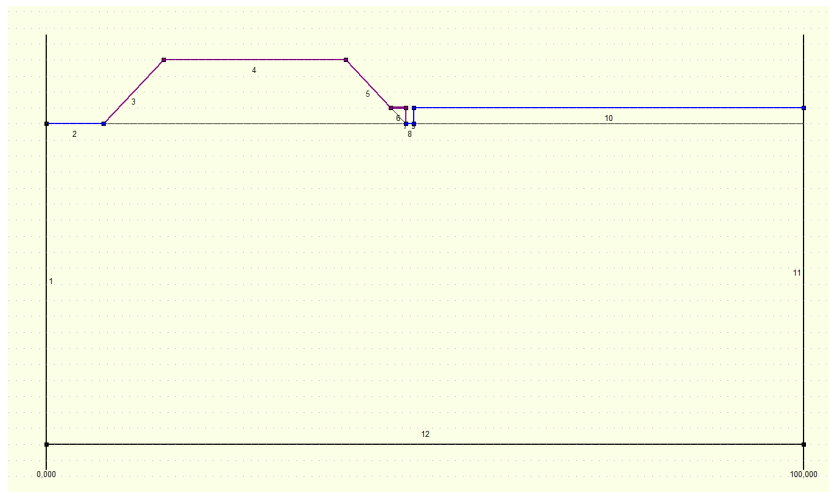


Figure F.5: Cross section of the dike showing the numbering of the different boundaries

F.2.4. Erosion

The erosion module was implemented in MSeep with a standard heave gradient of 0.5. The entrance point (intrede punt) was located directly at the inner toe of the dike. The exit point was located directly at the outer toe of the dike, resulting in a seepage length of 40 meters. The width of the ditch in which the exit point was located was equal to 1 meter. A mesh size of 0.5 meters was used.

F.2.5. Mesh size

The results of the piping simulations are dependent on the mesh size. The mesh size was chosen such that directly under the dike, the mesh is refined. At a larger depth, a more coarse mesh size was implemented. Such that the computation time of MSeep was limited.

F.2.6. Results

Critical hydraulic head

For each scenario, twenty four different simulations have been run (for the different values of the aquifer thickness). Six different scenarios were simulated each having a different value for the hydraulic conductivity of the cover layer. The results of these simulations are summarized in Table F.10. The results are plotted in Figure F.6.

Table F.10: Case II: Critical hydraulic gradient computed using MSeep for the various scenarios

D [m]	Critical hydraulic head (H_c) [m]						
	Hydraulic conductivity (k_{clay}) [m/day]						Sellmeijer DR
	0.013	0.065	0.130	0.648	1.296	6.480	
2	6.05	6.05	6.05	6.05	6.05	6.05	5.69
4	4.90	4.91	4.91	4.92	4.93	4.94	4.82
6	4.35	4.36	4.36	4.38	4.39	4.41	4.38
8	4.02	4.04	4.05	4.07	4.09	4.11	4.10
10	3.82	3.84	3.85	3.88	3.90	3.93	3.90
12	3.69	3.71	3.73	3.77	3.79	3.83	3.74
14	3.61	3.64	3.65	3.70	3.73	3.77	3.62
16	3.57	3.59	3.61	3.67	3.70	3.75	3.53
18	3.55	3.57	3.60	3.67	3.69	3.74	3.45
20	3.54	3.57	3.60	3.67	3.70	3.76	3.38
22	3.54	3.57	3.60	3.69	3.72	3.78	3.33
24	3.55	3.58	3.62	3.71	3.75	3.81	3.28
26	3.56	3.60	3.63	3.74	3.78	3.85	3.24
28	3.57	3.61	3.65	3.76	3.81	3.88	3.20
30	3.58	3.62	3.66	3.79	3.84	3.92	3.17
32	3.59	3.64	3.68	3.82	3.87	3.95	3.14
34	3.60	3.65	3.70	3.84	3.90	3.99	3.12
36	3.61	3.66	3.71	3.87	3.93	4.02	3.10
38	3.62	3.67	3.72	3.89	3.95	4.05	3.08
40	3.62	3.68	3.74	3.91	3.98	4.08	2.77
42	3.63	3.69	3.75	3.93	4.00	4.10	3.05
44	3.64	3.70	3.76	3.94	4.02	4.13	3.04
46	3.64	3.71	3.76	3.96	4.04	4.15	3.02
48	3.65	3.71	3.77	3.97	4.05	4.17	3.01

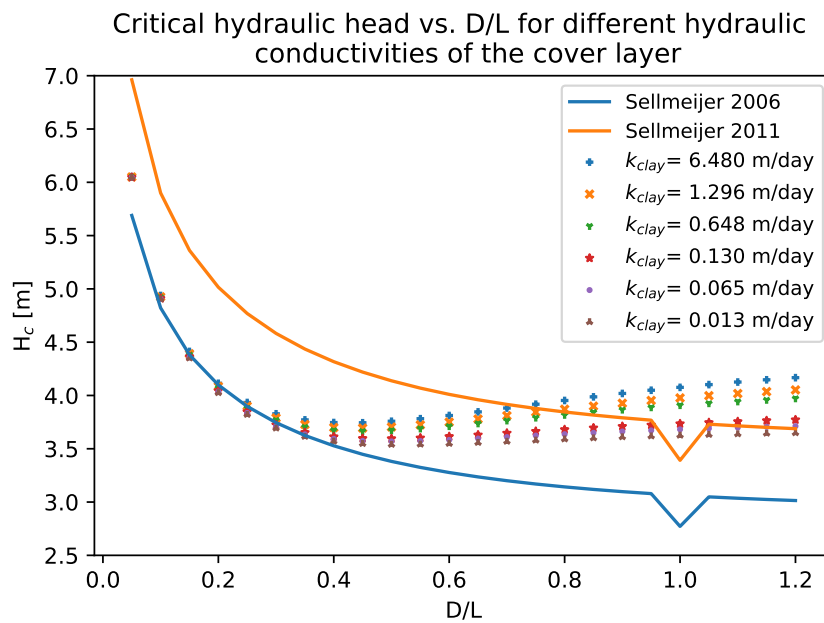


Figure F.6: Plot showing H_c vs. D/L for the different scenarios as well as the results of the 2006 version of Sellmeijer’s design rule.

Geometry factor

Table F.11 gives the results of the geometry factor computed from the MSeep simulations and using

Sellmeijer’s design rule. These results are plotted in Figure F.7.

Table F.11: Case II: Geometry factor for the computed critical hydraulic heads in MSeep for the various scenarios

D [m]	Geometry factor (F_g) [m]						
	Hydraulic conductivity (k_{clay}) [m/day]						Sellmeijer DR
	0.013	0.065	0.130	0.648	1.296	6.480	
2	1.98	1.99	1.99	1.99	1.99	1.99	1.87
4	1.61	1.61	1.61	1.62	1.62	1.62	1.58
6	1.43	1.43	1.43	1.44	1.44	1.45	1.44
8	1.32	1.33	1.33	1.34	1.34	1.35	1.35
10	1.25	1.26	1.26	1.27	1.28	1.29	1.28
12	1.21	1.22	1.22	1.24	1.24	1.26	1.23
14	1.19	1.19	1.20	1.22	1.22	1.24	1.19
16	1.17	1.18	1.19	1.21	1.21	1.23	1.16
18	1.16	1.17	1.18	1.20	1.21	1.23	1.13
20	1.16	1.17	1.18	1.21	1.22	1.23	1.11
22	1.16	1.17	1.18	1.21	1.22	1.24	1.09
24	1.16	1.18	1.19	1.22	1.23	1.25	1.08
26	1.17	1.18	1.19	1.23	1.24	1.26	1.06
28	1.17	1.19	1.20	1.24	1.25	1.27	1.05
30	1.17	1.19	1.20	1.24	1.26	1.29	1.04
32	1.18	1.19	1.21	1.25	1.27	1.30	1.03
34	1.18	1.20	1.21	1.26	1.28	1.31	1.02
36	1.18	1.20	1.22	1.27	1.29	1.32	1.02
38	1.19	1.21	1.22	1.28	1.30	1.33	1.01
40	1.19	1.21	1.23	1.28	1.31	1.34	0.91
42	1.19	1.21	1.23	1.29	1.31	1.35	1.00
44	1.19	1.21	1.23	1.29	1.32	1.35	1.00
46	1.20	1.22	1.24	1.30	1.33	1.36	0.99
48	1.20	1.22	1.24	1.30	1.33	1.37	0.99

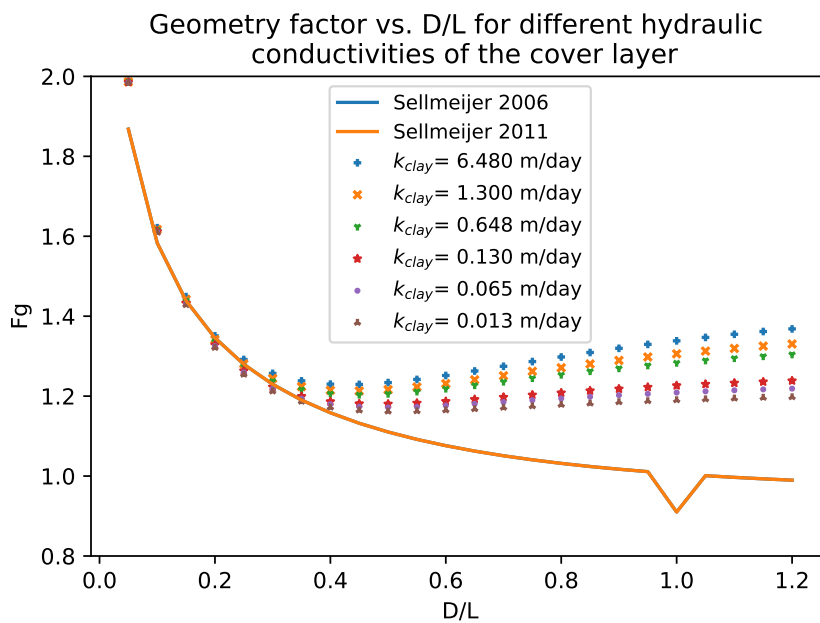


Figure F.7: Plot showing F_g vs. D/L for the different scenarios as well as the results of the 2006 versions of Sellmeijer’s design rule.

Effective depth

Table F.12 gives shows the effective depths extracted from the MSeep simulations. The effective depth is plotted versus the aquifer depth in in Figure F.8.

Table F.12: Case II: Effective depth of the different simulations

D [m]	Effective depth ($D_{effective}$) [m]					
	Hydraulic conductivity (k_{clay}) [m/day]					
	6.480	1.296	0.648	0.130	0.065	0.013
2	-0.67	-0.67	-0.67	-0.67	-0.67	-0.67
4	-1.33	-1.33	-1.33	-1.33	-1.33	-1.33
6	-2.17	-2.17	-2.42	-2.42	-2.42	-2.42
8	-2.67	-2.67	-2.67	-2.67	-2.67	-2.67
10	-3.42	-3.42	-3.67	-3.67	-3.92	-3.92
12	-3.67	-3.92	-4.17	-4.42	-4.42	-4.67
14	-4.17	-4.42	-4.67	-5.08	-5.17	-5.17
16	-4.67	-4.92	-5.17	-5.67	-5.67	-5.92
18	-5.08	-5.42	-5.67	-6.17	-6.42	-6.42
20	-5.42	-5.83	-6.08	-6.42	-6.83	-6.83
22	-5.67	-6.17	-6.42	-6.83	-6.83	-7.67
24	-5.92	-6.42	-6.67	-7.33	-7.67	-7.67
26	-6.08	-6.42	-6.83	-7.67	-7.67	-8.33
28	-6.17	-6.83	-6.83	-7.67	-8.33	-8.67
30	-6.42	-6.83	-6.83	-7.67	-8.67	-8.67
32	-6.42	-6.83	-7.33	-8.67	-8.67	-8.67
34	-6.42	-6.83	-6.83	-8.67	-8.67	-9.67
36	-6.42	-6.83	-7.67	-8.67	-8.67	-9.67
38	-6.42	-6.83	-7.67	-8.67	-9.67	-9.67
40	-6.42	-6.83	-7.67	-8.67	-9.67	-9.67
42	-6.42	-6.83	-7.67	-8.67	-9.67	-9.67
44	-6.42	-6.83	-7.67	-8.67	-9.67	-10.67
46	-6.42	-6.83	-7.67	-8.67	-9.67	-10.67
48	-6.42	-6.83	-7.67	-8.67	-9.67	-10.67

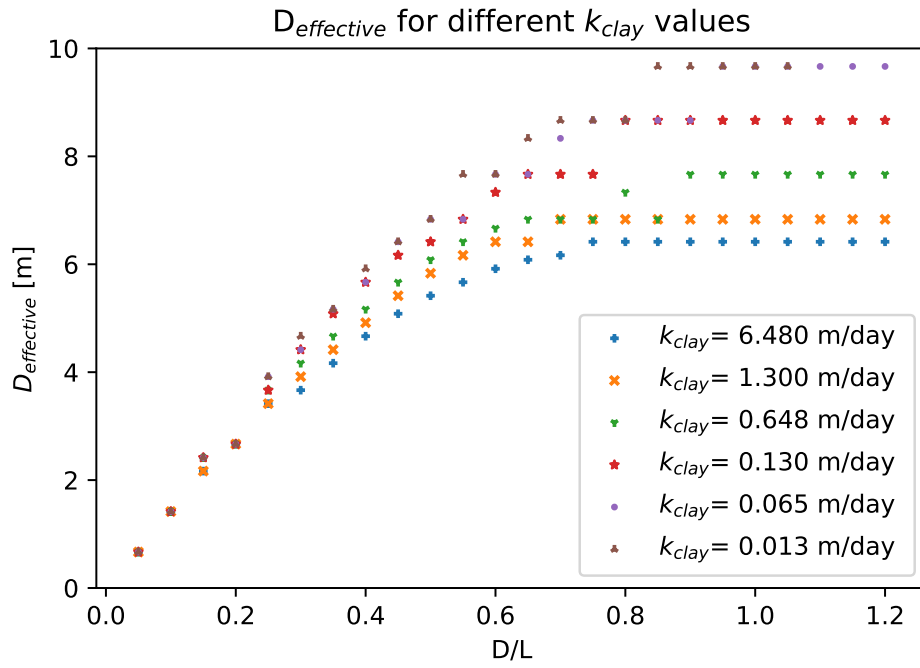


Figure F.8: Graph showing the difference in effective depth for the different scenarios (k_{clay}).

Discharge well for a pipe length of 1.5 meter

The discharge computed in MSeep for a pipe length of 1.5 meters is given in Table F.13.

Table F.13: Case II: Discharge of the well for a pipe of 1.5 meters for the various scenarios

D [m]	Discharge well (Q_{well}) [m^3/day]					
	Hydraulic conductivity (k_{clay}) [m/day]					
	6.480	1.296	0.648	0.130	0.065	0.013
2	2.74	2.74	2.73	2.72	2.71	2.69
4	3.38	3.36	3.35	3.31	3.28	3.22
6	3.68	3.64	3.62	3.55	3.52	3.43
8	3.84	3.81	3.78	3.69	3.65	3.54
10	3.95	3.91	3.88	3.78	3.73	3.61
12	4.03	3.99	3.95	3.84	3.78	3.65
14	4.09	4.04	4.00	3.89	3.82	3.69
16	4.13	4.09	4.05	3.92	3.86	3.71
18	4.17	4.12	4.08	3.95	3.88	3.73
20	4.20	4.15	4.11	3.97	3.90	3.75
22	4.22	4.17	4.13	3.99	3.92	3.76
24	4.24	4.19	4.15	4.00	3.93	3.77
26	4.25	4.21	4.17	4.02	3.94	3.78
28	4.27	4.22	4.18	4.03	3.95	3.79
30	4.28	4.23	4.19	4.04	3.96	3.79
32	4.29	4.25	4.20	4.05	3.97	3.80
34	4.30	4.25	4.21	4.05	3.97	3.80
36	4.30	4.26	4.22	4.06	3.98	3.81
38	4.31	4.27	4.23	4.07	3.98	3.81
40	4.32	4.27	4.23	4.07	3.99	3.81
42	4.32	4.28	4.24	4.07	3.99	3.81
44	4.32	4.28	4.24	4.08	3.99	3.81
46	4.33	4.29	4.24	4.08	4.00	3.82
48	4.33	4.29	4.25	4.08	4.00	3.82

Discharge well for a pipe length of 20 meters

The discharge computed in MSeep for a pipe length of 1.5 meters is given in Table F.14.

Table F.14: Case II: Discharge of the well for a pipe of 20 meter for the various scenarios

D [m]	Discharge well (Q_{well}) [m^3/day]					
	Hydraulic conductivity (k_{clay}) [m/day]					
	6.480	1.296	0.648	0.130	0.065	0.013
2	3.63	3.63	3.63	3.61	3.61	3.59
4	6.07	6.05	6.03	5.97	5.94	5.87
6	8.15	8.10	8.06	7.95	7.89	7.76
8	9.93	9.84	9.78	9.60	9.51	9.33
10	11.45	11.32	11.23	10.97	10.85	10.62
12	12.74	12.57	12.44	12.10	11.94	11.65
14	13.84	13.62	13.46	13.02	12.83	12.49
16	14.77	14.51	14.32	13.77	13.55	13.16
18	15.56	15.26	15.03	14.39	14.13	13.69
20	16.23	15.90	15.63	14.89	14.60	14.11
22	16.79	16.42	16.13	15.30	14.98	14.44
24	17.26	16.87	16.55	15.63	15.27	14.70
26	17.66	17.24	16.89	15.90	15.51	14.90
28	17.99	17.55	17.18	16.11	15.70	15.06
30	18.27	17.82	17.43	16.29	15.85	15.18
32	18.51	18.04	17.63	16.43	15.97	15.27
34	18.70	18.22	17.80	16.55	16.07	15.34
36	18.87	18.38	17.94	16.64	16.15	15.39
38	19.01	18.51	18.06	16.72	16.21	15.43
40	19.13	18.62	18.17	16.78	16.25	15.46
42	19.24	18.71	18.25	16.83	16.29	15.48
44	19.32	18.79	18.32	16.88	16.32	15.50
46	19.40	18.86	18.39	16.91	16.35	15.51
48	19.46	18.92	18.44	16.94	16.37	15.52

G

iMOD

In this chapter, a general background on iMOD is given followed by an overview of some of the basic functions of iMOD and packages used.

iMOD is a simple user interface, which uses the computational code of MODFLOW. MODFLOW is a finite difference model which has been derived in the United States. The program is used to simulate groundwater flow through aquifers. Before a simulation can run a number of different input parameters need to be defined. Each of these parameters are discussed briefly below.

G.1. Boundary conditions (BND)

In order for the simulation to run, boundary conditions need to be imposed for each model layer so that the end of the calculation are can be determined. Three different boundary values can be used:

- Boundary value < 0
Represent a fixed boundary, at these locations a fixed head is applied
- Boundary value = 0
These locations are excluded from the simulation, meaning that no groundwater will flow through these boundaries.
- Boundary value > 0
These are active areas, and therefore groundwater can flow through these areas, and the head can be computed. These open boundaries need to be connected to at least a single fixed boundary condition (either a boundary conditions < 0 , or a head-dependent boundary such as the RIVER of DRaiNage package).

An overview of the different boundaries in a model is given by Figure G.1.

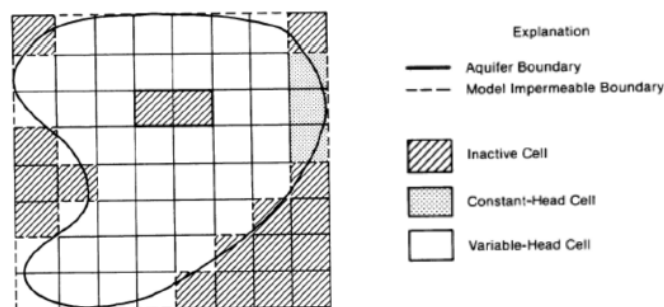


Figure G.1: Example of boundary conditions for a single layer (Vermeulen et al., 2012)

G.2. Starting Heads (SHD)

For each model layer, a initial value needs to be given for the head(in metres) in that layer.

G.3. Horizontal permeabilities (KHV)

In each layer, the horizontal permeability (in m/day) needs to be implemented. In the modelled simulations, a constant value was used through out the model domain for each of the layers.

G.4. Vertical permeabilities (KVV)

In each layer, the vertical permeability (in m/day) needs to be implemented. In the modelled simulations, a constant value was used through out the model domain for each of the layers.

G.5. Vertical anisotropy(KVA)

In iMOD the vertical anisotropy for each model layer needs to be defined. Through out the model, a anisotropy of 1.0 was used. The anisotropy is multiplied by the horizontal permeability to calculate the vertical permeability in the permeable parts of the model layer.

G.6. Top of aquifers

In each layer the elevation needs to be included. This can be defined in this file. The top of the layer represent the top layer of the permeable part of each layer.

G.7. Bottom of aquifers

The bottom layer of the permeable part of each model layer is defined by this file. Each layer needs to have confined by both a top and a bottom.

G.8. Pathline simulation

In order to study the streamlines under the aquifer, the interactive pathline simulator was used. First the particles studied needed to be included. A choice can be made in forward particle tracking or backwards particle tracking. Forward particle tracking determines where the particles end up. While the backward particle tracker determines where the particles originated from.

H

iMOD simulations

Here an detailed overview of the input parameters of the model are given as well as a detailed overview of the results.

H.1. Geometry

Before any simulations can be done, first the dimensions of the model domain need to be determined. For all of the simulations a domain of 200 meters by 300 metres was simulated. Along the whole Northern boundary a river was implemented with the use of a constant head boundary. The river has a width of 20 meters. Directly to the South of the river, a dike was placed of 4 meters high and 20 meters wide and consisted of very impermeable clay ($k_{dike} = 1.3 \text{ E-5 m/day}$). Further south, a cover layer of 1 meter thick was present along the whole model domain. An overview of the implemented features can be seen in Figure H.1

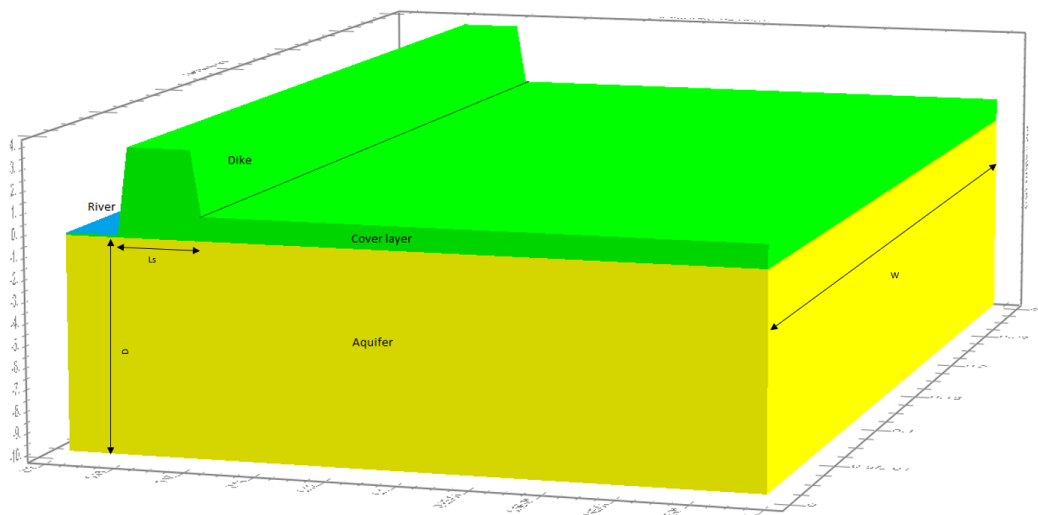


Figure H.1: Three-dimensional view of the geometry implemented in iMOD.

H.2. Mesh size

Through the model, a relatively small mesh size was chosen of 0.1 m by 0.1 m by 0.1 m. This is because in a later stage, a pipe will be simulated and will have these dimensions.

H.3. Boundary conditions

Two sets of boundary conditions were implemented. For the top layer, a constant head boundary was implemented both in the river and downstream of the dike. The fixed head in the river was equal to 2.1 meters and the fixed head in the hinterland was equal to 0.5 meters. For the remaining two layers, a constant head boundary of 0.5 meters was implemented at the southern boundary.

H.4. Input parameters

A number of different parameters need to be defined before the model can be simulated. In Table H.1 an overview is given of the main input values. In some of the simulations, these input values with be varied. For each simulations the range in which the value is varied will be given.

Table H.1: Input parameters for the different MSeep simulations

Parameter	L	k_{sand}	k_{dike}	n	d_{sand}	d_{clay}	$Stage_{river}$
Value:	20 m	13 m/day	1.3E-05 m/day	0.4	10 m	1 m	2.1 m

H.5. Piping

In iMOD backwards erosion piping cannot be simulated. However, in order to simulate the effect of a well on the groundwater flow, a very permeable strip was implemented in the cover layer. In order to simulate a pipe, a similar approach was used and a very permeable strip was implemented directly below the dike. The pipe has a length of 10 meters long a height of 0.1 meters and a width of either the hole model width or 0.1 meters. Figure H.2 and Figure H.3 show the two different set-ups for a quasi 3D simulation and a full 3D simulation.

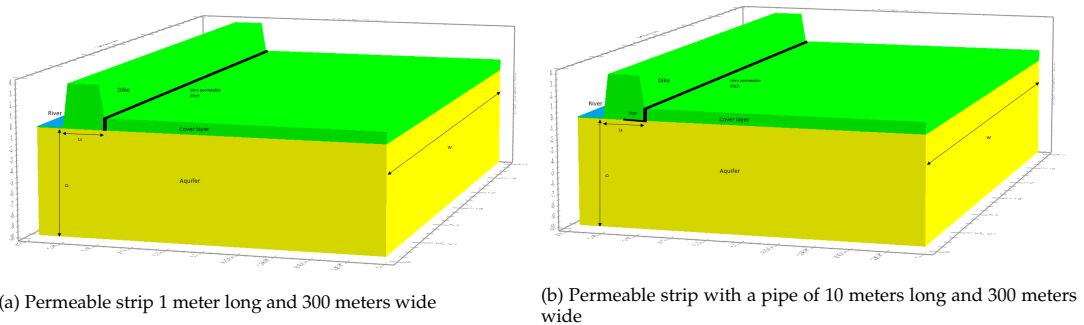


Figure H.2: Quasi 3D schematization of an exit point and a pipe

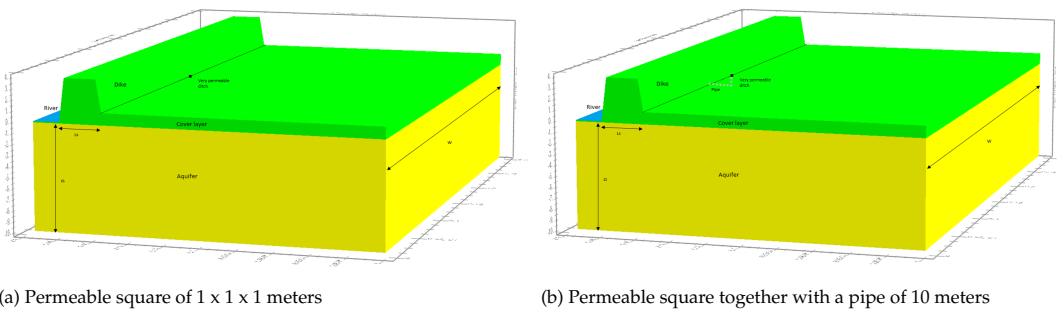


Figure H.3: 3D schematization of an exit point and a pipe

H.6. Results

As is mentioned in chapter 8, seven different sets of simulations were done in iMOD. An overview of the different simulations is given below:

1. A set of simulations where the hydraulic conductivity of the cover layer is constant throughout the model domain but has been varied according to the six different scenarios (Figure 8.1).
2. A set of simulations where the hydraulic conductivity is varied and a very permeable strip of 1 meter long by 1 meter deep is placed directly behind the dike along the whole model width (quasi 3D, Figure H.2a).
3. A set of simulations where the hydraulic conductivity is varied and a very permeable strip of 1 meter long by 1 meter deep is placed directly behind the dike along the whole model width (quasi 3D, Figure H.2b) together with a very permeable 'pipe' of 10 meters long and 0.1 meters deep along the whole model width.
4. A set of simulations where the hydraulic conductivity is varied and a very permeable strip of 1 meter long by 1 meter deep and 1 meter wide is placed directly behind the dike in the center of the model(3D, Figure H.3a).
5. A set of simulations where the hydraulic conductivity is varied and a very permeable strip of 1 meter long by 1 meter deep and 1 meter wide is placed directly behind the dike in the center of the model(3D, Figure H.3b). Together with a pipe of 10 meter longs and 0.1 meters deep and 0.1 meter wide.
6. A set of quasi 3D simulations (with a pipe) were the critical hydraulic head computed in MSeep was implemented as river water level.
7. A set of 3D simulations (with a pipe) where the critical hydraulic head computed in MSeep was implemented as river water level.

In each simulation the hydraulic conductivity was varied according to Table H.2.

Table H.2: Overview of the parameters varied in the six different scenarios

Parameter	Scenario 1	Scenario 2	Scenario 3	Scenario 4	Scenario 5	Scenario 6
k_{clay}	6.480 m/day	1.296 m/day	0.648 m/day	0.130 m/day	0.065 m/day	0.013 m/day

H.7. Base case

In this section the streamlines in the modelled are checked to determine if they behave according to what is expected. As well as to determine if the boundary conditions do not significantly effect the results of the simulations.

H.7.1. Simple groundwater models

First a comparison is done between the two different groundwater models; an MSeep model without a pipe, and an iMOD model without a pipe for both a quasi 3D and 3D model. In all of the simulations, the water level in the river is equal to 2.1 meters and the potential in the clay layer is equal to 0.5 meters. First the groundwater flow potentials in MSeep are compared to the streamlines of a quasi 3D iMOD simulation. This comparison can be made because the streamlines in MSeep are directly perpendicular to the contour potentials. An overview of the potentials and streamlines can be found in Figure H.4.

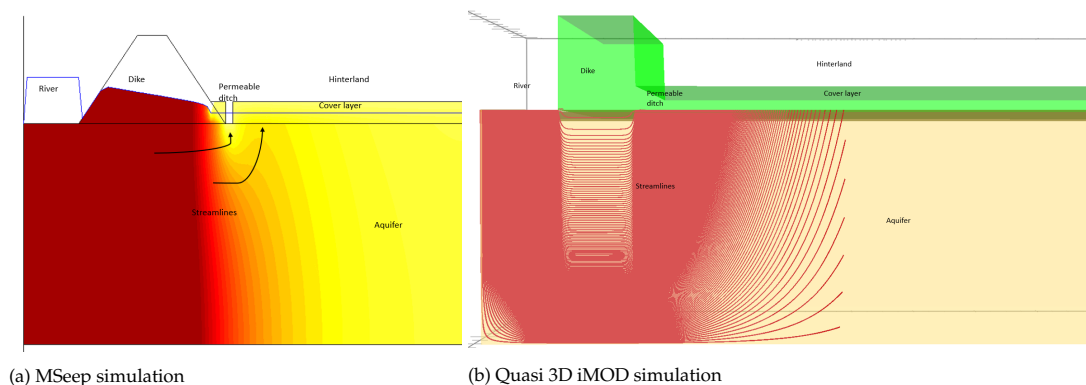


Figure H.4: Comparison of streamlines for an MSeep simulation and a Quasi 3D iMOD simulation

Similar patterns in for the streamlines can be observed for both the 2D MSeep simulation and the quasi 3D iMOD simulation. For a further comparison, the discharge through the ditch and the very permeable layer are compared for both a 2D, quasi 3D and a fully 3D simulations, where the permeable ditch is schematized by a cube of 1 meter wide 1 meter long and 1 meter deep. Table H.3 gives an overview of the results for the six different scenarios.

Table H.3: Discharge through the ditch (MSeep) and the very permeable cover layer(iMOD)

Model	Discharge (Q_{ditch}) [m^3/day]					
	Hydraulic conductivity (k_{clay}) [m/day]					
	6.480	1.296	0.648	0.130	0.065	0.013
MSeep	3.72	4.45	4.83	5.70	5.98	6.29
iMOD (Quasi 3D)	1.52	1.89	2.13	2.81	3.09	3.60
iMOD(3D)	2.48	3.99	5.02	8.24	9.82	13.11

It can be observed that there is a difference in magnitude between the MSeep model and the quasi 3D iMOD model. One of the reasons for this difference is that, in MSeep the discharge is computed at the nodes of the cells (Figure H.5a). While in iMOD the discharge is calculated that the center of the cells (Figure H.5b). This difference because MSeep is a finite element model and iMOD is a finite difference model.

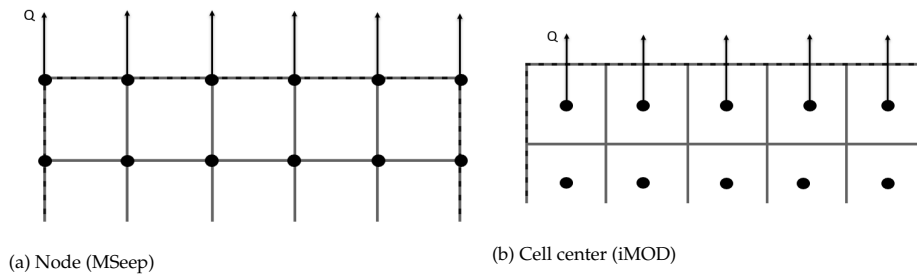


Figure H.5: Discharge is computed in MSeep in the nodes while in iMOD in the cell centers

Lastly, similar trends can be observed for all three models, a decrease in the hydraulic conductivity of the cover layer results in an increase in flow towards the ditch and therefore also an increase in discharge through the ditch.

H.8. Effect of leakage

Here, each of the four different simulations are compared. For each simulations, the six different scenarios are modelled (Table 8.2). For these simulations, both the effective depth, the effective width and the discharge through the cover layer is determined.

For all of the simulations, the effective depth was determined and an overview is given in Table H.4. It can be observed that the effective depth increases for less leaky layers. Smaller effective depths are observed for the two sets of simulations with a pipe. From Table H.4 it can be observed that the effective depth is smaller for the quasi 3D simulations. This is because for these simulations, the effective width also becomes important. The effective width for these two simulations can be seen in Table H.5.

Table H.4: Effective depth for the four different simulations(iMOD)

Model	Effective depth ($D_{effective}$) [m]					
	Hydraulic conductivity (k_{clay}) [m/day]					
	6.480	1.296	0.648	0.130	0.065	0.013
iMOD (Quasi 3D)	5.43	5.68	5.88	6.44	6.67	7.05
iMOD (3D)	1.47	1.79	2.07	3.27	4.05	6.08
iMOD (Quasi 3D) pipe	1.52	1.76	1.96	2.65	3.00	3.72
iMOD (3D) pipe	1.99	2.38	2.74	4.21	5.10	7.28

The presence of a pipe also effects the streamlines under the aquifer. The difference in streamlines as a result of a dike can be seen in Figure H.6.

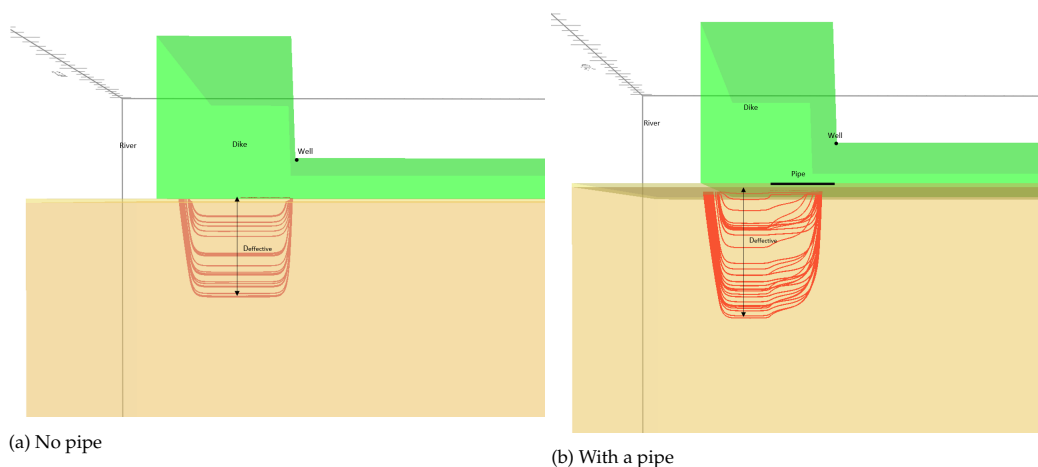


Figure H.6: Difference in streamlines under the dike for 3D simulations with and without a dike

For the 3D simulations, the effective width is also computed. For these simulations, the effective width increases as the hydraulic conductivity of the cover layer decreases, regardless of the presence of a pipe. Next, it can also be observed that the effective width is slightly larger for the set of simulations with a pipe. This is because as a result of the pipe, more lateral groundwater is attracted towards the pipe, that is the case for the simulations without a pipe.

Table H.5: Effective width for the fully three dimensional simulations(iMOD)

Model	Effective width ($W_{effective}$) [m]					
	Hydraulic conductivity (k_{clay}) [m/day]					
	6.480	1.296	0.648	0.130	0.065	0.013
iMOD(3D)	1.40	1.90	2.22	2.97	3.37	4.67
iMOD(3D) pipe	1.34	2.04	2.35	3.17	3.67	5.20

For these four sets of simulations, the area of influence was also calculated. For the 3D simulations, this was done by multiplying the effective width by the effective depth. For the quasi 3D simulaitons, this was done by multiplying the effective depth by the width of one cell which is equal to 0.1 meters. The results of these calculations can be found in Table H.6.

Table H.6: Effective area for the four different simulations(iMOD)

Model	Effective area($A_{effective}$) [m^3/day]					
	Hydraulic conductivity (k_{clay}) [m/day]					
	6.480	1.296	0.648	0.130	0.065	0.013
iMOD (Quasi 3D)	0.54	0.57	0.59	0.64	0.67	0.70
iMOD (3D)	2.06	3.40	4.59	9.73	13.63	28.41
iMOD (Quasi 3D) pipe	0.15	0.18	0.20	0.26	0.30	0.37
iMOD (3D) pipe	2.67	4.85	6.44	13.35	18.71	37.88

Finally, the discharge through the permeable cover layer was also determined. Table H.7, gives an overview of the computed discharge through the ditch. Here it can also be observed that an increase in discharge is paired with a decrease in the hydraulic conductivity of the cover layer. Secondly, for the simulations in which a pipe has been modelled, larger discharges through the ditch are observed.

Table H.7: Discharge through the very permeable cover layer for the four different simulations(iMOD)

Model	Discharge (Q_{ditch}) [m^3/day]					
	Hydraulic conductivity (k_{clay}) [m/day]					
	6.480	1.296	0.648	0.130	0.065	0.013
iMOD (Quasi 3D)	1.52	1.89	2.13	2.81	3.09	3.60
iMOD (3D)	2.48	3.99	5.02	8.24	9.82	13.11
iMOD (Quasi 3D) pipe	5.44	5.75	5.98	6.56	6.78	7.14
iMOD (3D) pipe	3.15	4.75	5.85	9.35	11.07	14.68

H.8.1. Comparison of MSeep and iMOD modules

In this section a comparison is made between two sets of simulations. A set of simulations done in MSeep for an aquifer depth of 10 meters with the piping module for the six scenarios and two sets of iMOD simulations (quasi 3D and 3D). The results and output of these simulations are implemented in iMOD. An overview of the input and the results of the MSeep simulations is given in Table H.8.

Table H.8: Overview of the MSeep simulations for the six different hydraulic conductivities

Model	Hydraulic conductivity (k_{clay}) [m/day]					
	6.480	1.296	0.648	0.130	0.065	0.013
H_c [m]	2.16	2.13	2.12	2.08	2.07	2.06
$D_{effective}$ [m]	2.42	2.92	2.92	3.17	3.42	3.42
Q_{pipe} [m^3/s]	8.74	9.01	9.15	9.48	9.58	9.69

In each iMOD simulation, the hydraulic conductivity and the critical hydraulic head was varied. In each simulation a constant pipe length was used of 10 meters. Since this is in accordance with Sellmeijer's design rule which assumes that the critical hydraulic head is reached at a pipe length of half the structure length. Lastly, the corresponding discharge through the pipe was also determined in MSeep.

As was mentioned two sets of iMOD simulations are done, quasi 3D and 3D. For these simulations, first the effective depth was determined. The results of these simulations can be seen in Table H.9. Here it can be seen that the effective depth of the MSeep simulations are smaller than for the quasi 3D iMOD simulations. While for the fully 3D simulations, the effective depth for the more permeable cover layers is first smaller than for the MSeep simulations. However, for less permeable cover layers, the effective depth is larger in 3D than in 2D.

Table H.9: Effective depth for the results of the MSeep simulations(iMOD)

Model	Effective depth ($D_{effective}$) [m]					
	Hydraulic conductivity (k_{clay}) [m/day]					
	6.480	1.296	0.648	0.130	0.065	0.013
iMOD (Quasi 3D) pipe	5.43	5.68	5.88	6.44	6.67	7.04
iMOD (3D) pipe	2.00	2.38	2.74	4.21	5.10	7.27

The effective width was also calculated, here the same trend can be observed as with the effective depth. The effective width also increases as the hydraulic conductivity of the cover layer decreases.

Table H.10: Effective width for the results of the MSeep simulations(iMOD)

Model	Effective width ($W_{effective}$) [m]					
	Hydraulic conductivity (k_{clay}) [m/day]					
	6.480	1.296	0.648	0.130	0.065	0.013
iMOD(3D) pipe	3.45	3.74	3.97	4.81	5.29	6.70

Lastly, the discharge through the permeable cover layer was also computed for both the quasi 3D and 3D simulations. The results of the quasi 3D iMOD simulations are quite similar in magnitude to the discharges computed in MSeep. From this it can be assumed that the models behave similarly. However, for the fully 3D simulations, the discharge through the permeable ditch is smaller for the more permeable cover layers ($k_{clay} > 0.65$) and larger for the less permeable cover layers ($k_{clay} < 0.65$).

Table H.11: Discharge through the very permeable cover layer for the results of the MSeep simulations(iMOD)

Model	Discharge (Q_{ditch}) [m^3/day]					
	Hydraulic conductivity (k_{clay}) [m/day]					
	6.480	1.296	0.648	0.130	0.065	0.013
iMOD (Quasi 3D) pipe	7.34	7.65	7.92	8.52	8.77	9.20
iMOD (3D) pipe	4.25	6.32	7.75	12.16	14.32	18.90